High-resolution integral modelling approach for flow and transport in groundwater-surface water interaction space

vorgelegt von
Master of Science
Katrin Tabea Christina Broecker, geb. Storck
ORCID: 0000-0001-7863-1062

an der Fakultät VI - Planen Bauen Umwelt
der Technischen Universität Berlin
zur Erlangung des akademischen Grades

Doktorin der Ingenieurwissenschaften
- Dr.-Ing. -

genehmigte Dissertation

Promotionsausschuss:

Vorsitzender: Prof. Dr.-Ing. Matthias Barjenbruch
Gutachter: Prof. Dr.-Ing. Reinhard Hinkelmann
Gutachter: Prof. Dr. rer. nat. Gunnar Nützmann
Gutachter: Prof. Dr.-Ing. Rainer Helmig
Gutachterin: Prof. Dr.-Ing. Nicole Saenger

Tag der wissenschaftlichen Aussprache: 8. Dezember 2020

Berlin 2021

Preface

First of all, I would like to thank my supervisor, Reinhard (Phillip) Hinkelmann, for his scientific and methodological support and for giving me the great opportunity to work within the Research Training Group “Urban Water Interfaces" (UWI). I am also very grateful for the valuable discussions and the feedback from my supervisor Gunnar Nützmann. I would like to thank all my former colleagues from the Chair of Water Resources Management and Modeling of Hydrosystems at TU Berlin as well as all members of the Research Training Group for the numerous discussions, advices and comments that allowed me to discover new aspects and approaches. Thanks as well for the many non-scientific and motivating conversations.

Especially I would like to thank Ralf Duda, who has always supported me with a lot of patience and great willingness to help in all technical matters. I would like to thank Katharina Teuber for the numerous discussions about OpenFOAM, and for being such a wonderful roommate and friend. Thanks also to Waldemar Elsesser with whom it was great to work together and who gave me excellent support in the beginning of my PhD studies. I am likewise very thankful for the administrational support and the encouragement by Gwendolin Porst and Tosca Piotrowski.

And my biggest thanks to my husband, our two sons, my parents and my sister for all the support and the patience.

Berlin, January, 2021

Publications of cumulative doctoral thesis

First author publications (in chronological order):

1. **Broecker, T.,** Elsesser, W., Teuber, K., Özgen, I., Nützmann, G. & Hinkelmann, R. (2018). High-resolution simulation of free-surface flow and tracer retention over streambeds with ripples. Limnologica, 68, 46-58, https://doi.org/10.1016/j.limno.2017.06.005.
2. **Broecker, T.,** Teuber, K., Sobhi Gollo, V., Nützmann, G., Lewandowski, J. & Hinkelmann, R. (2019). Integral Flow Modelling Approach for Surface Water-Groundwater Interactions along a Rippled Streambed. Water, 11(7), 1517, https://doi.org/10.3390/w11071517.
3. **Broecker, T**., Sobhi Gollo, V., Fox, A., Lewandowski, J., Nützmann, G., Arnon, S. & Hinkelmann, R. (2021). High Resolution Integrated Transport Model for Studying Surface Water–Groundwater Interaction. Groundwater, https://doi.org/10.1111/gwat.13071.

Book Chapter:

1. **Broecker, T.,** Teuber, K., Elsesser, W. & Hinkelmann, R. (2018). Multiphase Modeling of Hydrosystems Using OpenFOAM, in: Gourbesville P., Cunge J., Caignaert G. (eds). Advances in Hydroinformatics, Springer Water, 1013-1029, Singapore.

Conference paper:

1. **Broecker, T**., Schaper, J., El-Athman, F., Gillefalk, M., Hilt, S. & Hinkelmann, R. (2017). Surface water-groundwater interactions. Proceedings of the 37th IAHR (International Association for Hydro-Environment Engineering and Research) World Congress, Kuala Lumpur, Malaysia.

Supplementary contributions

Co-authored publications (in chronological order):

1. Teuber, K., **Broecker, T.,** Bentzen, T.R., Stephan, D., Nützmann, G. & Hinkelmann, R. (2019). Using computational fluid dynamics to describe H2S mass transfer across the water-air interface in sewers. Water Science and Technology, 79 (10), 1934-1946, https://doi.org/10.2166/wst.2019.193.
2. Teuber, K., **Broecker, T.,** Bayón, A., Nützmann, G. & Hinkelmann, R. (2019). CFD-modelling of free-surface flows in closed conduits. Progress in Computational Fluid Dynamics 19 (6), 368-380, https://doi.org/10.1504/PCFD.2019.103266.
3. Lewandowski, J., Arnon, S., Banks, E., Batelaan, O., Betterle, A., **Broecker, T.,** Coll, C., Drummond, J.D., Gaona Garcia, J., Galloway, J., Gomez-Velez, J., Grabowski, R.C., Herzog, S.P., Hinkelmann, R., Höhne, A., Hollender, J., Horn, M.A., Jaeger, A., Krause, S., Löchner Prats, A., Magliozzi, C., Meinikmann, K., Mojarrad, B.B., Mueller, B.M., Peralta-Maraver, I., Popp, A.L., Posselt, M., Putschew, A., Radke, M., Raza, M., Riml, J., Robertson, A., Rutere, C., Schaper, J.L., Schirmer, M., Schulz, H., Shanafield, M., Singh, T., Ward, A.S., Wolke, P., Wörman, A. & Wu, L. (2019). Is the Hyporheic Zone Relevant beyond the Scientific Community? Water, 11(11), 2230, https://doi.org/10.3390/w11112230.

An overview of all supplementary scientific work is given in section 6.

The thesis was carried out as project N7 of the Research Training Group ‘Urban Water Interfaces‘ (GRK 2032/1) and was funded by the German Research Foundation (DFG).

Abstract

While former research studies mainly considered groundwater and surface water separately, the importance of their interactions is nowadays widely acknowledged. Especially the hyporheic zone, which is the zone where stream and shallow groundwater exchange, is addressed in many investigations. This zone is recognized for retention, transformation and attenuation of solutes and enables to improve water quality significantly, while it additionally serves as refuge and habitat for many aquatic organisms.

But even though the importance of groundwater and surface water interactions is nowadays recognized to a large extent, in numerical models both resources are still investigated separately in most cases due to different temporal dimensions. For investigations at the hyporheic zone, flow and transport processes are commonly determined using coupled numerical models. A surface water model and a groundwater model are executed successively, often with no feedback from groundwater to surface water. In contrast to previous research with coupled models, in the prevailing work, processes at the groundwater-surface water interface are investigated with an integral numerical model. Since high computational effort is needed for the application of the integral solver, processes on a small-scale close to the interface of surface water and porous media are focused on. In a first step, the two-phase solver interFoam is extended for the investigation of tracer retention and free surface flow at rippled streambeds. The Navier-Stokes equations are solved in combination with an implemented advection-diffusion equation. The transport of tracer pulses from surface water to dead zones between ripples at the streambed with varying morphologies and different surface hydraulics are examined. Similar as for the coupled approaches, pressure gradients at the streambed are used to account for hyporheic exchange, assuming surface water moving from high to low pressure zones. It was found out that flow velocities, ripple sizes and spaces between the ripples show to significantly effect pressure gradients at the streambed. Parts of the injected tracer mass are temporarily retained between the ripples due to low velocities and recirculation. In a further step the sediment is included and the same ripple geometries and surface water velocities are assumed as in the previous step. The porousInter solver that extends the interFoam solver for the application in the subsurface is used to determine exchange processes of groundwater and surface water at a small-scale with high resolution. PorousInter solves an extended version of the Navier-Stokes equations and includes porosities as well as grain size diameters within an additional drag term. The validity for groundwater-surface water interactions is first demonstrated using analytical examples. In contrast to the one-way coupled models, the integral model shows the advantage to account for feedback from surface water to the sediment and vice

versa and is also applicable in non-Darcy flow areas. In- and outflowing fluxes at the interface of groundwater and surface water are determined for various hydrological and morphological factors. For all investigated cases with sand, non-Darcy-flow occurred in the upper part of the ripple, while for the cases with gravel non-Darcy-flow is observed over several decimetres in depth. Also, a feedback from the sediment to surface water flow is recognized.

Finally, the integral solver is further extended to determine transport processes at the interface. Observations of a conservative dye tracer that was injected into surface water and spread into rippled streambeds inside a flume are compared with modelling results gained with the integral solver. Neutral conditions as well as conditions with up- and downwelling groundwater flow are considered. The results gained with the integral solver show a good agreement with laboratory observations and provide additional information of prevailing flow processes at the interface. For downwelling groundwater flow the highest velocities within the sediment were found, which leads to shorter residence times compared to neutral conditions or upwelling groundwater, while under neutral conditions the hyporheic exchange was the largest.

The main outcome of this thesis is the description, validation and extension of a new integral solver for flow and transport processes at the interface of groundwater and surface water. Simulation results at various rippled streambeds show effects of small-scale topologies, groundwater and surface water velocities and grain sizes on flow and transport processes at the interface. The integral solver can be used for water management practices, e.g. engineering hyporheic zones, but is also applicable for further surface water-porous media interactions as simultaneous flow over and through dikes or breakwaters.

Kurzfassung

Während in früheren Forschungsstudien Grundwasser und Oberflächenwasser überwiegend getrennt betrachtet wurden, wird die Bedeutung ihrer Wechselwirkungen heutzutage weitgehend anerkannt. Vor allem die hyporheische Zone, in welcher sich Fluss- und oberflächennahes Grundwasser austauschen, wird in vielen Untersuchungen thematisiert. Diese Zone ist für die Rückhaltung, Umwandlung und Verdünnung gelöster Stoffe bekannt und ermöglicht eine erhebliche Verbesserung der Wasserqualität, während sie gleichzeitig vielen Wasserorganismen als Zufluchtsort und Lebensraum dient.

Doch obwohl die Bedeutung des Austausches von Grundwasser und Oberflächenwasser heutzutage weitgehend bekannt ist, werden in der numerischen Modellierung beide Ressourcen aufgrund unterschiedlicher zeitlicher Dimensionen in den meisten Fällen separat untersucht. Für Untersuchungen in der hyporheischen Zone werden Strömungs- und Transportprozesse üblicherweise mit gekoppelten numerischen Modellen bestimmt. Dazu werden Oberflächen- und ein Grundwassermodelle häufig nacheinander und ohne Rückkopplung vom Grundwasser zum Oberflächenwasser ausgeführt. Im Gegensatz zu früheren Forschungen mit gekoppelten Modellen werden in der vorliegenden Arbeit Prozesse an der Grenzfläche von Grundwasser und Oberflächenwasser mit einem integralen numerischen Modell untersucht. Da bei der Anwendung des integralen Lösers ein hoher Rechenaufwand erforderlich ist, werden vor allem kleinskalige Prozesse nahe der Grenzfläche zwischen Oberflächenwasser und porösen Medien untersucht. In einem ersten Schritt wird der Zweiphasen-Löser interFoam erweitert, um den Rückhalt eines Tracers zusammen mit dem freien Oberflächenfluss an einem Flussbett mit Rippeln zu untersuchen. Zusätzlich zu den Navier-Stokes-Gleichungen wird eine Advektions-Diffusions-Gleichung gelöst. Untersucht wird der Transport von Tracer-Zugaben vom Oberflächenwasser zu Totzonen an der Flussbettoberfläche, wobei unterschiedliche Rippelgeometrien und unterschiedliche hydraulische Verhältnisse berücksichtigt werden. Ähnlich wie bei den gekoppelten Ansätzen werden Druckgradienten am Strömungsbett analysiert, um auf den hyporheischen Austausch zu schließen, wobei das Oberflächenwasser von Hoch- zu Niederdruckzonen fließt. Strömungsgeschwindigkeiten, Rippelgrößen und Abstände zwischen den Rippeln zeigen einen signifikanten Einfluss auf die Druckgradienten am Strömungsbett. Ein Teil des injizierten Tracers wird aufgrund niedriger Geschwindigkeiten und Rezirkulation zwischen den Rippeln vorübergehend zurückgehalten. In einem weiteren Schritt wird das Sediment hinzugefügt und die gleichen Rippelgeometrien und Oberflächenwassergeschwindigkeiten wie im ersten Schritt angenommen. Der porousInter-Löser, der den interFoam-Löser um die Anwendung im Untergrund erweitert, wird zur

Bestimmung hochaufgelöster Austauschprozesse von Grundwasser und Oberflächenwasser auf kleinen Skalen verwendet. PorousInter löst eine erweiterte Version der Navier-Stokes-Gleichungen und berücksichtigt das Sediment durch Porositäten sowie Korngrößendurchmesser innerhalb eines zusätzlichen Widerstandsterms. Die Gültigkeit für den Austausch von Grundwasser und Oberflächenwasser wird zunächst anhand von analytischen Beispielen demonstriert. Im Gegensatz zu den Einweg-gekoppelten Modellen zeigt das integrale Modell den Vorteil, Rückkopplungen vom Oberflächenwasser zum Sediment und umgekehrt zu berücksichtigen und ist auch in Strömungsgebieten anwendbar, die außerhalb des Darcy-Bereichs liegen. Zu- und Abflüsse an der Grenzfläche von Grundwasser und Oberflächenwasser werden für verschiedene hydrologische und morphologische Faktoren bestimmt. In allen untersuchten Fällen mit Sand wurden an den oberen Zonen der Rippel Bereiche festgestellt, die außerhalb der Darcy-Gültigkeit liegen, während in den Fällen mit Kies diese Bereiche über mehrere Dezimeter in die Tiefe hinweg zu erkennen waren. Auch eine Rückkopplung vom Sediment- zum Oberflächenwasserfluss ist offensichtlich.

Zuletzt wird der integrale Löser dahingehend erweitert, Transportprozesse an der Schnittstelle zu bestimmen. Die Beobachtungen eines konservativen Farb-Tracers, welcher im Oberflächenwasser injiziert wurde und sich in einer Sohle mit Rippeln in einem Gerinne ausgebreitet hat, werden mit den Ergebnissen des integralen Lösers verglichen. Es werden neutrale Bedingungen sowie Bedingungen mit ab- und zufließendem Grundwasserfluss berücksichtigt. Die mit dem integralen Löser erzielten Ergebnisse zeigen eine gute Übereinstimmung mit Laborbeobachtungen und liefern zusätzliche Informationen zu den vorherrschenden Strömungsprozessen an der Schnittstelle. Für abfließende Grundwasserströmung wurden die höchsten Geschwindigkeiten innerhalb des Sediments festgestellt, was zu kürzeren Verweilzeiten im Vergleich zu neutralen Bedingungen oder zufließendem Grundwasser führt. Unter neutralen Bedingungen wurde das größte Ausmaß an hyporheischem Austausch festgestellt.

Das wesentliche Ergebnis dieser Arbeit ist die Beschreibung, Validierung und Erweiterung eines neuen integralen Lösers für Strömungs- und Transportprozesse an der Schnittstelle von Grundwasser und Oberflächenwasser. Simulationsergebnisse an verschiedenen gerippelten Flussbetten zeigen Auswirkungen kleinerer Topologien, Grundwasser und Oberflächenwassergeschwindigkeiten und Korngrößen auf Strömungs- und Transportprozesse an der Grenzfläche. Der integrale Löser kann für praktische wasserbaulichen oder wasserwirtschaftlichen Fragestellungen verwendet werden, beispielsweise für speziell konstruierte hyporheische Zonen, aber auch für weitere Interaktionen von Oberflächenwasser

und porösen Medien wie beispielsweise bei über- und durchströmten Deichen oder Wellenbrechern.

Contents

List of Figures

List of Tables

1. Introduction

1.1 Groundwater-surface water interactions

Groundwater and surface water are hydraulically connected. The exchange can occur between groundwater and streams, rivers, lakes, wetlands or the ocean (Toran, 2017). Depending on the distribution of hydrostatic and hydrodynamic pressure, surface water infiltrates into the sediment or groundwater exfiltrates into surface water (Brunke, 2001). After Winter et al. (1998) groundwater and surface water have to be considered as a single resource, but traditionally, groundwater and surface water are regarded separately. This separation exists on the one hand due to different accessibilities and on the other hand due to their different characteristics (Brunke, 2001). Over the last decades, the interest into the interaction of groundwater and surface water has increased significantly (Fleckenstein & Schmidt, 2009). This can be seen e.g. in the EU Water Framework Directive 2000/60/EU which prescribes explicitly an integral consideration of groundwater and surface water resources. Various research approaches highlighted the importance of the exchange. Especially the very specific biogeochemical conditions in the transition zone between groundwater and surface water and their relevance for aquatic ecology and water quality were emphasized (Khan & Khan, 2019). An increased focus on the exchange of groundwater and surface water was initiated by the development of new methods for quantification and new modelling approaches (see section 1.3), which had to be elaborated based on different spatial and temporal patterns for each domain (Fleckenstein & Schmidt, 2009; Schuetz & Weiler, 2011).

Today, there are several methods to investigate the exchange between groundwater and surface water (Anderson, 2005; Rahimi et al., 2015). The different quantification methods have their advantages and disadvantages depending on the focus of the study and depending on different spatial resolutions (Cook, 2015; Hatch et al., 2006). For measurements, direct and indirect methods can be distinguished (Cook, 2015; Kalbus et al., 2006). For direct measurements seepage meters can be used, ranging from simple collecting tanks to combined devices with built-in piezometers (see Figure 1-1) to ultrasound or electromagnetic instruments. However, seepage meters are only point measurements (Kalbus et al., 2006; McCallum et al., 2012), while exchange processes can be very heterogeneous and therefore exchange fluxes are not characterized sufficiently with point measurements (Toran, 2017). The indirect methods can be subdivided into methods based on the Darcy law and methods that are based on mass balance (Kalbus et al., 2006). Quantification methods based on the Darcy law use the proportionality

between the hydraulic gradient and water flowing through a cross section with a certain hydraulic conductivity (Darcy, 1856). By determining the piezometric heights in the flow and in the aquifer the hydraulic gradient and the flow direction can be determined. But again, these techniques are point measurements. Most of the current approaches work with mass balancing or with a combination of different methods as e.g. in Saenger (2002). Research studies using the mass balancing method are mostly based on the investigation of hydrochemistry and on tracer experiments (Irvine et al., 2015; Keery et al., 2007; Westhoff et al., 2007). For detailed measurements of the flow field, Particle Imaging Velocimetry (PIV) can be applied in laboratory experiments as e.g. in Blois et al. (2014). These field and laboratory measurement approaches are suitable to offer realistic observations under specific conditions. However, generalization is difficult – especially for field experiments. Deeper understanding of the complex dynamics at the interface can be gained with modelling studies, which can also be applied to offer predictions without the application of experiments. In section 1.3 various modelling approaches for the exchange of groundwater and surface water are presented.

Figure 1-1: Investigation of groundwater-river interactions within the SMART-project of the Leibniz Institute of Freshwater Ecology and Inland Fisheries (IGB) in the Schlaube, (Brandenburg, Germany), Image: Jörg Lewandowski, IGB.

Regarding the characteristics of groundwater-surface water exchange, a distinction is made between two main types. In the first case the groundwater table is higher than the surface water table and groundwater infiltrates into the surface water - in the following referred as ‘gaining

conditions' (see Figure 1-2a). In the second case, when the hydraulic gradient between surface water and groundwater level is reversed, water exfiltrates from the surface into the adjacent aquifer. This is the so-called 'losing conditions' (see Figure 1-2b). A special case of a losing system is when the surface water is separated from the underlying aquifer by an unsaturated zone (Kalbus et al., 2006) (see Figure 1-2c). When there is no hydraulic gradient between surface water and groundwater, this is referred to as 'neutral conditions' (Ivkovic, 2009; Silliman & Booth, 1993; Woessner, 2000). Since the exchange is related to groundwater and surface water tables, gaining and losing conditions can depend on weather and season (Gariglio et al., 2013). Next to the exchange due to different water tables, exchange of subsurface- and surface water is generated by water flow over streambed morphologies like meanders, pool-riffles, bars, ripples or others obstacles (Boano et al., 2014; Cardenas & Wilson, 2007a, 2007c; Mutz et al., 2007; Packman et al., 2004). After Toran (2017), the hyporheic flow (see section 1.2) is (strictly seen) not considered as groundwater-surface water exchange since the water is derived from the stream and flows back again. However, it could be seen to become groundwater as long as the water flows within the streambed or within the stream banks (Toran, 2017). As a consequence, hyporheic exchange is a special exchange type and is introduced more closely in section 1.2.

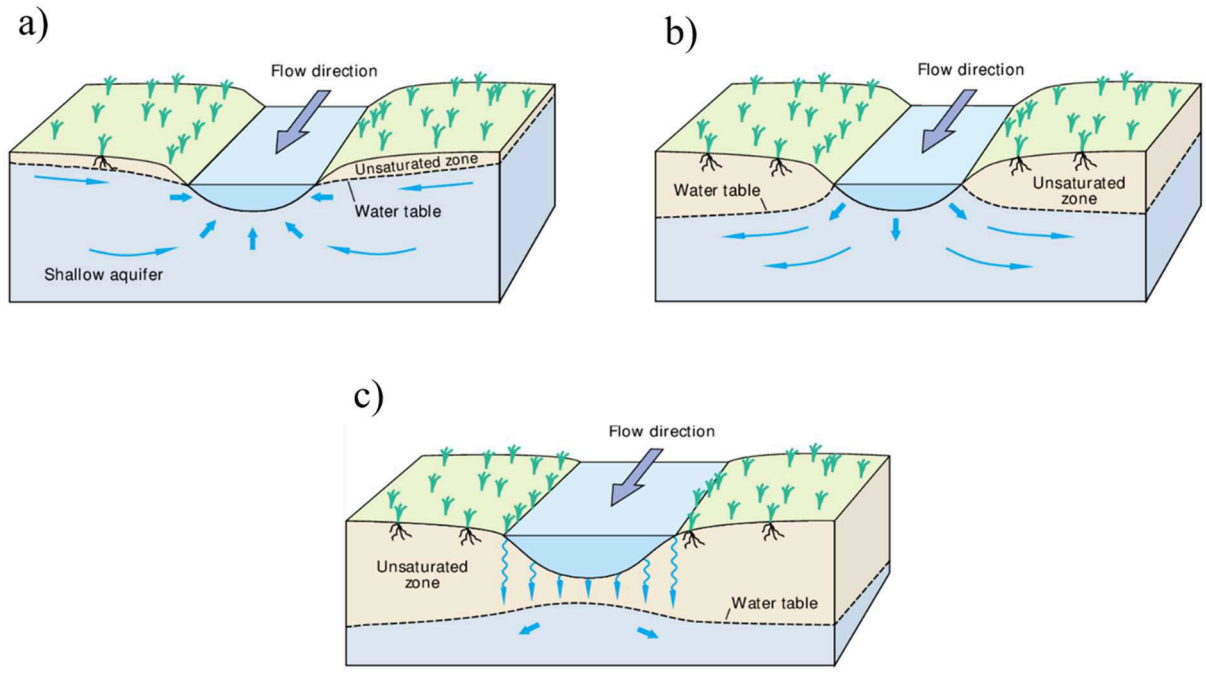

Figure 1-2: Groundwater-surface water exchange types: a) gaining conditions, b) losing conditions, c) disconnected, losing conditions after Winter et al. (1998).

With the exchange of water from surface to subsurface and vice versa, the transport of substances and corresponding reactions is enabled as well. As a consequence, a spreading of contaminants e.g. by industry, intense agriculture or sewage systems is possible. Therefore, the knowledge about exchange rates between groundwater and surface water is of central importance in order to predict consequences for drinking water and animal protection and to find appropriate management solutions (Becker et al., 2004; Kalbus et al., 2006). But next to the spreading of contaminants, the water quality can also be improved by interactions of groundwater and surface water. Critical substances can be transformed or degraded by biogeochemical reactions enabled by interactions of groundwater and surface water. The significance of reactive transport for the water quality is widely accepted, even though mechanistic understanding and standardized methods for the underlying processes are still not sufficient (Lewandowski et al., 2020). Especially the hyporheic zone was considered in many studies to investigate processes at sediment-water interfaces (Lewandowski et al., 2020). This zone is known for the impressive self-purification capacity including e.g. nutrient turnover, degradation of contaminants and the removal of trace organic compounds (Lewandowski et al., 2019). The hyporheic zone is introduced in the following section.

1.2 Hyporheic zone

The ‘hyporheic zone’ is a transition zone between surface water and groundwater, whose clear delineation depends on the point of view (Tonina, 2012). While the upper boundary of the sediment-water interface is relatively clear, the lower boundary depends on the perspective. It can be defined e.g. on the basis of hydrological, biological or chemical criteria (White & Hendricks, 2000). From the hydrological point of view, the hyporheic zone is characterized by infiltration of surface water with a following exfiltration into/out of the streambed (Bencala, 2000). Hydrology affects biogeochemistry and eco-hydrology through flow paths, since the investigated exchange fluxes control habitat characteristics like temperature and the mixing and transport of e.g. dissolved oxygen, nutrients and contaminants in spatio-temporal dependence (Krause et al., 2011). For biologists, the hyporheic zone is an important habitat and refugium for numerous organisms (Brunke & Gonser, 1997). Biologically, this zone is defined by the presence of hyporheic fauna, called ‘hyporheo’ (Orghidan, 1959). Whereas chemists delineate the hyporheic zone as a volume of mixed groundwater and surface water regarding chemical signatures. Classically, the amount of surface water in the sediment should indicate at least 10 % (Triska et al., 1989). But even within the disciplines, the definition varies sometimes (Gooseff, 2010; Ward, 2016). Most exchange processes occur in the limited geographical

transition zone at the bottom of surface waters with dimensions of a few centimetres to decimetres (DWA, 2013). Due to variations of surface water level, groundwater table, velocity or temperature, the depth of the hyporheic zone can vary over time.

The exchange of water at the sediment-water interface is caused by local pressure differences e.g. due to the unevenness in the riverbed (Elliott & Brooks, 1997a). Obstacles can cause high pressures at the upstream side, whereas the pressures at the downstream side of the structures decreases. As a result, the stream water infiltrates into the sediment at the upstream side of the obstruction and exfiltrates back into the stream at the downstream side (Elliott & Brooks, 1997a, 1997b; Harvey & Bencala, 1993; Packman et al., 2000; Thibodeaux & Boyle, 1987). Next to small scale phenomena, also valleys, bedrocks and aquifer properties can influence hyporheic exchange (Brunke & Gonser, 1997; Malcolm et al., 2005). At larger scales the ambient groundwater flow can have a significant impact on the hyporheic flow (Bayani Cardenas & Wilson, 2006). Moreover, turbulence in the surface water can lead to additionally pressure variations (O'Connor & Harvey, 2008). The transfer of turbulent momentum into the sediment is especially important for sediments with large grain sizes (Packman et al., 2004; Roche et al., 2018). Often various causes of exchange are superimposed (Bayani Cardenas & Wilson, 2006).

The hyporheic zone is characterized by high temporal dynamics (Ibisch et al., 2009; Kennedy et al., 2009) and spatial heterogeneity (Fleckenstein et al., 2006). Transport processes in surface waters are comparable fast, while transport velocities in groundwater are usually several orders of magnitude lower (Paton Née Mueller et al., 2014). The dynamic exchange of water, substances and energy (temperature) between groundwater and surface water as well as the intensive material turnover in the hyporheic zone lead to steep hydrological, biogeochemical and thermal gradients (Krause et al., 2011).

The blockage of the streambed by fine sediments and organic material through colmation/clogging controls the residence time and therefore also reaction times, which are of great importance for hyporheic biogeochemical cycling and habitat conditions (Nogaro et al., 2010). Moreover, aquatic vegetation can affect stream velocity and depth (Duff et al., 2001; Packman & Salehin, 2003) and can increase the degradation and retention of particulate matter (White & Hendricks, 2000). From the biogeochemical perspective, the hyporheic zone is of great importance considering especially the self-purification of rivers (Smith, 2005). Numerous studies of predominantly small streams indicated the significance of the hyporheic zone for the removal of nitrate and phosphate (Doyle, 2005; Fischer et al., 2005; Knapp et al., 2009). Trauth et al. (2014) emphases in this context the influence of the ambient groundwater flow on the

solute flux, the residence time and the size of the reactive zone. Basic requirements for the denitrification are anaerobic conditions and the availability of reductive agents like organic carbon next to nitrate concentrations (Hill & Cardaci, 2004). The hyporheic zone acts usually as an interface between oxidized surface water and reduced conditions in groundwater and is consequently very important for the aquatic environment. Based on the impact on the nitrogen and carbon cycling, Fischer et al. (2005) call the hyporheic zone 'the river's liver'.

Next to the nutrient transformation, the impact of the hyporheic zone for heavy metal concentrations (Feris et al., 2003a; Feris et al., 2003b), microplastics (Klein et al., 2015), pesticides (Boutron et al., 2011), organic stormwater contaminants (Peter et al., 2019) and pharmaceuticals (Riml et al., 2013; Schaper et al., 2019; Schaper et al., 2018) is examined in various research studies. Hancock (2002) described the human impacts on the stream-groundwater exchange zone and proposed to include the hyporheic zone into the river management.

Facing the interest of different disciplines in so many different processes within the hyporheic zone (see Figure 1-3), interdisciplinary cooperation is acquired to fulfil research challenges (Krause et al., 2011). For the understanding of hydrological processes at the groundwater-surface water interface, the development of high-resolution field measurement techniques and stable numerical models are essential, which in turn also affect other disciplines. In the next section the focus lies on the application and investigation of modelling tools for the exchange of groundwater and surface water.

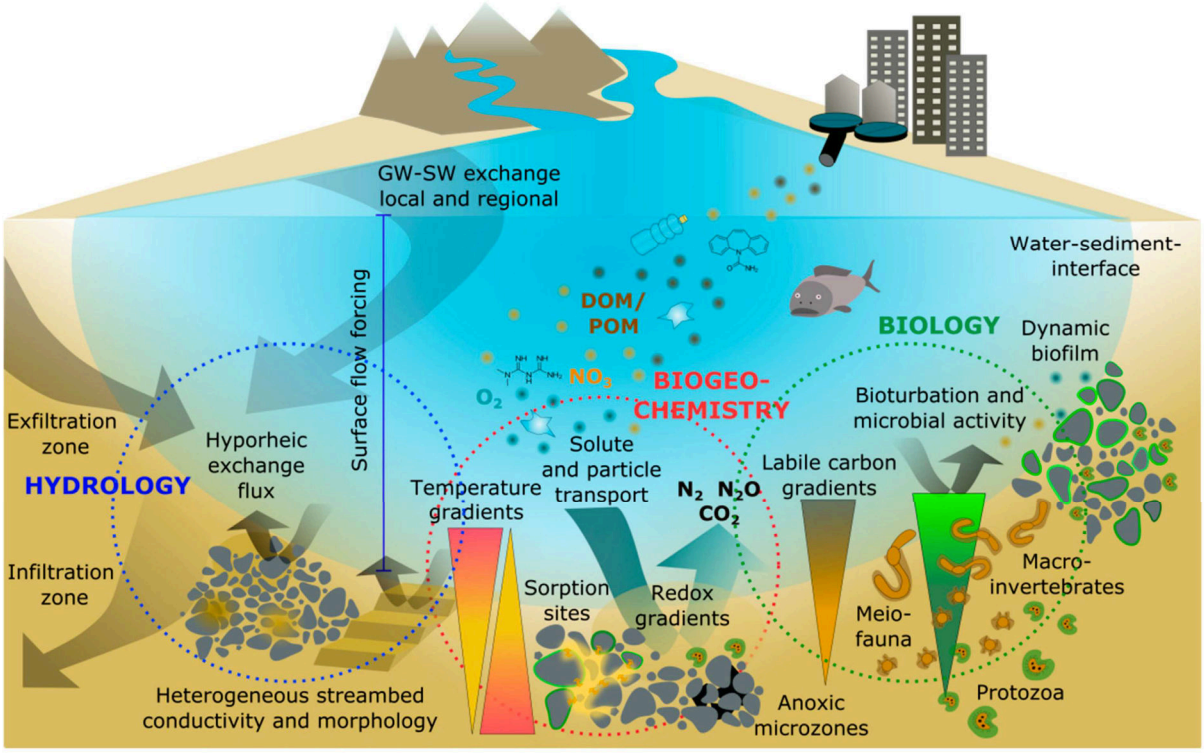

Figure 1-3: Major hyporheic zone drivers and processes from different disciplines after Lewandowski et al. (2019).

1.3 Conceptual modelling of groundwater-surface water interactions

Numerical models offer the possibility to make predictions and improve process understanding for even complex hydrodynamics and transport processes. For instance, the impact of planned river restoration structures on the flow field can be predicted by numerical modelling studies. This can comprise e.g. sediment coarsening (Ward et al., 2018), manipulation of flow path geometries through baffle walls (Herzog et al., 2016; Vaux, 1968) or the construction of a step into a river (Morén et al., 2017). Compared to field or laboratory measurements numerical models can show the advantage to provide high-resolution information for a broad range of applications. Moreover, information about variables that are difficult to measure or rather difficult to measure without disturbing the flow field itself can be obtained. They can serve as qualitative tool if different scenarios should be tested numerically without or with a reduced number of cost and time expensive experiments. They can be used e.g. as indicator for impacts by climate or land use change. In the context of groundwater-surface water interactions, numerical models can serve as a tool for the quantification of water and solute exchange as well as for understanding flow and transport processes under different conditions to protect or recover the aquatic ecosystem. But modelling the interaction of groundwater-surface water

requires the consideration of various processes on different time scales and require adequate modelling strategies with a sufficiently high-resolution.

In the numerical modelling at this interface, different coupling approaches can be found in the literature for one- as well as for two-domains. For the one domain approaches, one set of equations is used in the entire investigation area. On the microscale area it is possible to model the whole groundwater-surface water interaction space by solving the Navier-Stokes equations without any interface condition. For this modelling approach, each pore geometry needs to be described in detail. The computational cost of this model is of course enormous. Another known one-domain approach is the method by Brinkman (1949) who uses one set of equations for the entire domain by superposing the Navier-Stokes equations with the Darcy law with a gradual transition from surface to subsurface (see Figure 1-4). A key parameter for this equation is the effective viscosity, for which many different approaches exist how to choose this parameter (compare Brinkman (1949), Starov and Zhdanov (2001), Gupte and Advani (1997), Larson and Higdon (1987), Ochoa-Tapia and Whitaker (1995)).

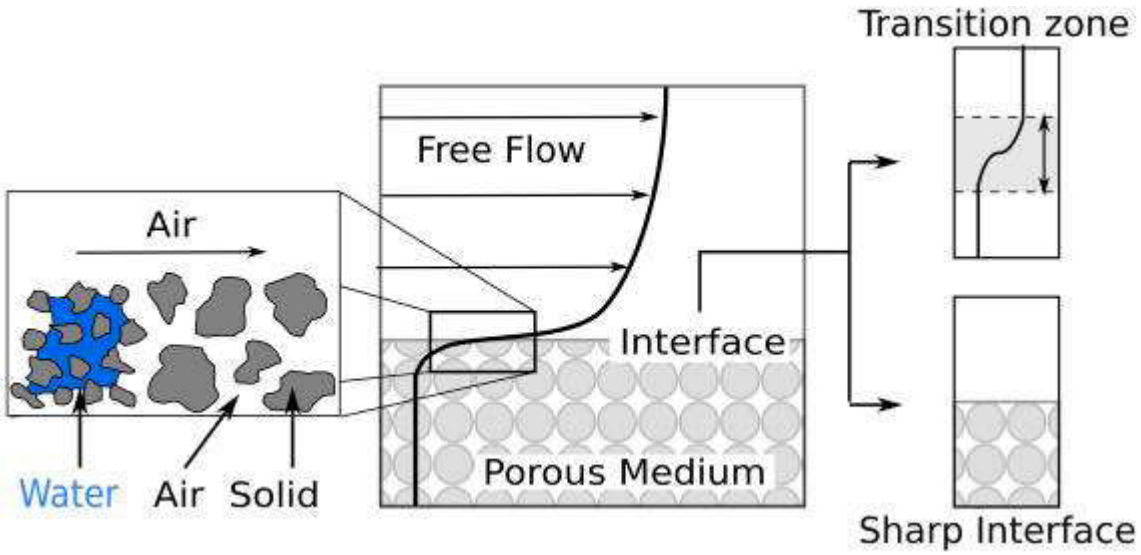

Figure 1-4: Interface description for coupled free flow after Mosthaf et al. (2011).

For the two-domain approach different sets of equations are used for two different domains. At the interfaces these domains are connected by appropriate conditions. One coupling strategy was developed by Beavers and Joseph (1967) as applied e.g. in Yang et al. (2019). Beavers and Joseph (1967) derived a boundary condition at the interface, for which they relate the free flow velocity and its gradient at the interface to the Darcy velocity. Again, an additional parameter, known as Beavers and Joseph slip coefficient, is needed to be adapted to each problem.

Numerous models which couple surface and groundwater flow models apply only one- or two-dimensional shallow water equations, but also three-dimensional models as e.g. applied in Trauth et al. (2013, 2014, 2015) exist. For the analysis of hyporheic exchange also transient storage models are widely used. Thereby the exchange rate is gained by fitting the model to determined solute breakthrough curves obtained from measurements of tracer experiments. Afterwards, the exchange parameters are commonly used for further applications as e.g. for reactive transport modelling (Zaramella et al., 2003). A very common coupling strategy for groundwater-surface water flow is a one-way sequential coupling via pressure distributions calculated with a surface water model that is used as a top boundary condition for the subsurface (Cardenas & Wilson, 2007a, 2007b; Janssen et al., 2012; Jin et al., 2010; Saenger et al., 2005; Tonina & Buffington, 2009a; Trauth et al., 2013; Trauth et al., 2014; Trauth et al., 2015). Some further approaches also consider feedback from the subsurface to the surface water (Nützmann & Mey, 2007) or fully couple surface and subsurface flow e.g. with Integrated Hydrology Model (VanderKwaak, 1999), MODHMS (Panday & Huyakorn, 2004) or HydroGeoSphere (Brunner & Simmons, 2011). They use either a common node technique (via superposition) or a dual node technique. For the common node technique exact same head values for each shared node is enforced, while for the dual node approach a flux between the surface water and groundwater is enabled. However, for the flux there is still the problem with the specification of the exchange coefficient.

While hydrological processes in catchment scales are simulated e.g. with the Integrated Hydrology Model or HydroGeoSphere, high resolution processes were modelled e.g. by Cardenas & Wilson (2007a, 2007b) or Trauth et al. (2013, 2014, 2015) on laboratory scales or small river stretches of several 10 meters.

The aim of the present thesis is, to develop a high-resolution integral modelling approach for flow and transport processes on small scales with the same conceptual approach for groundwater and surface water without the determination of any additional parameter for the interface. The approach uses the software OpenFOAM, which is introduced in the following.

1.4 Multiphase flow and transport modelling with OpenFOAM

OpenFOAM (Open-source Field Operation And Manipulation) is a free computational fluid dynamics (CFD) software which contains multiple solvers as well as pre- and post-processing utilities. The software package contains a large number of libraries, written in the object-oriented programming language C++. All uncompiled files are available in text format, which enables them to be viewed and manipulated. Consequently, the user can expand or change the

software for the individual requirements. Different numerical problems for compressible or incompressible, single or multiphase flow in one, two or three dimensions can be addressed. The Finite Volume Method is applied in space and the Finite Differences Method in time (Schulze & Thorenz, 2014).

Within the pre-processing step a computational mesh has to be generated to define a finite number of volumes where the solution for the relevant equations is calculated. Using the built-in utility ‘blockMesh’, it is possible to generate structured meshes. But the import of meshes created with other CFD programs is possible as well. Next to the generation of meshes, boundary conditions have to be defined, depending on the chosen solver. Dirichlet and Neumann boundary conditions or variations combining both types can be applied. A fast convergence can be reached with the help of good initial conditions.

The partial differential equations which describe the flow and transport processes need to be transformed to algebraic equations. This is done by integrating them over a certain time step and control volume. The spatial and temporal discretization schemes as well as the interpolation schemes have to be defined by the user (Schulze & Thorenz, 2014). This can be done by defining a default parameter for all terms or by defining a parameter for every single term in the solution procedure. Moreover, the procedure to solve the equations and the tolerances for the exact solution for each term have to be indicated by the user.

In the next sections, the equations and models applied in this thesis are presented. Due to the high computational effort of the high-resolution simulations presented in this thesis, most calculations were executed on supercomputers of the Norddeutscher Verbund für Hoch- und Höchstleistungsrechnen (hlrn) in Berlin and on high performance computing (HPC) clusters of the Technische Universität Berlin.

1.4.1 Modelling free flow

OpenFOAM offers a number of different solvers for multiphase flow. For this thesis the interFoam solver is chosen as a basis. InterFoam solves the three-dimensional Navier-Stokes equations for two incompressible, immiscible fluids (water and air). A two-phase model can be necessary to depict water level fluctuations which influence the pressure distribution in the domain. The Volume of Fluid (VOF) method is used for locating an interface in a control volume and introducing volume fractions of each fluid. Thus, a fluid is defined with changing fluid properties according to the volume fraction of each fluid.

The conservation of mass (Equation 1.1) and momentum (Equation 1.2) can be written as:

$$\nabla \cdot \vec{U} = 0 \tag{1.1}$$

with $\vec{U}$ for the velocity field (m/s)

$$\frac{\partial(\rho\overrightarrow{U})}{\partial t} + \vec{U} \cdot \nabla(\rho\,\vec{U}) = -\nabla p + (\mu_{phys} + \mu_{turb})\Delta\vec{U} + \rho f_b \tag{1.2}$$

ρ is the density (kg/m³); t is the time (s); p is the pressure (Pa); μ_{phys} and μ_{turb} are the physical and turbulent viscosity (Ns/m^2), where μ_{turb} is calculated by a turbulence model and f_b are body forces per unit mass (m/s²).

InterFoam uses a modified pressure term definition, which is called p_{rgh} and is defined as:

$$p_{rgh} = p - \rho g x \tag{1.3}$$

With g as acceleration vector due to gravity (m/s^2) and x as a spatial position vector (m).

For the four variables of the flow field, which are the pressure and the velocity in three directions, a solution procedure is needed. Since the velocity can be calculated with the Navier–Stokes equations, but the mass conservation equation is not capable to solve for the pressure, a pressure linking equation is implemented. The interFoam solver uses the PIMPLE algorithm which is based on the PISO (Pressure Implicit with Splitting of Operators) and on the SIMPLE (Semi-Implicit Method for Pressure Linked Equations) algorithm (Caretto et al., 1973; Greenshields, 2010; Issa, 1986).

Due to the VOF method, the density and the viscosity have to be weighted according to their fractions with the help of the volume fraction parameter α (-), which is strictly bounded between

0 and 1. In this thesis, we consider 0 for the air phase and 1 for the water phase, while values between 0 and 1 are in a transitional region. The density and viscosity are calculated as follows:

$$\mu = \mu_{water}\alpha + \mu_{air}(1-\alpha) \quad 1.4$$

$$\rho = \rho_{water}\alpha + \rho_{air}(1-\alpha) \quad 1.5$$

The water-air interface is described by the following convective transport equation:

$$\frac{\partial \alpha}{\partial t} + \nabla \cdot (\alpha \vec{U}) = 0 \quad 1.6$$

1.4.2 Turbulence models

Turbulence is characterized by movements on different spatial and temporal scales. Thereby eddies of different sizes can be formed, which also interact with each other. Moreover, turbulence is irregular and chaotic, which leads to a sensitivity of initial and boundary conditions. For transport simulations, the effect of mixing or diffusion caused by turbulent fluctuations has to be considered.

At low Reynolds numbers, the viscous forces dominate, which means that disturbances underlying a laminar flow have no influence, or turbulent structures are dampened immediately. At high Reynolds numbers the inertial forces dominate and lead to turbulence. For pipe and open-channel flow the critical Reynolds number, in which a laminar flow becomes turbulent, is about 2300. Further descriptions of turbulent flows can be found, for example in Lesieur (2007) and Hinze (1959).

Since the focus of this thesis lies on high-resolution results, a sophisticated turbulence model is required for the simulations. OpenFOAM offers a wide number of turbulence models. The most important methods for the numerical simulation of turbulent flows are the Reynolds-Averaged Navier-Stokes (RANS), the Large Eddy Simulation (LES) and the Direct Numerical Simulation (DNS). For the DNS the Navier-Stokes equations are fully resolved, whereby even the smallest turbulences are considered. The results show the highest accuracy but extremely high computational effort is needed (Maric et al., 2014). With the LES turbulence model the large-scale eddies are resolved, while the small-scale eddies are taken into account with a subgrid scale model. The computational effort is still very high, but the grid resolution is not as fine as for DNS. With the RANS turbulence model, no scales of turbulence are directly resolved but they are partially modeled. A wide range of turbulence models are available for RANS. In terms of computational effort, this is the fastest turbulence model of the three described methods.

However, with this model fluctuations in the flow velocity - which can be important for some applications - cannot be captured that good. For RANS, the turbulent flow is divided into an average velocity and a fluctuating velocity and leads to a Reynolds stress tensor in the Navier-Stokes equations (RANS) which is often computed with the help of two-equation models. Thereby, two extra transport equations represent the turbulent flow properties. Commonly, the transported variables are either k for turbulent kinetic energy and ε for the turbulent dissipation within the k-ε turbulence model or k and ω (specific dissipation) within the k-ω turbulence model or the k-ω Shear Stress Transport (SST) model. The k-ω SST model combines the advantages of the k-ε formulation with the advantages of the k-ω formulation as it uses uses the k-ε model for the free-stream and the k-ω model in the inner parts of the boundary layer.
In this thesis the LES and the RANS turbulence models are applied.

1.4.3 Transport modelling in free-flow

To investigate the movement of a tracer, transport processes have to be taken into account, which can be separated into conservative and reactive transport. In this thesis only conservative transport is studied. For conservative transport advection, diffusion and a combination of both have to be considered (see Figure 1-5).

Advection is the movement of a particle with the flowing fluid without any spreading. For the diffusion, molecular and turbulent diffusion have to be distinguished. Molecular diffusion is a physical exchange process which is based on the disordered movement of molecules by temperature-induced impact, known as Brown's molecular movement. It represents a movement mechanism that is independent of water movements. The diffusivity depends on the transport medium, on the substance itself and is also temperature dependent. For turbulent flow, the turbulent diffusion is significantly higher than the molecular diffusion and depends on flow velocity variations in space and time. It can be considered by employing the turbulent Schmidt number. A comprehensive review about the turbulent Schmidt number can be found in Gualtieri et al. (2017).

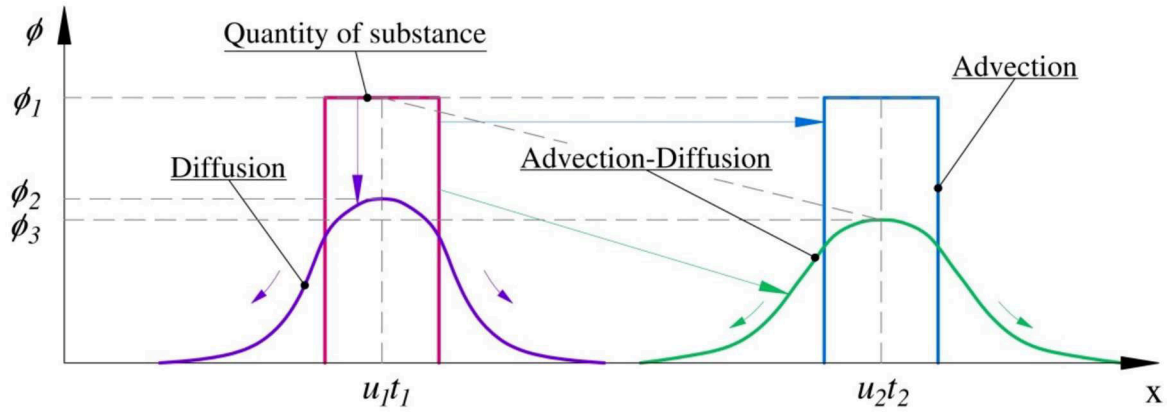

Figure 1-5: Transport processes after Badarch (2017).

The interFoam solver did not account for transport processes. Therefore, an advection-diffusion equation to describe the transport of a passive tracer with a concentration C (kg/m³) was implemented into the solver within this thesis:

$$\frac{\partial C}{\partial t}+\nabla\cdot(C\vec{U})+\nabla\cdot((D_{phys}+D_{turb})\nabla C)=0 \qquad 1.7$$

The diffusion is divided into D_{phys} (m²/s) for the physical diffusivity and D_{turb} (m²/s) for the turbulent diffusivity. The turbulent diffusivity is related to the turbulent viscosity by the turbulent Schmidt number:

$$Sc_t=\frac{\mu_{turb}/\rho}{D_{turb}} \qquad 1.8$$

The turbulent Schmidt number Sc_t (-) as well as the physical diffusivity have to be defined by the user.

1.4.4 Flow modelling for groundwater-surface water interactions

The equations of the interFoam solver were extended by Oxtoby et al. (2013) for the application in porous media for flow processes. For the developed solver, called porousInter, the solid fraction of the porous media is taken into account through the consideration of porosity and an additional drag term. All values which are represented by $[\ ]^f$ are averaged only over the void region filled with the fluids. The conservation of mass and momentum for the porousInter solver are defined after Oxtoby et al. (2013) as:

Mass conservation equation

$$\varphi\nabla\cdot\left[\vec{U}\right]^{f}=0 \qquad 1.9$$

Momentum conservation equation

$$\varphi\left(\frac{\partial([\rho]^{f}\left[\vec{U}\right]^{f})}{\partial t}+\left[\vec{U}\right]^{f}\cdot\nabla([\rho]^{f}\left[\vec{U}\right]^{f})\right)=-\varphi\nabla[p]^{f}+\varphi[\mu]^{f}\nabla^{2}\left[\vec{U}\right]^{f}+\varphi[\rho]^{f}\vec{g}+D \qquad 1.10$$

with φ for the soil porosity (-) and D for an additional drag term (kg/(m^{2}s^2)). The drag term accounts for momentum loss by fluid friction with the porous medium after Ergun (1952) and flow recirculation in the sediment within an effective added mass coefficient that is included after van Gent (1995). The porous drag term is described as:

$$D=-\left(150\frac{1-\varphi}{d_p\varphi}[\mu]^{f}+1.75[\rho]^{f}\left[\vec{U}\right]^{f}\right)\frac{1-\varphi}{d_p}\left[\vec{U}\right]^{f}-0.34\frac{1-\varphi}{\varphi}\frac{[\rho]^{f}\partial\left[\vec{U}\right]^{f}}{\partial t} \qquad 1.11$$

with d_p (m) as effective grain size diameter.

The water-air interface of the porousInter solver is captured by:

$$\varphi\frac{\partial[\alpha]^{f}}{\partial t}+\varphi\nabla\cdot([\alpha]^{f}\left[\vec{U}\right]^{f})=0 \qquad 1.12$$

Hitherto, the porousInter solver was mainly applied for coarse sediments, since the computational effort is extremely high for sediments with small grain sizes.

1.4.5 Tracer transport modelling for groundwater-surface water interactions

Next to advection and diffusion, dispersion is an important transport phenomenon in groundwater. Dispersion is the mixing of dissolved substances in the moving water of the subsurface, which is caused e.g. by different pore sizes, non-uniform velocity profiles within a pore or by distracting the flow through the grain structure (see Figure 1-6). The dispersion plays an important role and depends on the flow velocity as well as on the longitudinal and transverse dispersivities (Bear, 1972; Freeze & Cherry, 1979). In surface water, there is turbulent diffusivity (see section 1.4.3). Since the turbulent structures are comparable small in groundwater when compared to the surface water, turbulent diffusivity is of less importance within the subsurface. Generally, the flow in groundwater is laminar and the application of the Darcy law is possible when Reynolds numbers do not exceed a value between 1 and 10 (following Bear (1972)). In the interaction space of groundwater and surface water turbulent

diffusivity may play a certain role also in the groundwater depending e.g. on the Reynolds number.

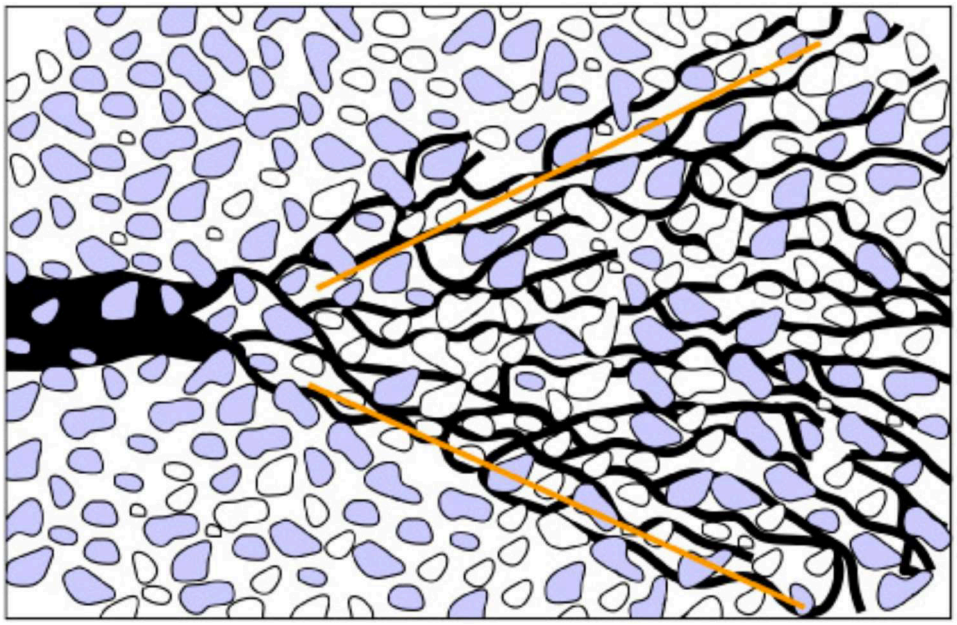

Figure 1-6: Hydrodynamic dispersion after Freeze and Cherry (1979).

For the integral solver an advection-diffusion equation for conservative transport is implemented within this thesis. The transport equation is defined as:

$$\frac{\partial C}{\partial t} + \nabla \cdot (C\vec{U}) + \nabla \cdot (D_{coeff} \nabla C) = 0 \qquad 1.13$$

with D_{coeff} as diffusion coefficient (m^2/s).

1.5 Scope of this thesis

In this thesis a novel integral modelling approach was developed for the correct description of high-resolution flow and transport processes occurring at the interface of groundwater and surface water. In contrast to the widely applied coupled approaches, the same conceptual approach is used for surface and for groundwater using the CFD code OpenFOAM. The three-dimensional two-phase solvers interFoam (implemented in OpenFOAM) and porousInter by Oxtoby et al. (2013) are applied and extended for conservative tracer transport. In a first step, a validation for the correct description of the hydrodynamics at rippled streambeds by the interFoam solver is performed and an additional transport equation is implemented and validated. The free surface modelling approach is applied to rippled streambeds. In a further step, the correct description of the porousInter solver for groundwater-surface water interactions is examined and again applied to rippled streambeds. Compared to the first approach, not only

surface flow, but also subsurface flow is considered. In a last step the porousInter solver is extended for transport investigations. The tracer spreading at rippled streambeds with ambient groundwater flow is investigated.

The thesis is structured in seven sections consisting of the current introduction, three peer-reviewed journal articles (two accepted, one submitted), one peer-reviewed conference contribution, one book chapter, further supplementary contributions and a synthesis.

In **section 2** several connections of this thesis to other projects within the Research Training Group 'Urban Water Interfaces' (UWI) and at the Chair of Water Resources Management and Modeling of Hydrosystems of the Technische University Berlin will be outlined. The first part focuses on groundwater-surface water interactions from different perspectives within UWI. Research activities investigating the hyporheic zone as well as on bank filtration will be presented considering flow processes, ecosystem functioning and chemical turnover rates. Furthermore, the cooperation within the chair concerning multiphase modelling using OpenFOAM with a focus on the interfaces of groundwater-surface water, water-air and fluid-structure are briefly introduced.

Section 3 describes high-resolution free surface flow and tracer retention at rippled streambeds with different ripple heights, lengths and distances between the ripples including different surface hydraulic conditions. The two-phase flow solver interFoam is extended by the implementation of an advection-diffusion equation for the examination of a tracer pulse injected into surface water and its retention between the ripples. The validation is carried out with analytical solutions and data of two experiments.

In **section 4** the same ripple geometries and surface hydraulics are considered as in **section 3**, but the sediment is included at the bottom with two different grain sizes. The solver uses an extended version of the three-dimensional Navier–Stokes equations which is also applicable in non-Darcy-flow layers. The integral solver porousInter is first validated based on two applications for groundwater-surface water interactions. The influence of ripple geometries, surface hydraulics and grain sizes on flow processes within the hyporheic zone is determined with high-resolution. This includes in- and outflowing exchange flux rates.

While in **section 4** the focus lies on the investigation of flow processes, in **section 5** tracer transport processes were studied under neutral, losing and gaining flow conditions at a rippled

sandy streambed. For this purpose, the porousInter-solver is extended by an advection-diffusion equation. The high-resolution transport simulations are compared to previous observations at a flume. Consequently, this study serves on the one hand as a further validation of the applied and extended solver and on the other hand high-resolution information about prevailing flow processes during the experiment can be presented.

An overview of the supplementary scientific work is presented in **section 6.** This section includes a brief introduction of three co-authored journal articles concerning flow, transport and mass transfer modelling in sewers and the relevance of the hyporheic zone.

Section 7 synthesizes the outcomes of the thesis. Moreover, limitations of the applied and extended modelling approach are discussed and an outlook on future research is presented.

2. Research embedded in larger context

2.1 Research on groundwater-surface water interfaces within the DFG Research Training Group 'Urban Water Interfaces'

This study was published as:

Broecker, T., Schaper, J., El-Athman, F., Gillefalk, M., Hilt, S. & Hinkelmann, R. (2017). Surface water - groundwater interactions. Proceedings of the 37th IAHR (International Association for Hydro-Environment Engineering and Research) World Congress, Kuala Lumpur, Malaysia.

This is the postprint version of the article.

The test cases' setups are listed in Appendix B (B1 Seepage through a homogeneous dam with an impervious foundation compared with analytical solutions after Casagrande and Kozeny, B2 Seepage through a homogeneous, rectangular dam with an impervious foundation).

2.1.1 Abstract

Almost all types of surface water are interrelated with the groundwater. Therefore, the knowledge of interactions between ground- and surface water is very important for understanding processes within the whole water cycle. This paper presents surface water-groundwater interactions from different perspectives and with various emphases including investigations of flow processes, the impact on the ecosystem functioning, the local biota and chemical turnover rates. The application and extension of an integral single-domain model for flow and transport processes in the groundwater - surface water interaction space is the objective of one research project. Most numerical investigations consider ground- and surface water as separate environmental compartments or couple the corresponding models. For the integral model concept, the three-dimensional Navier-Stokes equations are extended by the consideration of porosities using the open source CFD software OpenFOAM. In a further project the retention of chemical compounds in hyporheic reactors of urban freshwater systems is examined. Biogeochemical factors that affect retention and dynamics of micropollutants as a function of flow characteristics in hyporheic zones are determined with the help of laboratory

experiments and field approaches. A simple one-dimensional transport and reaction model will be extended for the quantitative prediction of trace compounds such as organic micropollutant dynamics in sediments. Furthermore, various effects of bank filtration are investigated in two projects. Passing the soil layers, different purification processes and chemical reactions are taking place resulting in a modified water quality and changed properties. The reductive metabolism of iodinated X-ray contrast media as important organic pollutants in urban surface water as well as changes in groundwater seepage including effects on lake ecosystems are examined. This contribution gives an overview on different research activities with special emphasis on the integral model concept for the surface water-groundwater interaction space.

2.1.2 Introduction

The Urban Water Interfaces Research Training Group (UWI), funded by the German Research Foundation, aims to achieve a broad process understanding in urban water systems, focusing on various natural and technical interfaces (Gessner et al., 2014). Engineers as well as natural scientists collaborate closely in different interdisciplinary topics. Surface water – groundwater interactions is one of these so-called common topics. Within this group, interactions between groundwater and surface water from lakes as well as from lotic systems are considered. These interfaces are characterized by diverse microbial communities and highly active biota leading to steep biogeochemical gradients (Birgand et al., 2007; Greskowiak et al., 2006). The temporal and spatial variability of surface water and groundwater exchange driven by steep hydrodynamic gradients and biogeochemical cycling are considered by experimental measurements as well as by modelling these processes. The very complex exchange processes require interdisciplinary approaches, exchanging knowledge, expertise and technology from different backgrounds. Within this group engineers as well as natural scientists collaborate for an advanced understanding of surface water-groundwater interactions with emphases on different researches. Figure 2-1 shows an overview of the four research topics, which are focused on the hyporheic zone as well as on bank filtration.

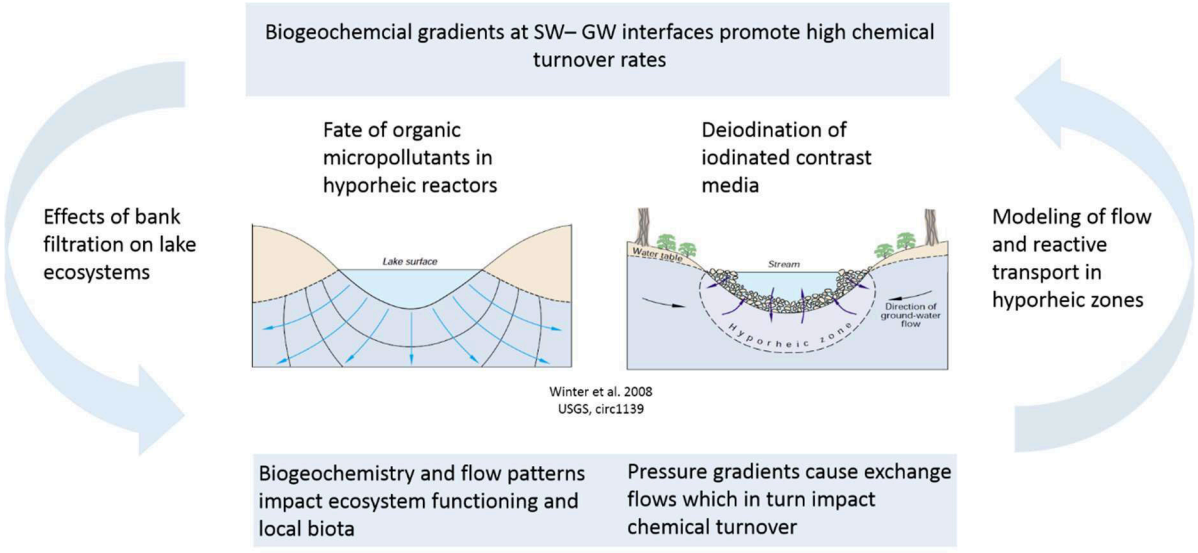

Figure 2-1: Research topics of UWI for surface water-groundwater interactions.

2.1.2.1 Hyporheic zone

The hyporheic zone is the transition zone between saturated river sediments and groundwater (Boano et al., 2014). This zone is considered to constitute a major sink for trace organic compounds from wastewater treatment plant in lotic systems and thus plays a pivotal role in urban water cycles, with regards to both, ecosystem functioning as well as drinking water protection (Hester & Gooseff, 2010; Lewandowski et al., 2011b; Z. Li et al., 2016). The stability of trace organic compounds in saturated sediments is generally thought to be dependent on biogeochemical conditions like the redox potential (e.g., Heberer et al. (2008)), availability of labile organic carbon or the distribution of reactive surfaces (Borch et al., 2010). The biogeochemical processes are significantly controlled by the fluxes, the flow paths and the residence time within the hyporheic zone, which can be calculated with the help of different model types. For the quantitative prediction of trace compounds a simple, one-dimensional model is sufficient. Spatially explicit results investigating hyporheic exchange processes can be achieved with numerical models and were applied on different scales. However, most numerical investigations consider groundwater and surface water as separate environmental compartments or couple a groundwater and a surface water model. The objective of one UWI research is to apply and extend an integral model in the groundwater-surface water interaction space for investigating flow and transport processes. The modelling results can be used for another UWI research, investigating the retention of chemical compounds in hyporheic reactors of urban freshwater systems. A quantitative as well as qualitative understanding of the behavior of many trace organic compounds as a function of the interactive effects of both transport characteristics and biogeochemical conditions, commonly encountered in hyporheic zones, is still lacking.

Likewise, chemical mechanisms that govern the numerous transformation and translocation processes of trace organic compounds in the subsurface are unclear. The lack of mechanistic understanding also results in a lack of predictive tools. Hitherto comprehensive models describing the dynamics of trace organic compounds in hyporheic zones as a function of both biogeochemical and hydrological conditions have not been developed. The primary goals of one research are thus to (i) further our conceptual understanding of the factors that control the overall efficiency of hyporheic zones with respect to trace organic compounds removal and ii) to determine first order attenuation rates for a variety of trace organic compounds under different environmental conditions.

2.1.2.2 Bank filtration

Two further research topics within this group are focused on bank filtration, which is one of the oldest techniques used for drinking water production and purification. Close to the bank of a river or lake, the groundwater level is lowered by water abstraction causing an infiltration of the surface water through the bank. Although bank filtration has been used for more than 100 years, especially purification efficiency and infiltration capacities were investigated so far, whereas significant knowledge gaps concerning the effects on the ecosystem of rivers and lakes still exist. Based on the present knowledge, various hypotheses are tested in order to examine whether bank filtration affects macrophytes in lakes and lake water quality in one research project.

Besides physical effects like filtration and sorption, microbiological degradation occurs for flow times of several weeks or months. Pathogens, but also different organic micropollutants can be partially removed or transformed by these processes. The degradability of many substances is dependent on the prevailing redox conditions which are changing along the flow length. In the first section, molecular oxygen is still available and allows for aerobic respiration. This section is followed by anoxic and anaerobic conditions with nitrate, manganese, iron and sulphate reduction (Baumgarten, 2013; Jekel & Czekalla, 2016).

Iodinated X-ray contrast media are found at much higher concentrations than any other pharmaceutical compound in wastewater and surface water (Ebert et al., 2014). Under aerobic conditions, an almost complete transformation of the contrast medium Iopromide has been observed, however, without any deiodination of the molecule (removal of iodine) (Wiese et al., 2011). A release of iodide has been found under anoxic/anaerobic conditions (Stieber et al., 2008). The deiodination is assessed by the decrease of the sum parameter adsorbable organic

bound iodine (AOI) which measures unchanged or partially deiodinated molecules as well as molecules with only altered side chains.

One research project of UWI concentrates on the deiodination of ICM in bank filtration of urban waters to achieve a better understanding of the already observed deiodination and to contribute to the further understanding of the decrease of anthropogenic trace substances in the aquatic environment. While the AOI decrease of contaminated water at the production side, e.g., by nanofiltration (Drews et al., 2003) or ozonation (Putschew et al., 2007) has been studied extensively, the deiodination in natural environments is still widely unknown.

2.1.3 Integral modelling approach for flow and transport in groundwater-surface water interaction space

One research project that is presented more detailed, applies and extends an integral modelling approach for the hyporheic zone. The concept behind as well as first results are presented in the following sections.

2.1.3.1 Governing equations and numerical model

The three-dimensional Navier-Stokes equations are extended by the consideration of the porosity φ and an additional drag term D. For all calculations, the free, open source computational fluid dynamics (CFD) software 'OpenFOAM' (Open Field Operation and Manipulation) is applied. The two-phase flow solver 'interFoam', which is usually applied for surface water simulations, serves as starting point for the integral solver and solves the three-dimensional Navier-Stokes equations. Values, that are represented by $[\ ]^f$ are averaged only over the void region, which means that the solid fraction is not considered. For the integral solver, the equations are defined after Oxtoby et al. (2013):

Mass conservation equation

$$\varphi \nabla \cdot \left[\vec{U}\right]^f = 0 \qquad 2.1$$

Momentum conservation equation

$$\varphi\left(\frac{\partial [\rho]^f \left[\vec{U}\right]^f}{\partial t} + \left[\vec{U}\right]^f \cdot \nabla([\rho]^f \left[\vec{U}\right]^f)\right) = -\varphi \nabla [p]^f + \varphi [\mu]^f \nabla^2 \left[\vec{U}\right]^f + \varphi [\rho]^f \vec{g} + D \qquad 2.2$$

with the following parameters

$$\mu = \alpha\mu_w + \mu_a(1-\alpha) \quad 2.3$$

$$\rho = \alpha\rho_w + \rho_a(1-\alpha) \quad 2.4$$

and the porous drag term D

$$D = -\left(150\frac{1-\varphi}{d_p\varphi}[\mu]^f + 1.75[\rho]^f\left[\vec{U}\right]^f\right)\frac{1-\varphi}{d_p}\left[\vec{U}\right]^f - 0.34\frac{1-\varphi}{\varphi}\frac{[\rho]^f\partial\left[\vec{U}\right]^f}{\partial t} \quad 2.5$$

For the drag term pressure loss, due to the friction of fluid with the porous medium (Ergun, 1952), is considered through the first term. The second term acts to increase the effective mass of the fluid due to flow recirculation caused by porous medium with an effective added mass coefficient after van Gent (1995).

Volume of Fluid equation

$$\varphi\frac{\partial[\alpha]^f}{\partial t} + \varphi\nabla\cdot([\alpha]^f\left[\vec{U}\right]^f) = 0 \quad 2.6$$

U is the velocity, t is time, ρ is the density with the subscripts a and w for air and water, α is a volume fraction which varies between 0 (for air) and 1 (for water), p is pressure, μ is the dynamic viscosity with the subscripts *a* and *w* as for the density and *turb* for turbulent and g is the gravitational acceleration.

First of all, an advection-diffusion equation was implemented into the interFoam solver (see Equation 2.7) to examine the transport of a passive tracer with a concentration C. The user can define the physical diffusivity D_{phys} as well as the turbulent Schmidt number Sc_{turb}, which defines the turbulent diffusivity coefficient D_{turb} (Equation 2.8).

Transport equation

$$\frac{\partial C}{\partial t} + \nabla\cdot(C\vec{U}) + \nabla\cdot(D_{phys} + D_{turb})\nabla C = 0 \quad 2.7$$

$$D_{turb} = \frac{\mu_{turb}/\rho}{Sc_t} \quad 2.8$$

2.1.3.2 Validation and results

First simulations relating to this research consider the upper boundary of the hyporheic zone focusing on flow and transport processes around varying ripple morphologies and flow

conditions using the interFoam solver with the implemented transport equation. The pressure distribution, related to the exact flow paths as well as the pressure gradient that is connected to the volumetric exchange flux in the hyporheic zone were significantly affected by the ripple geometries and the present flow rates. Moreover, the simulations showed the relevance of transport processes in surface waters for the spreading and retention of substances at the interface, probably influencing biogeochemical reactions within the hyporheic zone. The results of this research were submitted to 'Limnologica, Ecology and Management of Inland Waters' (see Broecker et al. (2018)). More information can be achieved by adding the sediment at the lower boundary with the help of the integral solver.

For the integral simulations, an algorithm by Oxtoby et al. (2013) simulating two-fluid flows in porous media with arbitrary heterogeneous porosity fields is tested. In a further step, a tracer transport equation will be implemented to this solver.

As first test, the seepage through a homogeneous earth dam with a height of 22 m and a constant water level of 17 m on the right side of the dam was simulated until steady state was achieved. The foundation is impermeable. The dam has a porosity of 0.25 and a median grain size radius of 1.59 cm which corresponds to a gravel material. Consequently, the influence of the drag term is relatively small. After 100 s steady state was achieved. The simulated water table is compared with an analytical solution by Kozeny (see Lattermann (2010)) and an improvement of this solution by Casagrande (1937). Close agreement is obtained between the numerical and the analytical results (see Figure 2-2). At the entrance of the water into the dam and at the outlet, a very good agreement can be observed between the numerical simulation and the solution after Casagrande (1937). Inside the dam, the water table is slightly higher in the numerical simulation.

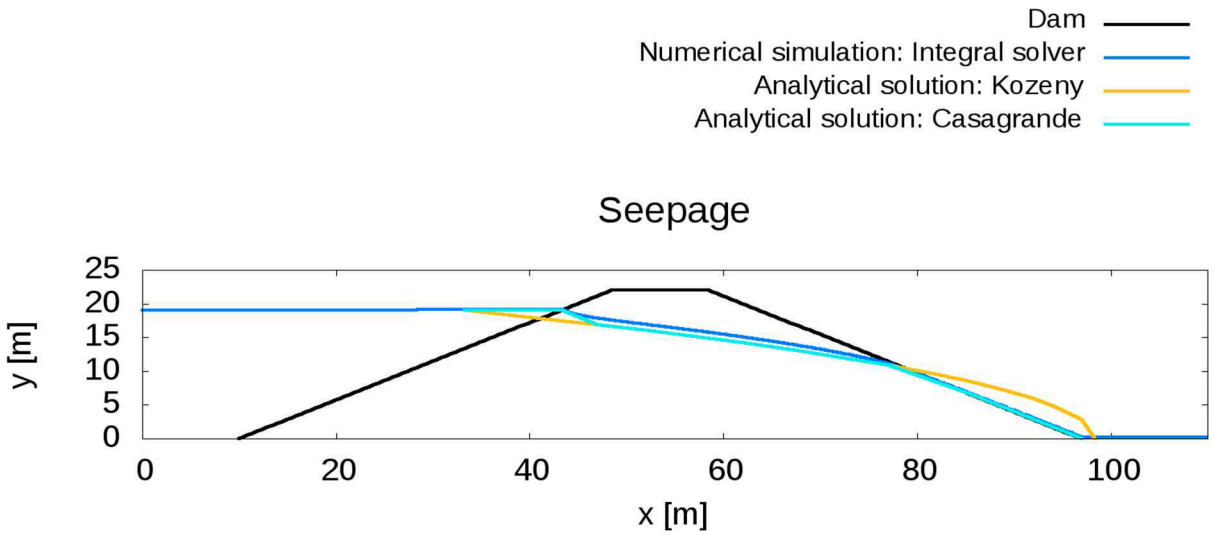

Figure 2-2: Comparison of seepages through a homogeneous dam with an impervious foundation for a numerical simulation using the integral solver and two analytical solutions.

For a second test case, a rectangular dam (again with an impermeable foundation) is considered with the same soil properties as for the previous simulation. The dam has a height of 24 m and a width of 16 m. For this test case, the seepage calculated with the integral solver is compared with: an analytical one-dimensional solution (after Kobus and Keim (2001)), an analytical two-dimensional solution (after Di Nucci (2015)) and two further numerical solutions (Aitchison & Coulson, 1972; Westbrook, 1985). Figure 2-3 (left) shows the seepages for each approach. The lowest seepage is calculated for the analytical one-dimensional solution. With a look at the velocity vectors inside the dam calculated with the integral solver (Figure 2-3, right) it is obvious, that a one-dimensional solution is not sufficient for this case. In contrast to the analytical one-dimensional solution, the analytical two-dimensional solution shows very similar results compared to the seepage calculated with the integral solver. The numerical solutions by Westbrook (1985) and Aitchison and Coulson (1972) show slightly lower seepages, but are still in a similar range.

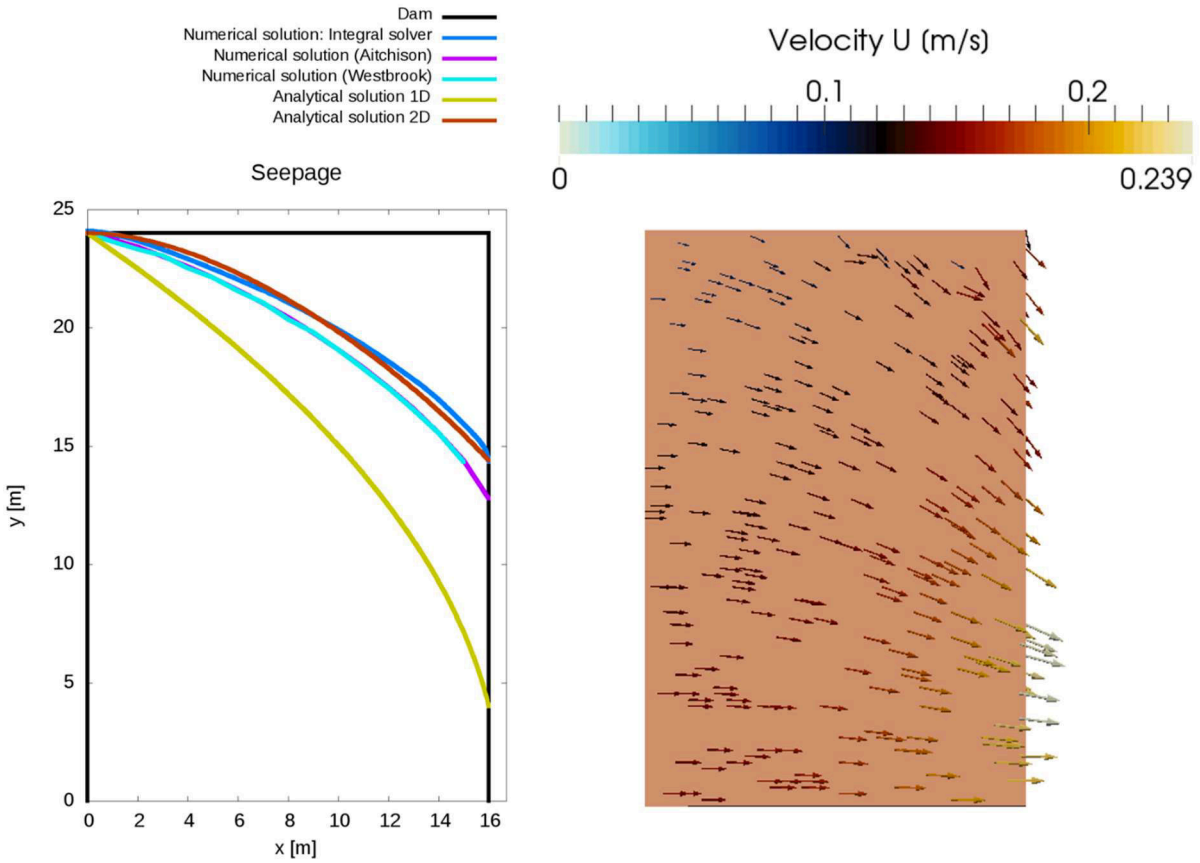

Figure 2-3: Comparison of seepages through a homogeneous, rectangular dam for three numerical and two analytical solutions (left) as well as velocity vectors inside the dam for the integral solver (right).

The integral solver is further examined concerning the applied drag term using the test case with the rectangular dam. In a first test, the drag term is completely deleted. Inside the dam the water level decreases and at the left side of the drag, disproportionately high turbulences can be observed even after 300 s simulation time due to the absence of a drag.

The test cases showed, that the integral solver shows good results for groundwater-surface water interactions as long as the median grain size diameter of the soil is not too small. In a next step, smaller grain sizes will be applied and an advection-diffusion equation for the investigation of a passive tracer will be implemented. The model will be validated with the help of a flume experiment by Fox et al. (2014). After a successful validation, the presented study for varying ripple morphologies and flow conditions can be examined again considering surface water and groundwater at the same time in one model. Moreover, field measurements from partners within this group will be used for further simulations. In this context, modelled flow paths and residence times can be used to explain the retention of chemical compounds within the

hyporheic zone for a further research project working on groundwater-surface water interactions (see section 2.1.4).

2.1.4 Retention of chemical compounds in hyporheic reactors of urban freshwater systems

Next to flow and transport dynamics within the hyporheic zone, biogeochemical aspects are investigated in a further project. In this project it is hypothesized that the overall behaviour of trace organic compounds in river sediments and the overall effectiveness of the hyporheic zone in removing trace organic compounds is to a large extent controlled by transport limitations. Hydraulic conditions in hyporheic zones do not only influence the availability of terminal electron acceptors and electron donors and the spatial distribution of reactive surfaces. They also determine flow velocities and flow path lengths and hence reaction times and bioavailability on the pore scale. We further hypothesize, that under similar flow characteristics, differences in attenuation rates between various trace organic compounds will reflect their relative stability under different biogeochemical conditions and hence may provide mechanistic insights into their attenuation processes.

In order to derive relevant and transferable results experiments were predominantly conducted in situ, in wastewater treatment plant influenced lotic systems. Hydrological methods such as temperature depth profiles (Anderson, 2005; Gordon et al., 2012), heat pulse sensors (Lewandowski et al., 2011a) and seepage meters (Solder et al., 2016) were used to characterize hyporheic flow with respect to both direction and magnitude. A novel approach to determine flow velocities and hydrodynamic dispersion coefficients employing time series of pore water electrical conductivity is currently developed and tested in the field. In conjunction with flow measurements, samples of interstitial water are taken using both active and passive pore water sampling techniques. Porewater peepers, for instance, were deployed to obtain time integrated concentration profiles of trace organic compounds and various biogeochemical parameters in the hyporheic zone of a wastewater treatment plant effluent urban river in Berlin, Germany. At the same site, a novel Mini Point Sampler was successfully used to obtain porewater time series over the course of 32 h. A 1D - transport and reaction model was subsequently used to calculate first order attenuation rate constants from the measured concentration profiles and flow characteristics. The findings of this project will be compared with those of the integral solver explained in section 2.1.3.

Preliminary results show that, under losing conditions, the hyporheic zone of an urban lowland river can indeed be considered a sink for wastewater treatment plant derived trace organic

compounds. The overall magnitude of calculated first order attenuation rate constants reflects the general compound susceptibilities to biodegradation and sorption. The influence of biogeochemical conditions on trace organic compounds stability in the hyporheic zone was found to be compound specific. For most trace organic compounds studied, biogeochemical conditions such as the redox potential and the availability of respective reactive surfaces only had a minor influence on attenuation rates. These results indicate that, at the field site investigated, the effectiveness of the hyporheic zone is primarily controlled by hyporheic exchange and transport characteristics rather than by biogeochemical parameters.

While the majority of field experiments so far have been conducted in urban lowland rivers in central Europe, current efforts targets montane streams under more arid conditions. Using similar methods over climatic, geomorphological and geological gradients will not only broaden our mechanistic understanding of trace organic compound dynamics in hyporheic zones. It will also improve our predictive capabilities and offer river management and engineering guidelines, which in turn will be useful to meet the water quality challenges of urban areas.

2.1.5 Deiodination of iodinated contrast media during bank filtration

While the first two presented projects dealt with the interface of groundwater and lotic systems, the following project is related to the interface between groundwater and lakes with the focus on degradation processes of iodinated contrast media.

2.1.5.1 Biological deiodination

For environmentally relevant chlorinated and brominated substances, a reductive dehalogenation by corrinoid containing enzymes of dehalorespiring microorganisms has been shown in various studies. As part of this UWI project, genus *Dehalococcoides mccartyi* strain CBDB1 was cultivated in culture bottles under anaerobic conditions with the iodinated substances Iopromide, Diatrizoate as well as 2,3,5- and 2,4,6-Triiodobenzoic acid (TIBA) as electron acceptors. In addition to the iodinated compounds, positive controls additionally included hexachlorobenzene which can be completely dechlorinated by strain CBDB1. A CBDB1 culture previously cultivated with hexachlorobenzene was used as inoculum and titanium(III)citrate was added for reducing conditions. During a period of several weeks, the concentrations of the added iodinated compounds, iodide and the sum parameter AOI as well as the cell density were measured. In additional tests, the enzyme activity of CBDB1 with iodinated substances was photometrically determined by the extinction decrease of methyl

viologen which served as artificial electron donor and redox indicator changing color from blue in its reduced state to colorless in its oxidized state.

The degradation tests in culture bottles showed a deiodination of Iopromide of up to 95% but no cell growth in the absence of the additional electron acceptor hexachlorobenzene. Abiotic controls without microorganisms showed a similar deiodination degree, implying that the deiodination is not traced to microbiological activity. The activity tests with different iodinated substances in the presence of CBDB1 cells indicated a high electron transfer resulting in a deiodination (correlation was proven in preliminary tests). The specific activity is defined here as the amount of product (iodide) formed per second and protein mass and was calculated from the initial extinction decrease of the assays (Table 2-1). Control assays with heat-inactivated enzymes (5 min at 100°C) did not show any activity.

Table 2-1: Enzyme activity and specific enzyme activity for Dehalococcoides mccartyi strain CBDB1 with different iodinated substances (300 µM).

Compound	**activity (pmol iodide / s)**	**spec. activity (nmol iodide / (mg protein × s))**
Iopromide	0.20	0.50
Diatrizoate	0.20	0.50
2,3,5- TIBA	2.45	6.02
2,4,6-TIBA	1.84	4.51
Iopromide	0.20	0.50

2.1.5.2 Abiotic deiodination in the presence of corrinoids

Abiotic activity tests were conducted with commercially available corrinoids cyanocobalamin (synthetic form of vitamin B_{12}) and dicyanocobinamide. For dicyanocobinamide, the photometric measurement showed a significant extinction decrease for all three tested iodinated substances (Figure 2-4a). A decrease of the extinction was also shown in the presence of cyanocobalamin with Iopromide and 2,3,5-TIBA but not with 2,4,6-TIBA (Figure 2-4b).

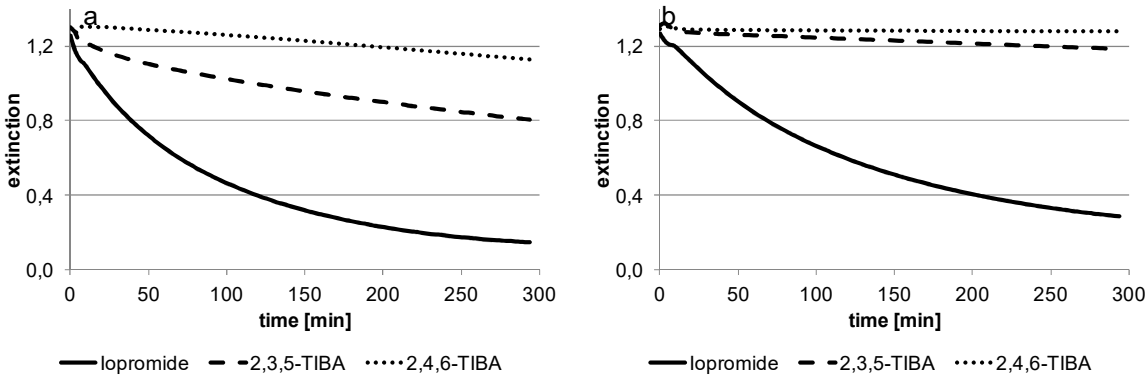

Figure 2-4: Extinction decrease (578 nm) by oxidation of reduced methyl viologen in the presence of 100 µM Iopromide, 2,3,5- or 2,4,6-TIBA and dicyanocobinamide (a) respectively cyanocobalamin (b). Blank values (extinction decrease in the absence of corrinoids) are subtracted from the graphs.

In contrast to the biotic enzyme tests, the catalytic activity of the tested corrinoids is much higher for Iopromide than for the two Triiodobenzoic acids. The results found here will be discussed with those explained in section 2.1.6.

2.1.6 Bank filtration: potential effects on surface water quality

There are many studies made on bank filtration, but almost all of them focus on water abstraction capacity and/or purification efficiency (e.g. Hoffmann and Gunkel (2011); Othman et al. (2015); Romero et al. (2014)). However, there might also be effects of bank filtration on surface water quality and one of the research projects within UWI focuses on this question. This new research field is being opened using mainly three different approaches: 1) Critical literature review of potential effects, 2) Modelling of shallow lakes using the ecosystem model PCLake and 3) Field investigations and laboratory work.

2.1.6.1 Review of potential effects

Bank filtration may affect physical, chemical and biological parameters and processes and these might in turn affect one another, resulting in consequences for the surface water quality. Among the physical parameters water level, retention time, flow velocity and water temperature are subject to be affected. Taking water temperature as an example, as the groundwater is hindered to enter the surface water by water abstraction wells its cooling effect in summer and its warming effect in winter will disappear, an impact that potentially will change the conditions for water-living organisms and their interactions (e.g. Alvarez and Nicieza (2005); Boisneau et al. (2008); Boscarino et al. (2007); Harper and Peckarsky (2006); Imholt et al. (2010); Wehrly

et al. (2007)). Among the chemical parameters, nutrients, toxic substances, dissolved organic and inorganic carbon (DOC and DIC) might be changed by bank filtration. Taking dissolved inorganic carbon as an example, groundwater often has higher concentrations than surface waters (Cole et al., 1994). When this source of DIC is removed, especially macrophytes solely relying on free CO_2 as their carbon source might disappear (Hilt, 2001). This has been shown in cases not directly related to bank filtration, but under other circumstances (e.g. Maberly et al. (2015)). The review assesses how the impact on physical and chemical parameters in turn might change the biodiversity, the macrophyte abundance and harmful blooms in surface waters. All in all, a comprehensive assessment of the potential effects on surface water quality by bank filtration is in progress.

2.1.6.2 Modelling of effects on shallow lakes

The shallow-lake model PCLake (Janse, 2005) provides the possibility of simulating whole-lake effects of bank filtration. Compared to what is possible in a field or a lab setting, the opportunity arises to examine the effects on more parameters and under more various conditions. PCLake is constantly being developed and adapted to extend its original applications, for example as shown with the study of deep lakes by (Sachse et al., 2014). Early trials show promising prospects for the model to provide relevant results that will give insight to potential effects of bank filtration on (shallow) lakes.

2.1.6.3 Field investigations and laboratory work

Field investigations are being conducted in Lake Müggelsee, which is located in eastern Berlin and is fed by water from the Spree River. Around the lake bank filtration has been conducted since more than 100 years and at the moment approximately 50 million m^3 water per year is being abstracted in the area around the lake (Wasserbetriebe, 2015), the water being a mixture of groundwater and bank filtrated lake water.

Early results from a minor field campaign indicate that higher rates of bank filtration increases the sediment organic content in Lake Müggelsee, a result that is in accordance with studies performed in Lake Tegel, Berlin (Hoffmann & Gunkel, 2011). The results from Lake Müggelsee still need to be confirmed by conducting a more comprehensive field campaign. Next to this, field experiments aimed at investigating the effect of different levels of CO_2 on the water plant *Fontinalis antipyretica* will be conducted. While this has been done in a laboratory setting (Maberly, 1985a, 1985b) it has not been performed in a field setting.

2.1.7 Conclusions

Interactions of groundwater and surface water are complex. They are related to the quantitative exchange of water, but also to chemical and ecological aspects. The UWI thematic group groundwater-surface water interactions addresses various knowledge gaps from different scientific disciplines, facing parts of all mentioned aspects. Within this group, engineers as well as natural scientists work on different projects, but at the same time knowledge as well as technologies are exchanged. Two projects are related to the hyporheic zone, while further two projects consider bank filtration. Overall, we expect to achieve a new quality of process understanding.

One project investigates flow and transport processes within the hyporheic zone with an integral numerical model. First of all, the upper boundary of the hyporheic zone was examined injecting a pulse of a passive tracer with various streambed morphologies. It was shown that the streambed morphology significantly influences where and for how long a tracer reaches the hyporheic interface. In a next step, the integral solver was applied and tested for two cases that account for groundwater as well as for surface water. For the validation of the integral solver, analytical as well as numerical results were compared. A good agreement was observed for big medium grain sizes of the soil. In a next step, smaller grain sizes will be investigated and an advection-diffusion equation will be implemented in the integral solver. The solver will then be validated with the help of a flume experiment and data from another project within UWI, which includes field experiments. The field experiments are conducted to elucidate next to flow and transport processes also biogeochemical processes. Moreover, the project aims to improve measurement techniques for the hyporheic zone. Control factors for the efficiency of trace organic compound removal in the hyporheic zone are investigated, using next to field experiments also a 1D – transport-reaction model. Present results from a wastewater treatment plant effluent urban river in Berlin show, that biogeochemical conditions had only a minor influence on attenuation rates. Consequently, the effectiveness is predominantly affected by flow and transport characteristics at the investigated field site. Actual analysis targets montane streams under more arid conditions.

Next to the hyporheic zone, the interaction of lake and groundwater is examined in two further projects. One project concerns the degradation process of iodinated contrast media during bank filtration. Iodinated X-ray contrast media are known for their persistence in the aquatic environment. The results to date indicate a deiodination of these compounds during anoxic/anaerobic bank filtration quantifiable by the sum parameter AOI. The microbiological

deiodination of iodinated contrast media with Dehalococcoides mccartyi strain CBDB1 could not be demonstrated by cell growth. However, an enzymatic activity with CBDB1 cells was shown for two contrast agents and two other iodinated aromatics. High deiodination rates, especially for Iopromide, were also achieved by using synthetic dicyanocobinamide as catalyst. Further microbiological experiments are planned with other dehalogenating bacteria strains. Abiotic batch tests will be conducted under nature related conditions in the presence of manganese(II), iron(II), iron(II) sulfide or sodium. One other project is also examining effects of bank filtration, but with a different focus, namely that of the effects on surface water quality. Since it is a new research field much work has been done to think of potential effects and to come up with hypotheses to test using the ecosystem model PCLake as well as field investigations. Early results indicate that there are noticeable effects, for example by increased sediment organic matter content in the littoral zone of lakes.

ACKNOWLEDGMENTS

The funding provided by the German Research Foundation (DFG) within the Research Training Group ’Urban Water Interfaces’ is gratefully acknowledged.

2.2 Research on multiphase modelling of hydrosystems at the Chair of Water Resources Management and Modeling of Hydrosystems, TU Berlin

This study was published as:

Broecker, T., Teuber, K., Elsesser, W. & Hinkelmann, R. (2018). Multiphase Modeling of Hydrosystems Using OpenFOAM, in: Gourbesville P., Cunge J., Caignaert G. (eds) Advances in Hydroinformatics, Springer Water, 1013-1029, Springer, Singapore.

This is the abstract of the book chapter (postprint).

This paper presents three computational fluid dynamics applications regarding multiphase modeling of hydrosystems with the open source software OpenFOAM. The first model investigates flow processes of groundwater and surface water using an integral approach which solves the three-dimensional Navier–Stokes equations, extended by the consideration of porosities. For the validation, seepages through homogeneous dams with impervious foundations were compared with analytical and numerical solutions. A further application examines the water–air interface in sewer systems. The focus of the model lies on the description of in-sewer water–air flow and transformation processes, reaeration and hydrogen sulfide emission which highly depend on the three-dimensionality of the hydraulic behaviour in the closed duct. A test case analyzing the hydraulic behaviour in a sewer stretch showed a good agreement of the numerical results with measured water levels. In the third model, fluid–structure interaction is investigated applying FOAM Extend Project. Calculations of the fluid phase are linked with the solid phase via a coupling algorithm to achieve an equilibrium state. To describe the time-varying position of the fluid boundary, caused by the structural response, dynamic meshes are considered. A technical case, consisting of the air flow around a thin tower as well as a natural case, describing the water flow around aquatic vegetation and its response, were examined.

3. Stream flow and tracer retention at rippled streambeds

This study was published in Limnologica as:

Broecker, T., Elsesser, W., Teuber, K., Özgen, I., Nützmann, G. & Hinkelmann, R. (2018). High-resolution simulation of free-surface flow and tracer retention over streambeds with ripples. Limnologica, 68, 46-58, https://doi.org/10.1016/j.limno.2017.06.005.

This is the postprint version of the article.

The test cases' setups are listed in Appendix B (B3 One-phase channel flow over a single ripple, B4 Two-phase flow over triangular ripples, B5 One-dimensional tracer transport in surface water, B6 Two-phase flow and tracer transport over rippled streambeds).

3.1 Abstract

This study presents a novel high-resolution simulation of free-surface flow and tracer retention over a streambed with ripples based on varying ripple morphologies, surface hydraulics and the transport of a tracer pulse from surface water to surface dead zone. For the simulations, the computational fluid dynamics (CFD) model OpenFOAM was used to solve the three-dimensional Navier-Stokes equations in combination with an implemented transport equation. Pressure gradients at the streambed were used to account for hyporheic exchange, assuming water flow from high pressure zones to low pressure zones. Flow velocities, ripple sizes and spacing showed to significantly affect these pressure gradients, but also the transport of a passive tracer at the streambed, which was not investigated so far. Due to the velocity field, large parts of the tracer mass were transported alongside the main stream above the ripples. Tracer mass reaching the space between the ripples was temporarily retained due to low velocities and recirculations. It was shown that the retention is depending on the ripple size and space between the ripples as well as on the flow velocity. Decreasing ripple sizes and higher flow velocities lead to a smaller tracer retention. Furthermore, we showed that the ripple length to height ratio controls the generation of recirculation zones which affect the residence time of the tracer significantly. Ripple spacing leads to temporarily higher tracer concentration at the streambed, but smaller tracer retention. We conclude that the impact of the streambed

morphology on the hydraulics in combination with tracer retention should be addressed for a comprehensive understanding of compound movement, exchange and transformation within the hyporheic zone.

3.2 Introduction

The hyporheic zone is the transition zone between aquifer and river (Buss et al., 2009). Processes within this zone are essential for the water balance, the movement of water and the substances transported and transformed therein. Consequently, the hyporheic zone has a strong influence on the health of fluvial systems e.g. through biogeochemical processes (Bardini et al., 2012; Dahm et al., 1998; Harvey & Fuller, 1998). These exchange processes occur at a wide range of spatial scales (Stonedahl et al., 2010) reaching from small scale riverbed topographies like ripples and dunes (Boano et al., 2007; Cardenas & Wilson, 2007c; Elliott & Brooks, 1997a; Packman & Brooks, 2001) to larger geomorphological features like meander bends (Boano et al., 2006; Cardenas, 2008; Revelli et al., 2008). A driving force for the exchange are pressure differences along the streambed (Buffington & Tonina, 2009; Elliott & Brooks, 1997a; Thibodeaux & Boyle, 1987).

Considering the complexity of turbulent flow and accompanied hyporheic exchange, it is quite challenging to perform adequate flume experiments or field studies of the groundwater-surface water interaction. Therefore, computational fluid dynamics (CFD) models are often a good alternative. CFD models offer high-resolution information on flow field characteristics which help to get a better insight into complex flow and transport processes. Especially three-dimensional models have the potential to consider the complex mechanisms of flow dynamics in all three directions (Chen et al., 2015; Lane et al., 2002; Y. Shen & Diplas, 2008; Tonina & Buffington, 2007, 2009b; Trauth et al., 2013; Trauth et al., 2014; Trauth et al., 2015), whereas vertically-averaged one- and two-dimensional hydraulic models are based on the hydrostatic pressure assumption. Therefore, it is not possible to determine vertical velocities using the latter models (Hinkelmann, 2005). Especially for the examination of turbulence, which also can cause hyporheic exchange (Tonina & Buffington, 2009a) and affect the flow of substances, the investigation of all three directions is important. Here, one-, two- or multiphase models can be applied. According to Stoesser et al. (2008) a shear-free symmetric boundary condition assumption suffices for high water levels as long as the Froude number is not bigger than 0.8, whereas for relatively shallow turbulent flow over streambed structures a two-phase model is appropriate (Yue et al., 2005).

A large number of publications have reported numerical simulations of flow, transport and reaction processes within the hyporheic zone (Bardini et al., 2012; Cardenas et al., 2008; Trauth et al., 2014). However, according to the author's knowledge, only the flow of surface water into the ground, not the transport of a tracer pulse from surface water into surface dead zones and the ground was simulated with numerical models. Furthermore, previous studies investigating the influence of amplitudes and wavelengths of dune-like structures on the hyporheic exchange did not include structure spacing.

This study aims to improve the understanding of flow and transport dynamics of a passive tracer in surface water with a focus on the processes occurring between the ripples using a three-dimensional computational fluid dynamics (CFD) model. High-resolution simulations are carried out to analyse pressure and velocity distributions. Several simulations are investigated using a one phase as well as a two-phase flow and transport model. In contrast to previous studies, where hyporheic exchange was quantified or the residence times in the hyporheic zone were presented, this study investigates pressure fluctuation and the generation of recirculation zones between ripples which cause a tracer retention between the ripples and thus has impact on hyporheic exchange. We hypothesize that ripple dimensions, lengths and spacing as well as varying flow rates have a clear impact on the flow dynamics as well as on tracer spreading and retention at the river bed which in turn will affect the hyporheic exchange.

3.3 Governing equations and numerical method

The OpenSource CFD software OpenFOAM (Open Field Operation and Manipulation) version 2.4.0 is used to simulate flow processes over a rippled streambed. As in most hydraulic engineering applications using OpenFOAM, the interFoam-solver is applied (Schulze & Thorenz, 2014). InterFoam is a multiphase solver for immiscible fluids that solves the three-dimensional Navier-Stokes equations using the Finite-Volume-Method in space and the Finite-Differences-Method in time. The OpenFOAM toolbox allows parallel computations on a theoretically unlimited number of processor cores and enables the user to take full advantage of the computer hardware. Regarding the simulation of water channels with complex stream bed morphologies, flow and pressure distributions can most realistically be depicted with the full Navier-Stokes equations (Cardenas & Wilson, 2007c; Janssen et al., 2012; Tonina & Buffington, 2009a). A common assumption for free surface flow is that it may be considered to be incompressible. This can be estimated if the Mach number (the ratio of the flow velocity to the sound velocity) is below 0.3 (Young et al., 2010). For incompressible flow, the conservation of mass (Equation 3.1) and momentum (Equation 3.2) are written as:

$$\nabla \cdot \vec{U} = 0 \tag{3.1}$$

$$\frac{\partial \rho \vec{U}}{\partial t} + \vec{U} \cdot \nabla \rho \vec{U} = -\nabla p + (\mu_{phys} + \mu_{turb}) \Delta \vec{U} + \rho g \tag{3.2}$$

where ρ represents the density of the fluids, v is the flow velocity, t is time, p is pressure, μ_{phys} and μ_{turb} are the physical and turbulent dynamic viscosity, respectively, and g is the gravitational acceleration. The interface is captured by a Volume-of-Fluid-Method (Hirt & Nichols, 1981). A single variable value per element, the indicator fraction α, expresses the proportion of the fluids. It considers the fluids to be a single multiphase fluid with properties (dynamic viscosity and density) that are weighted according to the fractions of each fluid (Equation 3.3 and 3.4). The indicator fraction α varies between 0 (air) and 1 (water). The movement of the water-air interface is described by a convective transport equation (Equation 3.5).

$$\mu = \mu_{water} \alpha + \mu_{air} (1 - \alpha) \tag{3.3}$$

$$\rho = \rho_{water} \alpha + \rho_{air} (1 - \alpha) \tag{3.4}$$

$$\frac{\partial \alpha}{\partial t} + \nabla \cdot \alpha \vec{U} = 0 \tag{3.5}$$

For the pressure-velocity coupling the PIMPLE algorithm is used. It is a combination of the widely used SIMPLE and PISO algorithms which uses the outer-correction tool of SIMPLE and the inner-corrector loop of PISO to gain a more robust coupling (Rodrigues et al., 2011). Turbulent features can be resolved directly with a very fine mesh or – like in most cases – are partially or completely modeled. In the following, a large eddy simulation (LES) model is applied to predict turbulent flows. LES turbulence models simulate eddies of a certain size directly. Only small turbulent structures are separated by a low-pass filter and subsequently treated with an algebraic model. In this case, the Smagorinsky subgrid scale model is used with a van Driest damping function. The purpose of the van Driest damping is to reduce the eddy viscosity in the near-wall region allowing to reproduce the characteristics of direct numerical simulations at the near-wall region which solve the three-dimensional Navier-Stokes equations for all eddies directly.

Since the interFoam-solver does not provide an application for the transport of a passive tracer, an advection-diffusion equation was implemented into the interFoam-solver (Equation 3.6). This additional implementation allows to investigate the transport of a passive tracer with a concentration C through the channel. Regarding the diffusivity, the user can define the physical

diffusivity coefficient D_{phys} as well as the turbulent Schmidt number Sct. According to Equation 3.7 the turbulent diffusivity coefficient D_{turb} will be calculated.

$$\frac{\partial C}{\partial t} + \nabla \cdot (C\vec{U}) + \nabla \cdot (D_{phys} + D_{turb}) \nabla C = 0 \qquad 3.6$$

$$D_{turb} = \frac{\mu_{turb}/\rho}{Sc_t} \qquad 3.7$$

3.4 Validation

In order to verify the numerical results concerning the hydraulics, the model was validated based on two laboratory experiments which are described in the following.

Almeida et al. (1990) performed and presented a flume experiment with a single ripple on the bottom of a channel (see Figure 3-1a). This experiment was used to ensure a reliable physical behaviour of the developed model – especially concerning velocity distributions around ripples. Flow velocities in two dimensions over a polynomial-shaped obstacle were measured using a Laser-Doppler Velocimeter up to 2 mm from the surface of the ripple and the bottom of the channel. The top of the channel consisted of a wall, while the whole channel was filled with water. The mean velocity at the inlet was 2.147 m/s.

The boundary conditions were adjusted slightly, since only one phase instead of two-phases as well as a fixed wall on the top instead of an atmospheric boundary had to be imposed according to the experimental setup. Furthermore, velocities were only measured in two dimensions. Therefore, a two-dimensional model was adequate for this validation. The model entry was extended in front of the hill to achieve fully developed velocity profiles. Since a velocity function was set as inlet boundary, an entrance length of 1 m in front of the hill was sufficient to receive a fully developed flow. Velocity profiles of the simulations in x- and y-direction at six different locations were compared to the measurements. The geometry of the model is presented in Figure 3-1a (top). Various turbulence models (three Reynolds Averaged Navier Stokes turbulence models and a Large-Eddy-Simulation) are applied to investigate the turbulence. Comparing the measured data of the experiments with the simulation data using different turbulence models, the LES turbulence model indicated the best agreement. Moreover, Figure 3-1a shows the resulting velocities in x- and y-direction for the simulation with the LES model and the experimental data at three locations. A good agreement with the measured data was observed.

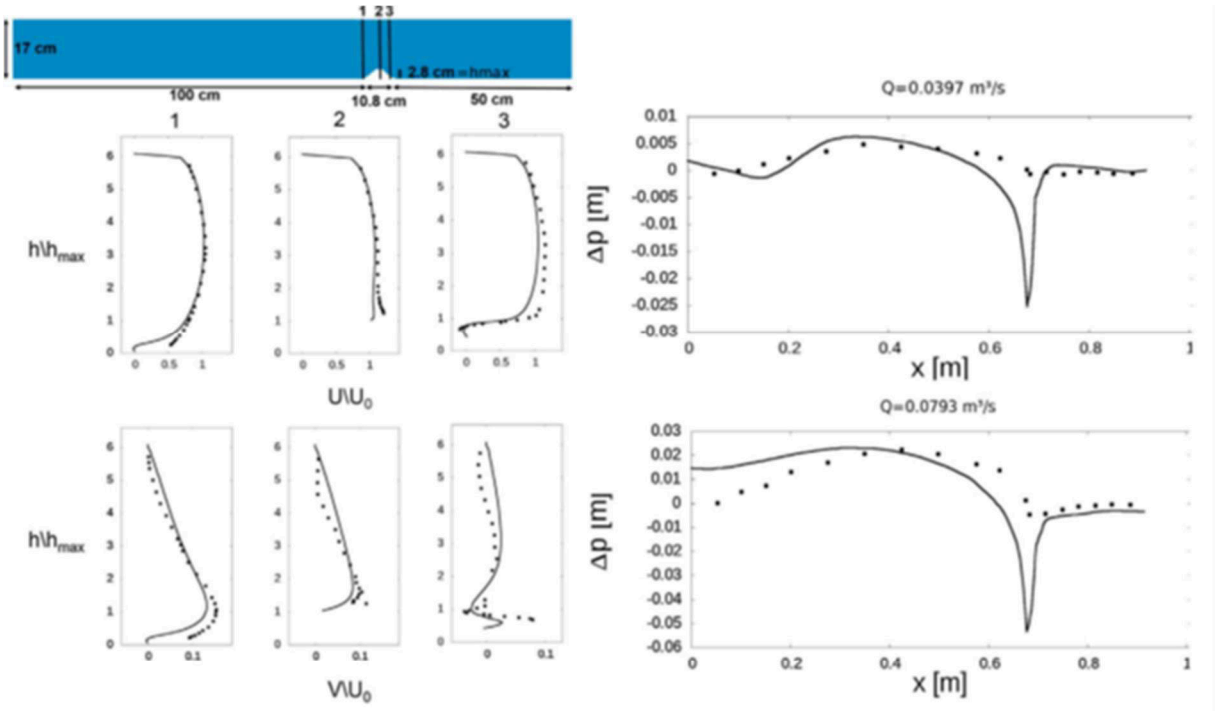

(a) Velocity profiles in a flume with a single ripple (b) Pressure difference profiles along triangular bedform

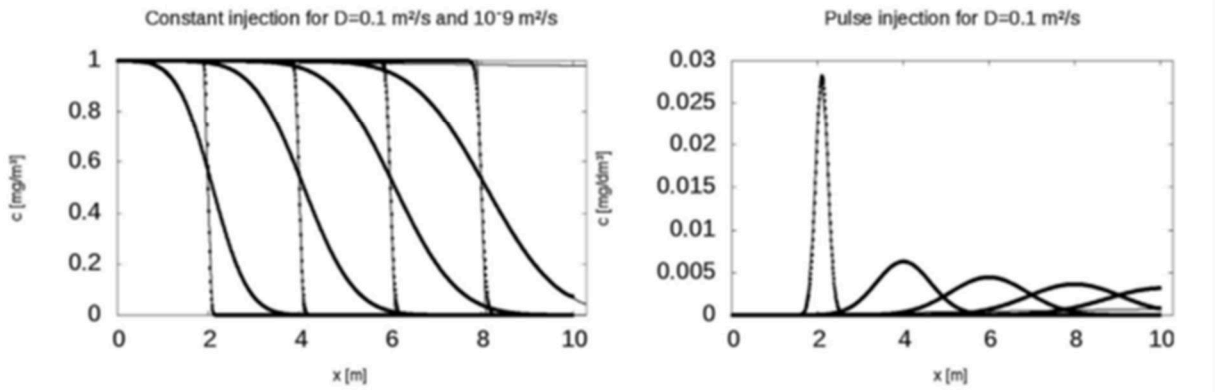

(c) Tracer breakthrough curves

Figure 3-1: Comparison of measured or with analytical solutions calculated data (points) with simulated data (lines).

Next to the measurements by Almeida et al. (1990), flume data by Fehlman (1985) were used to validate the model. Compared to Almeida et al. (1990), the data by Fehlman (1985) were used to ensure reliable pressure distribution of a three-dimensional, two-phase model. Fehlman (1985) investigated flow over beds with triangular ripples for twelve runs with discharges between 0.021 m^3/s and 0.140 m^3/s and examined pressure variations (see Figure 3-1b).

The geometry of Fehlman's flume including the triangular bed forms was discretized with the help of three-dimensional meshes. The results of the simulations were compared with

experimental data of two different discharges (Run 4 and Run 10) of Fehlman's examinations. Figure 3-1b shows a comparison of measured and simulated differences in pressure heads between the bed form surface and the crest of the ripple for a discharge of 0.0397 m^3/s and of 0.0793 m^3/s.

In this context it should be emphasized, that there were no pressure taps at the crest and consequently the pressure was linearly interpolated. Trauth et al. (2013) and Cardenas and Wilson (2007c) used the same experiment for the validation and pointed out that the crest is a singularity with an adverse pressure gradient which is challenging to capture numerically or experimentally. Therefore, it is very difficult to compare the measured and the simulated results. To improve the comparability, pressure heads for a point downstream of the crest are subtracted instead of the value directly at the crest. Despite this singularity at the crest, which was also depicted by Cardenas and Wilson (2007c) and Trauth et al. (2013), the simulated variations along the bed forms were in good agreement with the experiments.

For the validation of the transport, four analytical one-dimensional solutions after Kinzelbach (1992) were used for a constant tracer injection as well as for a tracer pulse for two different diffusion values: $D_{phys}=10^{-9}$ m^2/s (neglecting turbulent diffusion) and $D_{phys} = 0.1$ m^2/s (strong turbulent diffusion). We are aware that the value for the turbulent diffusion is very high, however we thus could check the implementation of the diffusion term. A good agreement was achieved between the simulations and the analytical solutions as it can be seen in Figure 3-1c.

In summary, the model concept was tested against data of two flume experiments as well as against analytical solutions. Different parameters were examined and the simulations demonstrate that the surface model shows good accuracy concerning the pressure head distributions, the calculated velocities and the tracer concentrations.

3.5 Simulations of flow and transport over streambeds with ripples

Based on the successful validation of the model, flow velocities, water elevations and pressure distributions as well as the transport of a passive tracer pulse were investigated for differing ripple geometries and flow rates as shown in Figure 3-2a. Firstly, the reference case will be presented. Based on these results, the influence of above-mentioned cases is analyzed.

3.5.1 Geometry and mesh

Figure 3-2b shows the geometry of the system and the bathymetry with the initial water level for the reference case. For all simulations, the domain is a prismatic rectangular channel with a

height and width of 1 m and a length of 40 m. After an inflow area of 6 m, a field with varying number of ripples (7 to 64) with differing geometries and distances is introduced. The length of this field comprises approximately 3 m. The length of the whole system was set to guarantee an undisturbed outlet in order to set proper boundary conditions – especially for larger ripple heights which affect the water surface.

Case	1	2	3	4	5	6	7
Ripple height [cm]	5.6	1.4	11.2	5.6	5.6	5.6	5.6
Ripple length [cm]	20	5	40	40	20	20	20
Ripple distance [cm]	0	0	0	0	20	0-56	0
Flow rate [m^3/s]	0.5	0.5	0.5	0.5	0.5	0.5	0.25
Schmidt number [-]	1 & 0.5	1	1	1	1	1	1

(a)

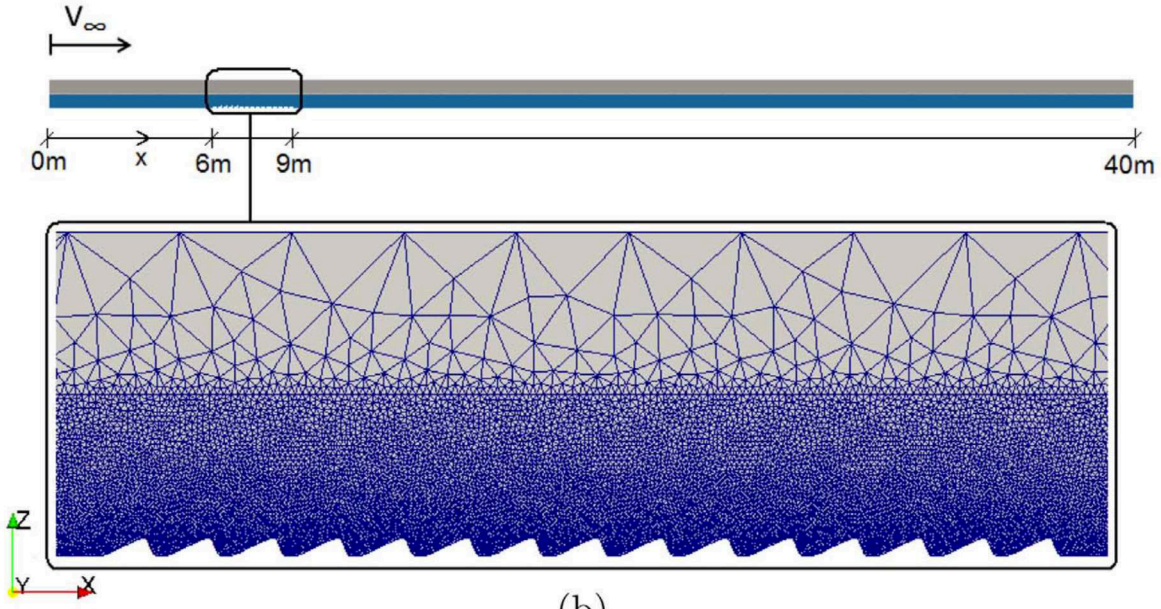

(b)

Figure 3-2: Simulation cases (a), model geometry and mesh for the reference case (b).

The ripples show a small gradient at the upstream face and a steep gradient at the downstream face. For different simulation runs, the height is varied from 0.014 m to 0.112 m, the length is varied between 0.05 m and 0.4 m and the distance between the ripples is varied from 0 m to

0.56 m. The mesh in the nearfield of the ripples is refined as shown exemplarily in Figure 3-2b. Due to the curved profile in the x-z-plane, unstructured elements were chosen. The elements were extruded with 10 layers in the y-direction to produce prismatic volumes. 6 three-dimensional meshes with up to 1.27 10^6 cells were created. Fixed bed forms were assumed for all cases, which means that no sediment transport is examined for this study. Since the air-phase as well as the outflow are not of interest for this study, larger element sizes were chosen for these areas. The minimum cell area in the x-z-plane amounts to 1.75 10^{-5} m (located at the rippled streambed) and to the maximum of 0.04 m (within the air-phase) for the reference case. All cases show similar mesh conditions.

3.5.2 Initial and boundary conditions

The boundary conditions are constant over time to represent steady state flow. An initial water depth (see Figure 3-2b) as well as an initial flow velocity are specified to achieve the steady state faster. The inlet is divided into two fractions. In the lower fraction only water enters the domain, in the upper half only air flow is possible. The discharge of the water that enters the domain is fixed. For the air fraction at the inlet as well as on the upper boundary atmospheric pressure is defined. At the outlet a mean velocity for the water phase is set. The velocity profile as well as the water depth are not fixed due to zero gradient boundary conditions at the outlet. At the streambed the velocity is set to 0 m/s. For the transport simulations zero concentration is assumed at the inlet as well as at the upper boundary, the rest is set to a zero gradient condition. Starting from steady state, a passive tracer with a density of 1 kg/m^3 is placed into the water phase as initial condition nearby the inlet with a volume of 0.5 m × 0.5 m × 1 m in the x-, z- and y-direction. For the turbulent diffusivity, a turbulent Schmidt number of 1 is set. The physical diffusivity coefficient is 10^{-9} m^2/s. All boundaries in the third dimensions contain slip conditions. Thereby normal components and the gradient of tangential components are set to zero. Consequently, the water is able to pass and no influence through lateral walls is given.

3.5.3 Reference case

For the first case the inlet discharge is set to 0.5 m^3/s, the initial water depth is set to 0.5 m. Hence, the inlet velocity is 1 m/s. The density of the water is 998.2 kg/m^3, the density of the air 1.2 kg/m^3, the physical kinematic viscosity of the water is 10^{-6} m^2/s and the physical kinematic viscosity of the air is 15.3 10^{-6} m^2/s. Each ripple has a length of 0.2 m, a height of 0.056 m (see Figure 3-2a). Since a semi-implicit time-difference scheme is imposed for all simulations, a time step of 0.05 s is sufficient.

A one-phase as well as a two-phase model were investigated for the reference case. A comparison of the results indicated that the application of a two-phase model is important to depict water level fluctuations which influence the pressure distribution in the domain. These pressure distributions are important for the exchange of surface water with groundwater and should therefore be determined as precisely as possible. Due to the rippled streambed the water surface raises slightly in front of the ripples from z = 0.5 m to z= 0.508 m. At the area of the ripples the water surface decreases down to z= 0.483 m due to subcritical flow (Froude number of 0.45) over an elevated ground (see Jirka (2007)). Since a relatively shallow turbulent flow (e.g. a small river or creek) is considered, the structure is better represented by a two-phase model.

Figure 3-3a shows the velocity distribution in x- and z-direction at the crest height for the first ten ripples as well as the velocity in x-direction for the rippled streambed (Figure 3-3b). The flow accelerates at the first ripple up to 1.49 m/s. The maximum velocity occurs near the crest at the stoss side. Compared to the following ripples, the flow is particularly accelerated at the first ripple. Behind the crest the flow velocity is very low, but accelerates again at the next ripple crest. The flow velocity at the streambed changes from positive to negative values up to −0.525 m/s. Negative velocities indicate the separation zone of the flow downstream of the crest. Starting with the second ripple, the velocity distribution is periodical for each ripple: small velocities between the ripples, flow acceleration at the crest.

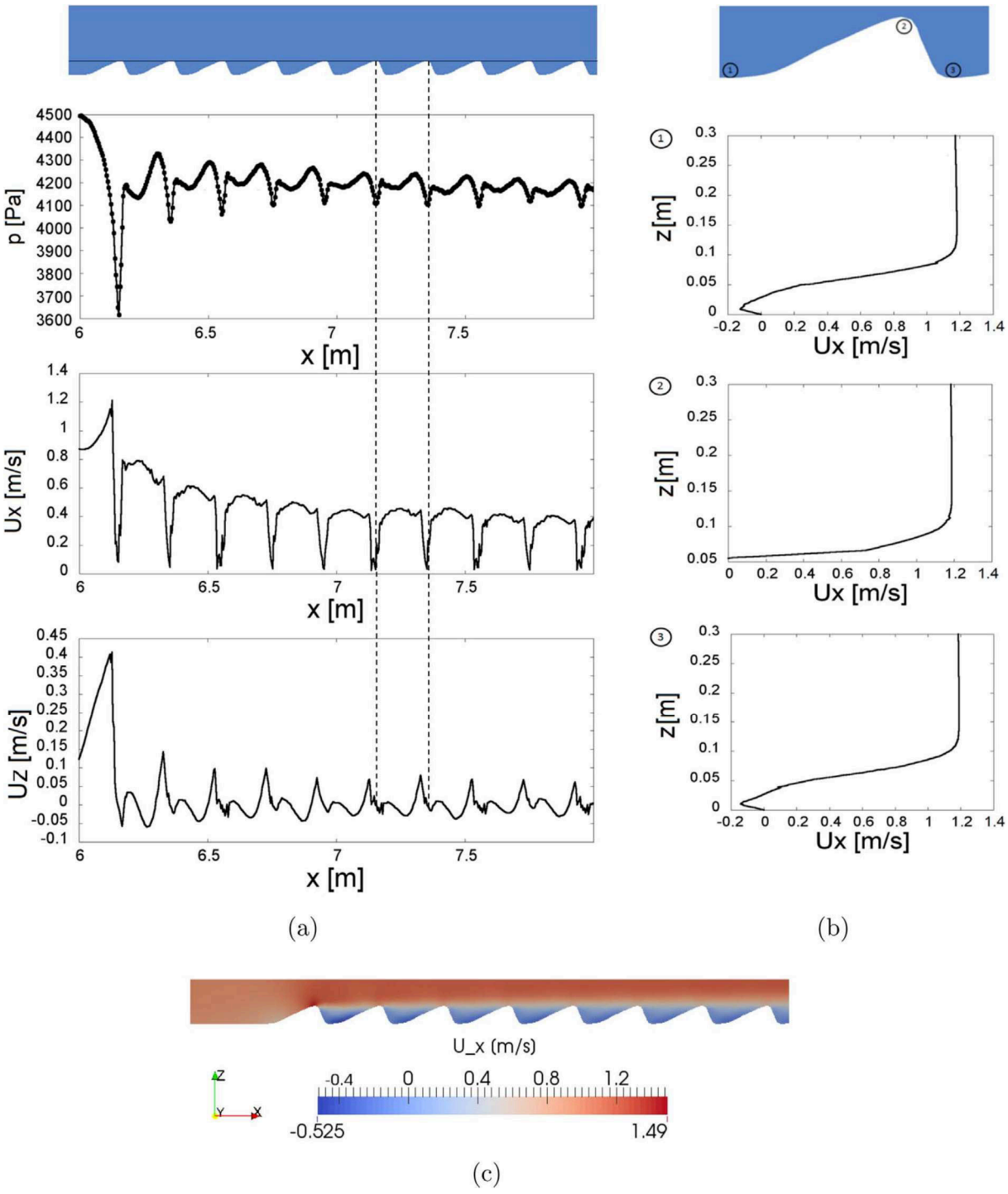

Figure 3-3: Pressure and velocity distribution for the reference case for the whole ripple domain (a), velocity profile at a ripple in the middle of the rippled bedform (sixth ripple) (b), velocity distribution in the domain (c).

In the z-direction, the flow accelerates from 0 m/s at the inlet up to 0.44 m/s upstream of the first ripple. Here, the three-dimensional Navier-Stokes model shows considerable differences in the third dimension which also will have a strong impact on the exchange with the underlying hyporheic zone. At the ripple crest the flow decelerates and reaccelerates at the ripple lee. At

the next ripple stoss the flow decelerates and turns initially negative. A constant variation pattern of negative and positive flow velocities in z-direction can be recognized starting with the second ripple. A recirculation zone with a three-dimensional structure can be observed behind each ripple.

Figure 3-3b shows the velocity profiles at a ripple located in the middle of the rippled bedform (the sixth ripple) at three different points. Each profile starts with 0 m/s at the wall. Up- and downstream of the ripple negative velocities are determined. The minimum velocity amounts −0.12 m/s at point 1 and −0.13 m/s at point 3. At half of the ripple height, the velocity turns positive. On top of each crest the flow accelerates compared to the mean inflow velocity of 1 m/s with a maximum of 1.19 m/s. Comparing the velocity of the rippled bedform with the flow field at the flat streambed, a faster flow can be observed above the ripples, whereas a zone of small velocities appears between the ripples.

Simulated pressure distributions near the streambed are of interest for predicting the hyporheic flow since water flows from high pressure zones to low pressure regions. The solver interFoam solves the pressure term p_rgh which is defined as p_ rgh = p− ρgz with the hydrostatic pressure p and z as coordinate vector. p_rgh is used – rather than p – 'to avoid deficiencies in the handling of the pressure force/buoyant force balance on non-orthogonal and distorted meshes' (see OpenFOAM (Greenshields, 2010)). In front of each ripple the pressure increases (see Figure 3-3a). At the crest an adverse pressure gradient can be observed with a maximum pressure difference of 1060 Pa – corresponding to a water level of 0.106 m. The highest pressure difference is determined at the first crest.

Figure 3-4 shows the tracer distribution at the beginning, after 3 s, 6 s, 7 s and after 10 s for the reference case. Next to the streambed the tracer is transported slower, compared to the mainstream, due to smaller velocities near the bottom. Most of the tracer is transported advectively with a velocity around 1 m/s, which is the mean velocity. After 6 s the tracer reaches the first ripples. The tracer is firstly accumulated in front of the first ripple. Due to the velocity profile at the ripple stoss, the tracer can flow across the first ripple. The advective transport of the tracer is now concentrated on the flow above the ripples. The main tracer concentration passes the rippled section after less than 9 s.

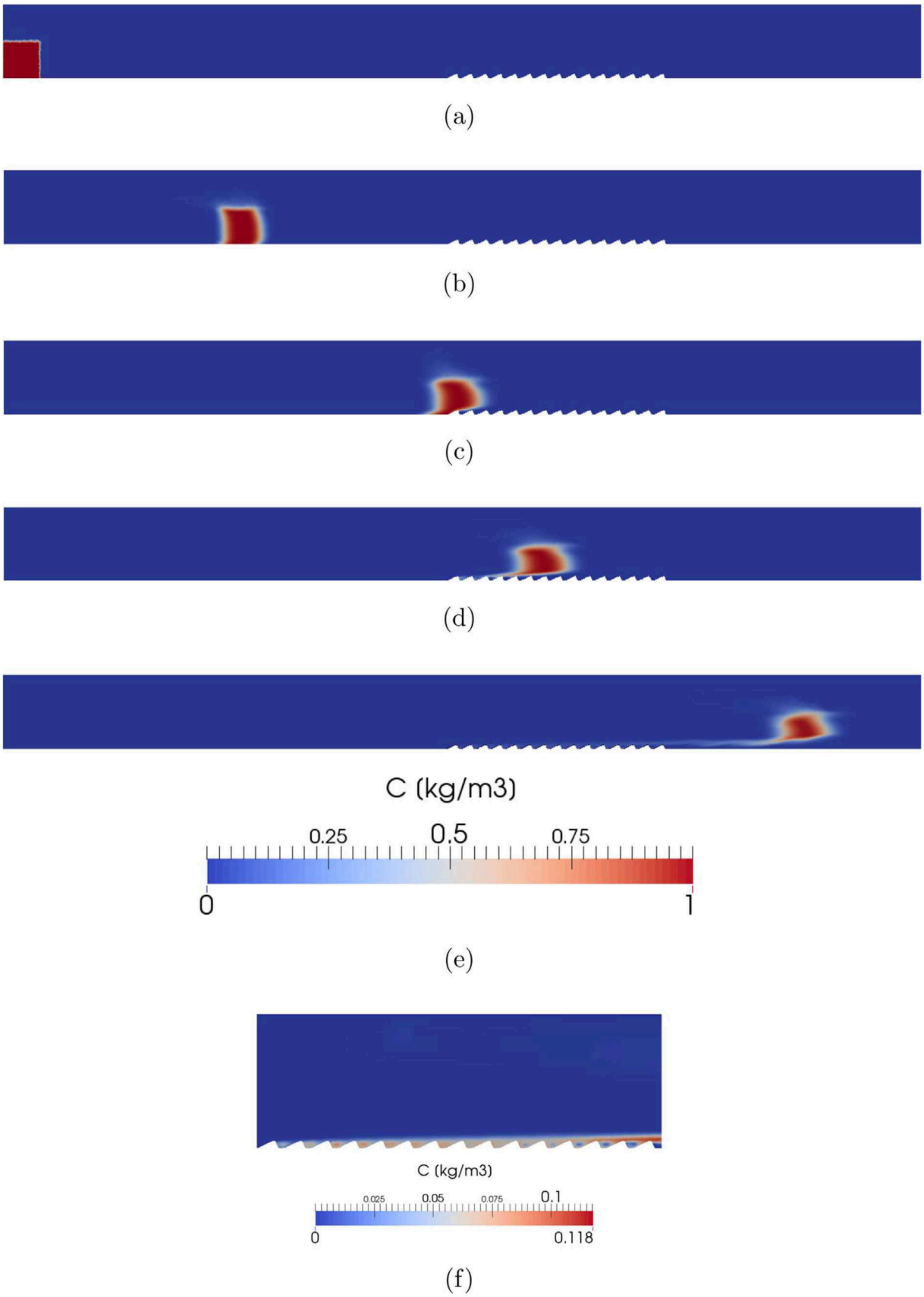

Figure 3-4: Tracer distribution at t = 0 s (a), t = 3 s (b), t = 6 s (c), t = 7 s (d), t = 10 s (e) (from section x = 0m to x = 12 m, top) and for the rippled area (section from x = 6 m to x = 9 m, bottom) at t = 10 s (f) for the reference case.

The simulation indicates that the tracer moves slightly in all directions driven by turbulent diffusion. Considering this fact and the local flow field, the tracer spreads also into the area between the ripples. The tracer shows a relatively long residence time in this area as result of the eddies between the ripples and their inherent small velocities. After 10 s a maximum tracer concentration of 11.8% of the initial concentration is still determined in the area around the ripples (see Figure 3-4f). Maximum tracer concentrations of 5% and of 1% at the rippled streambed are observed after 18.5 s and 39 s at the stoss side of the last ripple. The volume between the ripples can act as a storage volume for tracer which can lead to an increased and temporarily shifted exchange of tracer between surface and groundwater.

For a decreased Schmidt number from 1 to 0.5 the turbulent diffusion increases from maximum $3 * 10^{-7}$ m^2/s to maximum $6 * 10^{-7}$ m^2/s (see Eqation 3.7). This leads to less retention, with a maximum tracer concentration of less than 5% already after 14 s and 1% after 31 s (8 s less than for a Schmidt number of 1).

3.5.4 Variation of ripple dimensions

Next to the reference case two simulations were executed with the same settings like the reference case, only varying the ripple dimensions (see Figure 3-2, case 2 and 3): for case 2 the ripple is quartered (length: 0.05 m, height: 0.014 m) and for case 3 it is doubled (length: 0.20 m, height: 0.112 m).

For a ripple height of 0.014 m a maximum velocity of 1.09 m/s and a minimum of −0.334 m/s were observed in the x-direction. Thus, an absolute difference of 0.4 m/s (reference case: 1.49 m/s) for positive velocities and 0.191 m/s for negative velocities were determined compared to the reference case with higher ripples (reference case: −0.525 m/s). In the z-direction the negative values are 0.048 m/s higher and the positive values 0.154 m/s lower than the reference case with 0.44 m/s. The maximum pressure difference at the streambed amounts to 580 Pa which corresponds to about half of the reference case. Therefore, compared to the reference case, a significantly smaller hyporheic exchange is expected as shown by Cardenas and Wilson (2007a). The maximum pressure difference is concentrated at the area of the first ripple. For the following ripples the difference is even smaller. Next to the change of the pressure values, a variance of the location of the minimum pressure is determined: a shift of the minimum pressure from the crest for the reference case to the ripple lee for the simulation with smaller ripples is observed. The slight increase of the water level at the upstream of the first ripple is about 0.007 m and similar to the reference case, though the decrease of only 0.004 m is definitely lower (reference case: 0.017 m). Due to the less accelerated flow in the rippled area

(compared to the reference case), the tracer needs more time to pass this area. Therefore, after 10 s the maximum tracer concentration is with 14.6% almost 3% higher than for the reference case (see Figure 3-5a). But already after 17 s the maximum tracer concentration is less than 5% and even after 23 s the maximum tracer concentration is less than 1% (16 s difference compared to the reference case). Consequently, smaller ripples lead to a less accelerated flow above the ripples, supported by less water level fluctuations, whereby the tracer needs more time to pass the ripples. Between the ripples the tracer is stored for a shorter time. Including the fact, that the maximum pressure difference is about half of the reference case, a definitely lower tracer exchange with groundwater is expected for smaller ripples.

For the simulation of case 3 (see Figure 3-2), waves develop at the water surface. Due to the ripple height the water cross-section is significantly decreased and the flow velocities increased. This leads to a supercritical flow, whereas upstream and downstream of the rippled area subcritical flow is present which results in an undular hydraulic jump (Chanson & Montes, 1995). A comparison of the water level change is therefore difficult. The water level affects also the pressure and velocity distribution at the streambed. Nevertheless, small velocities between the ripples and accelerated flow at the crests can be observed over the whole rippled streambed. The maximum velocity in the x-direction at the first ripple amounts 1.68 m/s after 1000 s which corresponds to an absolute difference of 0.19 m/s compared to the reference case (reference case: 1.49 m/s). The minimum velocity amounts −1.19 m/s at the same time which corresponds to an absolute difference of 0.665 m/s compared to the reference case (reference case: −0.525 m/s). Thus, the ripple height has a large effect on the velocities in the x-direction. In the z-direction, the difference between the maximum velocity is 1.08 m/s and more than twice as high as for the reference case (reference case: 0.44 m/s). The minimum velocities are almost three times lower. Due to the disturbed water surface for a ripple height of 0.112 m, the maximum and minimum velocities do not occur periodically for each ripple. The pressure difference at the streambed after 1000 s is with 3220 Pa around three times higher than for the reference case. Next to the low pressure zones at the crests, low pressure zones are recognized also between the ripples.

The undular hydraulic jump has an immense effect on the tracer transport. Figure 3-5b–f shows the tracer distribution between 6 s and 10 s. Compared to the reference case the transport of the tracer is much more disturbed. There are still some eddies which store the tracer between the ripples, but due to the hydraulic jump the turbulent flow field is definitely higher than for the reference case and leads to a higher spreading of the tracer. After 10 s the maximum tracer concentration at the rippled area amounts to 28.5%, after 15 s to less than 5% and after t=20 s

the tracer concentration amounts to less than 1%. This means, that the tracer retention is much lower compared to the reference case and even lower compared to the smaller ripple dimensions of case 2 due to the flow field. However, considering the significantly higher pressure gradient, probably more tracer mass will reach the hyporheic zone compared to the reference case and case 2 even if the retention of tracer between the ripples is smaller.

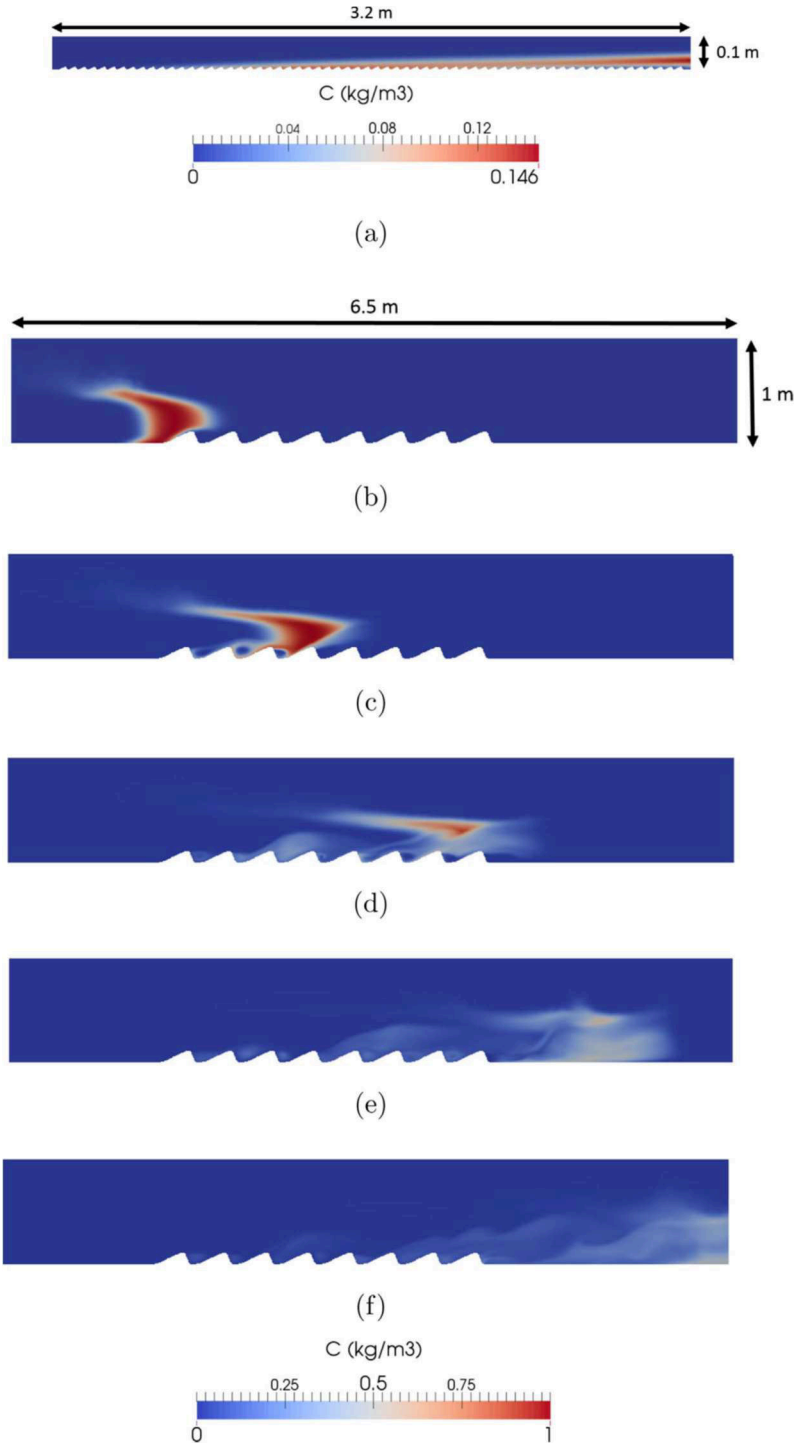

Figure 3-5: Tracer distribution for case 2 at t = 10 s (a) and for case 3 at t = 6 s (b), t = 7 s (c), t = 8 s (d), t = 9 s (e), t = 10 s (f).

3.5.5 Variation of ripple length

For case 4 with a ripple length of 0.4 m (twice as long as the reference ripple, see Figure 3-2), the flow is decelerated between the ripples, but no negative velocities occur in the x-direction. At the crests, the ripples indicate accelerated flow with a velocity of about 1.5 m/s in the x-direction, thus slightly higher velocities as in the reference case with 1.49 m/s. Figure 3-6a shows the velocity vectors. In contrast to all other simulated cases no recirculations were determined between the ripples. Regarding a backward facing-step it is evident, that a limit in the geometry for the descending part of the ripple is exceeded, which causes the flow to not produce eddies because of the smooth geometry. Due to the jam between the ripples, higher pressure is observed just like in front of the first ripple.

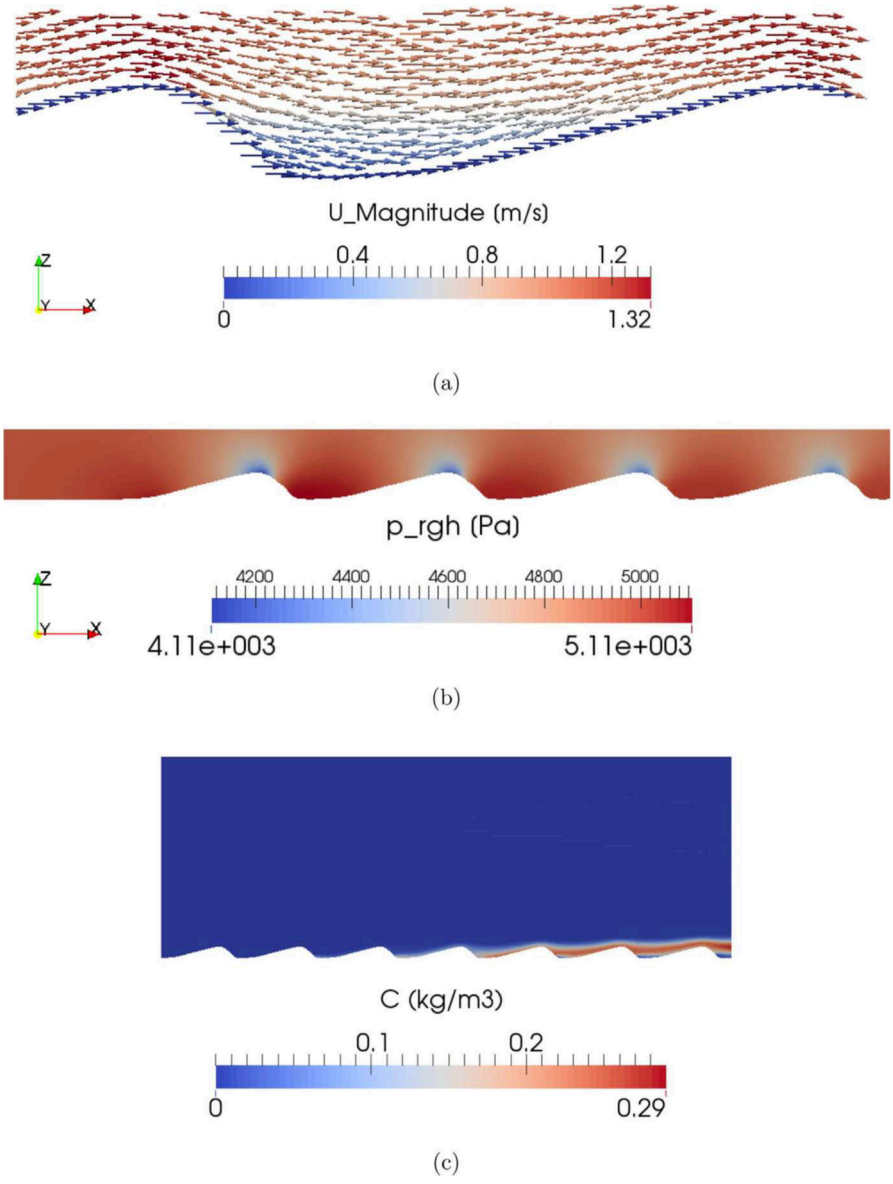

Figure 3-6: Velocity vectors (a), pressure distribution (b) and tracer distribution (c) after 10 s for case 4.

The maximum velocity in the z-direction is 1.6 times smaller than the maximum velocity in the z-direction for the reference case with 0.44 m/s. Unlike the reference case, the velocity at the first crest is similar to the following ripple crests. The same applies for the pressure distribution: the first ripple shows the same pressure distribution as the following ones (see Figure 3-6b) in contrast to all other cases, where the pressure differences between ripple stoss and crest where much higher for the first ripple. The difference of the maximum and the minimum pressure is 1000 Pa and thus similar to the reference case. This leads to the assumption, that a similar hyporheic exchange can be assumed.

Figure 3-6c depicts the tracer distribution after 10 s. With a maximum of 29% this case shows a higher concentration than for the reference case at that time. Comparing the whole tracer distribution of both cases, it is obvious, that a pulse tracer injected in the area of streambed with a higher ripple length has a significantly shorter residence time between the ripples. A maximum tracer concentration of 5% is observed after 15 s and a maximum concentration of 1% after 19 s – consequently the shortest residence time of all examined cases. The shorter residence time probably leads to varying hyporheic reactions compared to the other cases. This is most likely based on the flow field which shows no recirculation zones between the ripples retaining the tracer between the ripples (see Figure 3-6a).

3.5.6 Variation of ripple distances

While for the reference case no distance was defined between two ripples, for case 5 a constant distance of 0.2 m, i.e. a horizontal bed, is defined between each ripple pair (see Figure 3-2). For the constant ripple distance, the velocities in x-direction were in a similar range as the reference case. The area with small flow velocities has increased due to the distances. Figure 3-7a shows that the increased distance leads to a wider recirculation zone in the ripple lee. Due to the LES model, turbulent effects can also be seen in the third dimension. For an increased distance, the maximum velocity in the y-direction is higher.

Due to the expanded area with small velocities around the ripples, more tracer mass is retained in the rippled area after 10 s compared to the reference case (see Figure 3-7b). However, it takes only 16 s until the maximum tracer concentration is less than 5% and 28 s for less than 1%. Compared to the reference case, a slightly higher hyporheic exchange flow rate is expected due to higher pressure gradients (pressure difference case 5: 1170 Pa for reference case: 1060 Pa). However, the residence time is smaller for an increasing distance between the ripples.

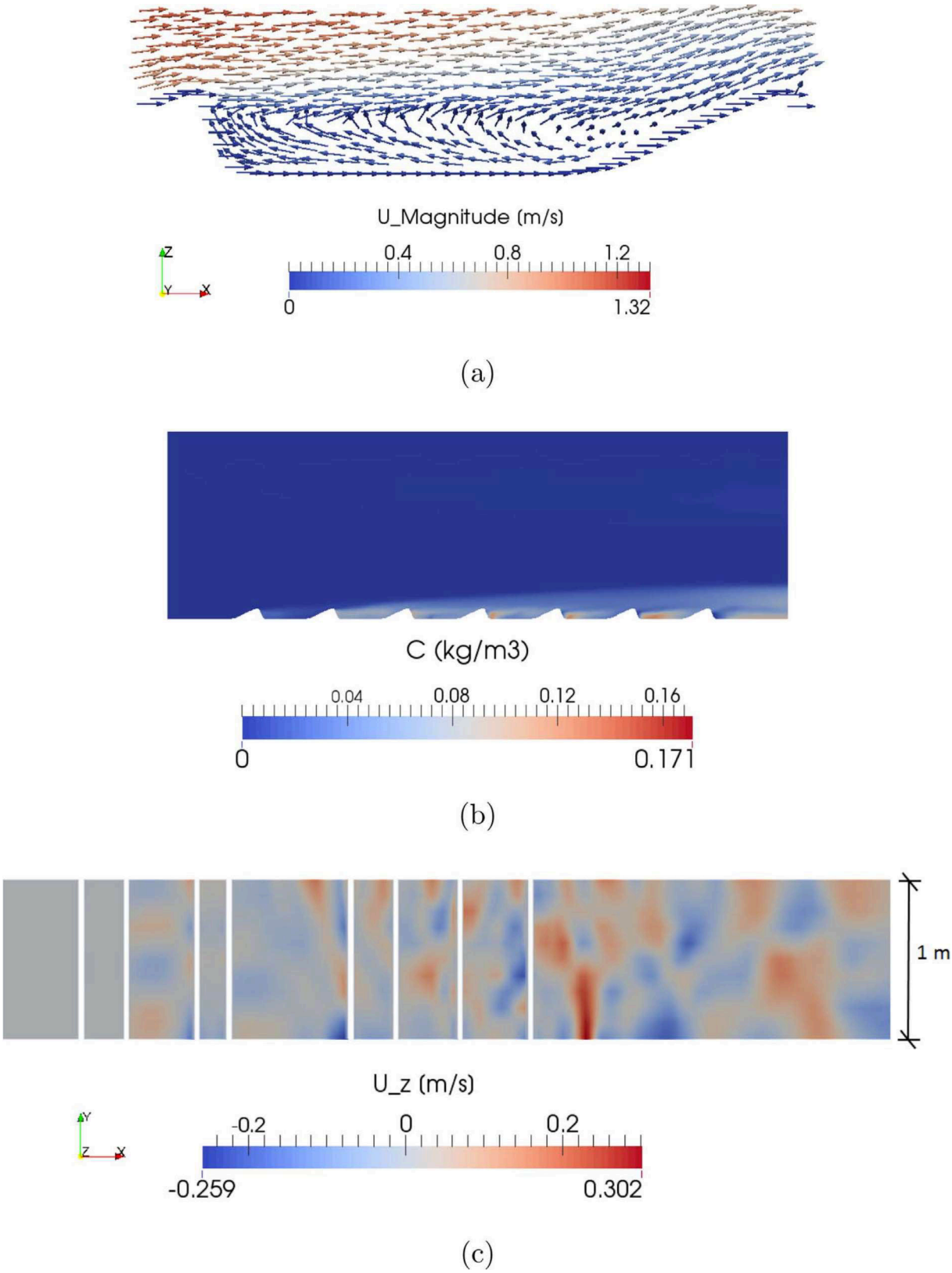

Figure 3-7: Velocity vectors (a) and tracer distribution (b) after 10 s for case 5 and velocity in z-direction at z = 0.05 m for case 6 (c), white lines illustrating the crest (bottom).

Following the simulation run with constant distance, the ripple distance is varied between 0 m and 0.56 m for case 6 (see Figure 3-2). The previous result is confirmed by the simulation with

varying distances, also showing an influence of the flow in the third dimension (see Figure 3-7c). The maximum difference between the pressure at the ripple stoss and the crest is 100 Pa higher for the reference case. High pressure fields occur at the first ripple stoss and at ripple stosses downstream of big distances. As for the maximum ripple length, a zone with small pressure between the ripples and the ripple crests was determined. After 10 s the maximum tracer concentration amounts to 13.7%, which is higher than for the reference case. A tracer concentration of less than 1% is observed after 33 s. For case 5 and case 6 a lower retention than for the reference case is noticed. Due to larger distances the tracer mass between the ripples is less protected against the flow.

3.5.7 Comparison of tracer retention based on ripple geometry

The simulations indicated that the ripple geometry has a significant influence on the retention of a passive tracer in surface dead zones. While the special characteristics of each case were discussed in detail before, in this section a comparison is made between cases 1–6. Figure 3-8a shows an overview of the maximum pressure differences across the middle ripple and the maximum concentrations at the middle ripple's toe for each case. In all cases, it was observed that the ripples had a protective function for tracer penetration into the surface dead zone: The maximum tracer concentration that was simulated at the toe of the middle ripple was less than 33% (see Figure 3-8a).

a)

	max. pressure difference across the middle ripple	max. concentration at the middle ripple's toe
Case 1	170 [Pa]	0.032 [-]
Case 2	30 [Pa]	0.115 [-]
Case 3	2130 [Pa]	0.323 [-]
Case 4	670 [Pa]	0.168 [-]
Case 5	680 [Pa]	0.191 [-]
Case 6	360 [Pa]	0.114 [-]

b)

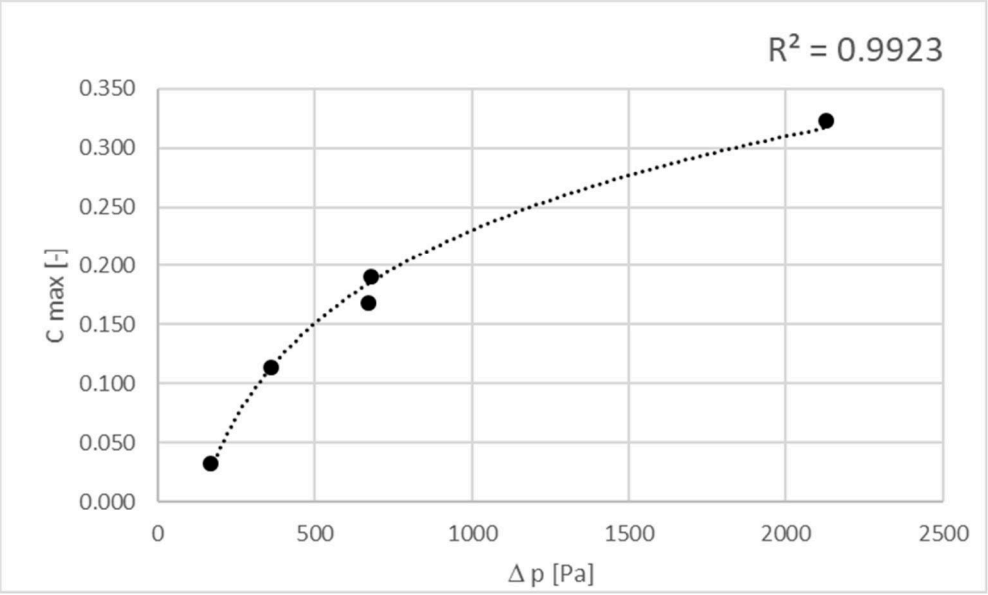

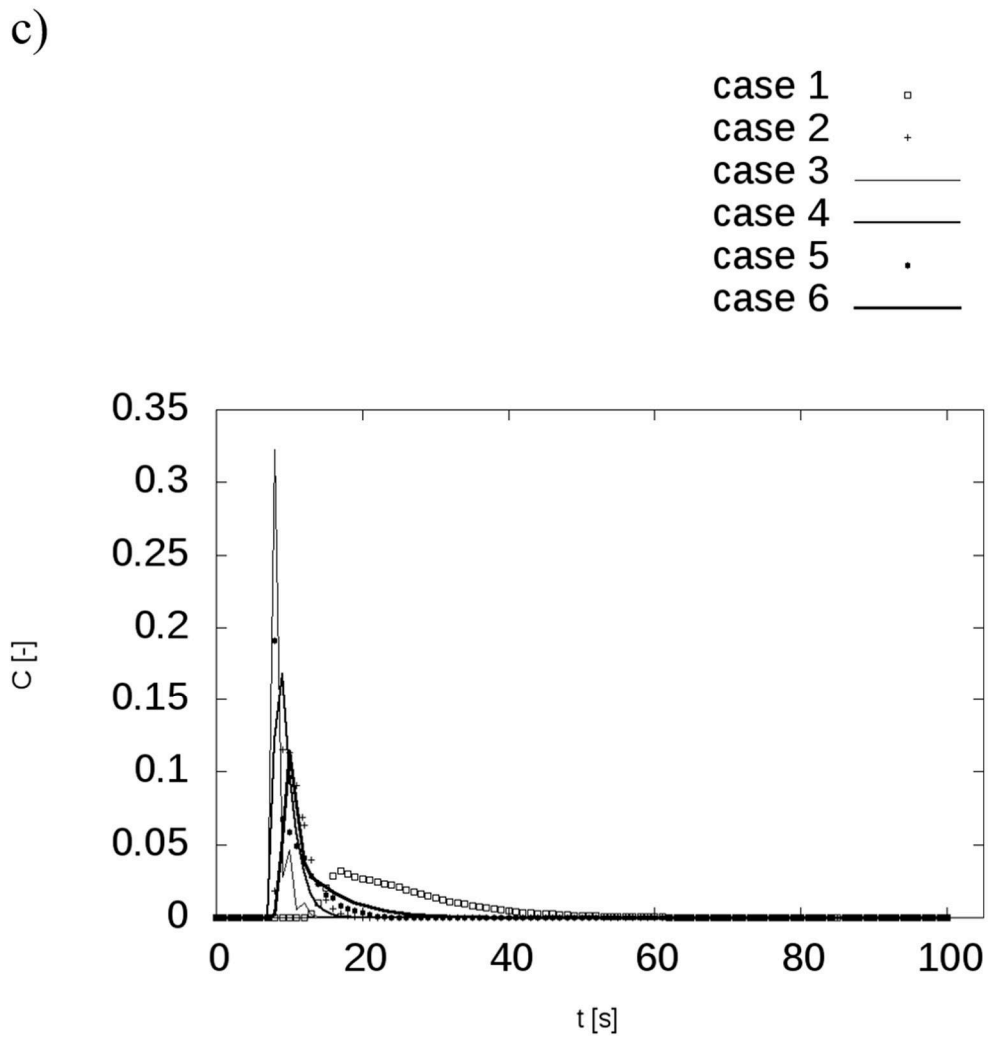

Figure 3-8: Maximum pressure differences and tracer concentrations for the ripples in the middle (a and b) and tracer breakthrough curves for the middle ripple's toe (c) for cases 1–6.

Excluding case 2, the maximum tracer concentrations at the middle ripples' toes increase with the maximum pressure differences across the middle ripples, being strongly related by a R^2 of 0.99 for a logarithmic regression function (see Figure 3-8b). We excluded case 2, with the smallest ripple height and the lowest ripple length. Due to the small ripples, low pressure differences were observed. At the same time the small ripples show a smaller protective role towards the streambed. It might be that a certain threshold has not been reached for this case, which leads to higher tracer concentrations despite low pressure differences. Another explanation could be, that due to the less accelerated flow above the ripples, the tracer has more time to enter the area between the ripples and consequently reaches a higher tracer mass.

Whereas the lowest pressure difference was observed for the smallest ripple (case 2), the maximum pressure difference was measured for the highest ripple (case 3), where the maximum

tracer concentration was noticed as well. But as it can be seen in Figure 3-8c, for this case the retention was comparatively low. Due to the hydraulic jump the tracer disappeared very fast. Moreover, fluctuations of the tracer concentration were determined. For case 5 a relatively large maximum concentration was detected as well. Due to the absence of eddies, the tracer disappears also very fast. The lowest maximum tracer concentration was determined for the reference case (case 1). Also the maximum pressure difference was relatively low compared to the other cases. In case 1 the duration of the tracer to reach the dead zone between the ripples was longest. However, the retention of the tracer was highest in this case (Figure 3-8c). Cases 5 and 6 considered different distances between the ripples (see Figure 3-2). Therefore, the tracer could enter the space between the ripples easier which lead to higher tracer concentration compared to case 1. However, the tracer was less protected and consequently less retention was observed (Figure 3-8c).

3.5.8 Variation of flow rate

Next to the simulations with a mean flow velocity of 1 m/s, a simulation with a mean inlet velocity of 0.5 m/s has been performed using the geometry and water depth of the reference case (see case 7, Figure 3-2). The inlet discharge amounts to 0.25 m^3/s. The velocity distribution seems to be similar to the reference case, but with smaller maximum velocities and larger minimum velocities (max case 1: 1.49 m/s, max case 7: 0.66 m/s, min case 1: −0.525 m/s, min case 7: −0.179 m/s in the x-direction). In z-direction the range is approximately half of the range of the reference case and consequently ranges around the ratio of the inlet velocities for both cases. The maximum pressure was again determined at the first ripple. The maximum pressure difference with 240 Pa is 4.4 times lower than for the reference case with 1060 Pa. A decreasing hyporheic exchange is consequently expected for a lower flow rate.

Due to the lower flow velocity the tracer reaches the rippled area after 12 s. After 18 s the main part of the tracer has passed the rippled area. To compare the tracer distribution of the reference case with a flow velocity of 1 m/s after 10 s for this case with 0.5 m/s the tracer distribution after 20 s is compared. Like in the reference case, the tracer is retained between the ripples. A maximum tracer concentration of 12% is determined at the last ripple, similar to the reference case. After 25 s the maximum tracer concentration in the rippled area amounts to 5%. For the reference case even after 18.5 s the concentration was below this value. It takes 74 s until the tracer concentration is lower than 1%. Following this result, it can be deduced that the flow rate is directly related to the residence time if geometry remains the same. Due to lower pressure gradients lower hyporheic exchange is expected, but at the same time the retention of the tracer

between the ripples is higher. Which influence is higher for a tracer pulse, still has to be investigated including the porous media below.

3.6 Conclusions

Ripples in natural stream flows cause disturbances in the water level and enhance turbulent flows which lead to pressure fluctuations and the generation of recirculation zones between the ripples which cause tracer retention and thus has an impact on hyporheic exchange. Pressure distribution can be used to locate an exchange of stream- and groundwater and pressure gradients provide information about the amount of exchange. Previous transport investigations at the surface water groundwater interface, considered the upper boundary of the hyporheic zone mainly with respect to pressure distributions, the exchange of water and the transport within the ground, but they did not consider tracer retention in surface waters. In this study, the retention of a tracer in a rippled streambed was investigated together with pressure fluctuations, flow fields and the generation of recirculation zones between the ripples. Turbulent two-phase open-channel flow and transport processes over idealized ripples with different geometries and two different flow rates were presented. Next to the variation of ripple heights and lengths, the distance between the ripples varied. The effect of ripple spacing was not studied so far. The high-resolution pressure and flow fields can have an impact on the movement and reaction of compounds like oxygen, carbon, nitrogen-species or contaminants (pesticides) in the hyporheic zone.

The model has been validated with data of two experiments as well as with the help of analytical solutions. The flow characteristics and tracer concentration were successfully reproduced with the computational fluid dynamics model OpenFOAM. The LES turbulence model has proven to be most suitable here and it allows to determine eddies for a certain size directly in three-dimensions.

The simulations verified our hypothesis that the ripple geometry (dimension, length and spacing) has significant influence on the hydraulics of the flow, i.e. flow velocity and pressure fluctuations as well as on the tracer spreading and retention. The main tracer transport occurred above the ripples for all cases, where the flow velocity was comparatively high. Between the ripples increased tracer retention was observed due to small velocities and recirculation zones. For decreasing ripple sizes, pressure gradients and tracer retention time were decreasing. Ripples of a certain size may even cause waves at the water surface due to an undular hydraulic jump with very high pressure gradients. The observed hydraulic jump had a significant effect on the tracer spreading with a significantly reduced retention. The study showed, that turbulence

leads to significant changes of residence times for the tracer between the ripples. No recirculations were determined for the highest ripple length to height ratio which led to a fast disappearance of the tracer, whereas the pressure gradient remained at the same size as in the reference case. Consequently, less tracer mass will flow into the subsurface for ripple geometries where no recirculations occur. For increased ripple distances the recirculation zone expands in the flow direction. More tracer mass reaches the interface, but less retention was determined. Observing lower flow velocities, the pressure gradients decrease whereas the residence time increases due to lower flow velocities. The research showed that the examination of transport processes at the upper boundary including the riverbed morphology is very important for the hyporheic zone. Already small-scale ripples influence whether, where, and for how long a tracer is retained in the surface water dead zones and may enter the subsurface.

For a more precise investigation about the change between surface water and the subsurface, the subsurface must be included. This work is currently underway where the surface water and a part of the river bed soil are modelled using an integral approach.

3.7 Acknowledgements

Most of the simulations were computed on the supercomputers of Norddeutscher Verbund für Hoch- und Höchstleistungsrechnen in Berlin. The funding provided by the German Research Foundation (DFG) within the Research Training Group ‘Urban Water Interfaces’ in project N7 is gratefully acknowledged.

4. Flow simulations for groundwater-surface water interactions at rippled streambeds

This study was published in Water as:

Broecker, T., Teuber, K., Sobhi Gollo, V., Nützmann, G., Lewandowski, J. & Hinkelmann, R. (2019). Integral Flow Modelling Approach for Surface Water-Groundwater Interactions along a Rippled Streambed. Water, 11(7), 1517, https://doi.org/10.3390/w11071517.

This is the postprint version of the article.

The test cases' setups are listed in Appendix B (B1 Seepage through a homogeneous dam with an impervious foundation compared with analytical solutions after Casagrande and Kozeny, B2 Seepage through a homogeneous, rectangular dam with an impervious foundation, B7 Flow simulations for groundwater-surface water interactions at rippled streambeds).

4.1 Abstract

Exchange processes of surface and groundwater are important for the management of water quantity and quality as well as for the ecological functioning. In contrast to most numerical simulations using coupled models to investigate these processes, we present a novel integral formulation for the sediment-water-interface. The computational fluid dynamics (CFD) model OpenFOAM was used to solve an extended version of the three-dimensional Navier–Stokes equations which is also applicable in non-Darcy-flow layers. Simulations were conducted to determine the influence of ripple morphologies and surface hydraulics on the flow processes within the hyporheic zone for a sandy and for a gravel sediment. In- and outflowing exchange fluxes along a ripple were determined for each case. The results indicate that larger grain size diameters, as well as ripple distances, increased hyporheic exchange fluxes significantly. For higher ripple dimensions, no clear relationship to hyporheic exchange was found. Larger ripple lengths decreased the hyporheic exchange fluxes due to less turbulence between the ripples. For

all cases with sand, non-Darcy-flow was observed at an upper layer of the ripple, whereas for gravel non-Darcy-flow was recognized nearly down to the bottom boundary. Moreover, the sediment grain sizes influenced also the surface water flow significantly.

4.2 Introduction

Hyporheic exchange—the exchange of stream and shallow subsurface water—is controlled by pressure gradients along the streambed surface and subsurface groundwater gradients. Over multiple scales, the bedform induced hyporheic exchange was identified as a crucial process for the biogeochemistry and ecology of rivers (Boulton et al., 1998; Brunke & Gonser, 1997; Cardenas, 2015; Dahm et al., 1998; Findlay, 1995; Gomez-Velez et al., 2015; Harvey & Gooseff, 2015; Schaper et al., 2018; Stonedahl et al., 2013; Stonedahl et al., 2010). On large and intermediate scales, stream stage differences, meander loops or bars can generate hyporheic exchange. Accordingly, it is possible to control surface water-groundwater exchange by river stage manipulation e.g., to manage the inflow of saline groundwater into a river (Alaghmand et al., 2014). A decrease of the groundwater level, in turn, impacts surface water infiltration up to a maximum where groundwater and surface water are disconnected. This condition is achieved when the clogging layer does not cross the top of the capillary zone above the water table (Brunner et al., 2009). On small scales, river sediments usually form topographic features such as dunes or ripples. The flowing fluid encounters an uneven surface on the permeable streambed, which results in an irregular pattern in the pressure along that surface and induces hyporheic exchange (Harvey & Bencala, 1993; Winter et al., 1998; Wondzell & Gooseff, 2013). Within theoretical, experimental, and computational studies the general mechanics of the bedform induced hyporheic exchange were examined over the past decades. By manipulating streambed morphology, stream discharge, and groundwater flow, experiments have been used to study driving forces for the hyporheic exchange intensively (Elliott & Brooks, 1997a; Mutz et al., 2007; Packman et al., 2004; Tonina & Buffington, 2007). At submerged structures such as pool-riffle sequences or ripples, turbulences, eddies or hydraulic jumps may occur. Packman et al. (2004), Tonina and Buffington (2009b), Voermans et al. (2017) and other studies showed, that turbulence influences hyporheic exchange and should not be ignored. Facing these complex three-dimensional flow dynamics at the sediment-water interface, it can be challenging to establish suitable flume experiments or field studies. Computational fluid dynamics has proven to be a viable alternative. The majority of these studies have focused on surface-subsurface coupled models. Reasons for the application of different models for the surface and the subsurface are for example the strong temporal variability in streams including relatively high

velocities, whereas the velocities and temporal variabilities in the groundwater are usually several orders of magnitude smaller, leading to different applied equations for the stream and the subsurface. Often, the two computational domains are linked by pressure. Pressure distributions from a surface water model are consequently used for a coupled groundwater model (Bardini et al., 2012; Cardenas & Wilson, 2007a; Chen et al., 2015, 2018; Saenger et al., 2005; Trauth et al., 2013; Trauth et al., 2014). However, also fully coupled models such as the Integrated Hydrology Model (VanderKwaak, 1999) or HydroGeoSphere have already been successfully applied (Alaghmand et al., 2014; Brunner et al., 2009; Brunner & Simmons, 2011). Within these models, open channel flow is described by the two-dimensional diffusion-wave approximation of the St. Venant equations, whereas the three-dimensional Richards equation is used for the subsurface. Water and solute exchange flux terms enable to simultaneously solve one system of equations for both flow regimes.

For many coupled surface-subsurface models, the Darcy law is applied within the sediment. However, especially for coarse bed rivers, this law may cause errors in the presence of non-Darcy hyporheic flow (Packman et al., 2004). Following Bear (1972), the linear assumption of the Darcy law is only valid if the Reynolds number does not exceed a value between 1 and 10. Applying Darcy's law in non-Darcy-flow areas leads to an overestimating of groundwater flow rates (Freeze & Cherry, 1979). Packman et al. (2004) investigated hyporheic exchange through gravel beds with dune-like morphologies and applied the modified Elliot and Brooks model (Packman et al., 2000). They realized that the model did not perform well - among other reasons—due to non-Darcy flow in the near-surface sediment which was not considered in the model. One possible solution to model groundwater in non-Darcy-flow areas is e.g., to use the Darcy-Brinkmann equation instead of the Darcy law. However, there is an additional parameter - the effective viscosity - which has to be determined.

In the present study, an extended version of the three-dimensional Navier–Stokes equations after Oxtoby et al. (2013) is used for the whole system comprising the stream as well as the subsurface. For the application in the groundwater, sediment porosity, as well as an additional drag term, are included into the Navier–Stokes equations. The model is consequently also applicable for high Reynolds numbers within the subsurface where the Darcy law cannot be applied. To our knowledge, this solver was never used for the hyporheic zone before. We apply the new integral solver to evaluate the effect of ripple geometries and surface hydraulics on hyporheic exchange processes, based on the study by Broecker et al. (2018) who investigated free surface flow and tracer retention over streambeds and ripples without considering the subsurface. In Broecker et al. (2018) the three-dimensional Navier–Stokes equations were

solved in combination with an implemented transport equation. In that study, ripple sizes, spacing as well as flow velocities affected pressure gradients and tracer retention considerably. Seven simulation cases were examined varying ripple height, length, distance, and flow rate. The investigated ripple geometries and flow rates are mainly transferred to the present study. Only case 6 is not used for the present study, as the irregular distance between the ripples gave no significant new findings compared to equal distances (Broecker et al., 2018). In contrast to Broecker et al. (2018), the present study examines both free surface flow and subsurface flow. The aim of the present study is to evaluate the impact of ripple dimensions, lengths, spacing and surface velocity on flow dynamics within the hyporheic zone using a new integral model.

4.3 Materials and methods

4.3.1 Geometry and mesh

The analyzed geometry consists of a prismatic domain with a length of 15 m, a width of 1 m and a height of 1.5 m at the inlet and 1 m at the outlet. A weir structure is included in front of the outlet to fix the water level. A rippled area of approximately 3 m is introduced 6 m downstream of the inlet. The model geometry of the reference case with the corresponding initial water depth can be seen in Figure 4-1.

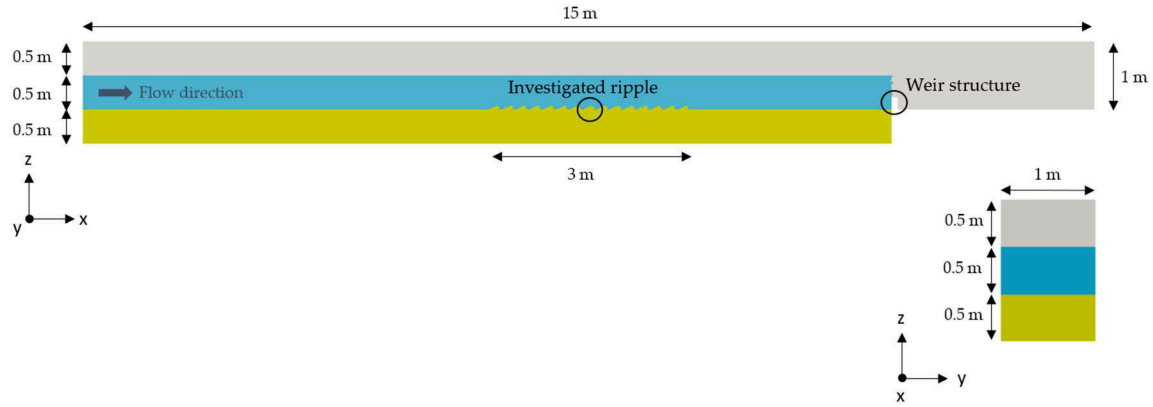

Figure 4-1: Model geometry and initial condition for the water level (sediment: yellow, water: blue, air: grey); top: front view, bottom right: cross-section.

The mesh has been discretized using the three-dimensional finite element mesh generator gmsh. The ripple parameters are based on the approach of Broecker et al. (2018). Table 4-1 summarizes the most important ripple parameter values. Unstructured elements were chosen in the *x*-*z*-plane to depict the curved profile of the ripples. Thereafter the elements have been extruded with 10 layers in the *y*-direction to produce a three-dimensional mesh. Different

meshes with similar mesh conditions have been created for the varying ripple geometries. Smaller element sizes were chosen for surface water and the subsurface, as detailed processes in the air phase are not of interest for the present study. The air phase was only included to account for water level fluctuations which showed to have a significant effect on the pressure distribution at the streambed (Broecker et al., 2018). The mesh resolution has been examined by calculating the fraction of the turbulent kinetic energy in the resolved motions after Pope (2004), who suggest to resolve 80% of the turbulent kinetic energy for a well resolved large eddy simulation (LES). In our simulation we are around this range with 75–83% resolution for the water phase with the applied meshes using the LES turbulence model (see section 4.3.3). Lower resolutions were observed for the air-phase, which is not of interest for our simulations.

Table 4-1: Simulation cases including ripple geometries and flow rates.

Case	**1 (Reference Case)**	**2**	**3**	**4**	**5**	**6**
ripple height (cm)	5.6	1.4	11.2	5.6	5.6	5.6
ripple length (cm)	20	5	40	40	20	20
ripple distance (cm)	0	0	0	0	20	0
flow rate (m^3/s)	0.5	0.5	0.5	0.5	0.5	0.25

4.3.2 Numerical model

To simulate exchange processes of surface water and groundwater, the open source software Open Source Field Operation and Manipulation (OpenFOAM) version 2.4.0 has been used. A solver called ‘porousInter’ has been applied. This solver was developed by Oxtoby et al. (2013) and is based on the interFoam solver by OpenFOAM. PorousInter is a multiphase solver for immiscible fluids and extends the three-dimensional Navier–Stokes equations by the consideration of soil porosity and effective grain size diameter. For our simulations two phases—water and air—are considered to allow water level fluctuations. Since the porousInter–solver does not account for the solid fraction of the soil, values that are represented by $[\ ]^f$ are averaged only over the pore space volume. The conservation of mass and momentum are defined after Oxtoby et al. (2013) as:

Mass conservation equation

$$\varphi \nabla \cdot \left[\vec{U}\right]^f = 0 \tag{4.1}$$

Momentum conservation equation

$$\varphi\left(\frac{\partial [\rho]^f \left[\vec{U}\right]^f}{\partial t} + \left[\vec{U}\right]^f \cdot \nabla([\rho]^f \left[\vec{U}\right]^f)\right) = -\varphi \nabla [p]^f + \varphi [\mu]^f \nabla^2 \left[\vec{U}\right]^f + \varphi [\rho]^f \vec{g} + D \tag{4.2}$$

where φ is the soil porosity (-); $\vec{U}$ is the velocity (m/s); ρ is the density (kg/m^3); t is time (s); p is pressure (Pa); μ is the dynamic viscosity (Ns/m^2), g is the gravitational acceleration (m/s^2) and D an additional drag term (kg/(m^{2}s^2)). The drag term was developed by Ergun (1952) and accounts for momentum loss by means of fluid friction with the porous medium and flow recirculation within the sediment. To consider flow recirculation, an effective added mass coefficient is included after van Gent (1995). The porous drag term is defined as:

$$D = -\left(150\frac{1-\varphi}{d_p \varphi}[\mu]^f + 1.75[\rho]^f \left[\vec{U}\right]^f\right)\frac{1-\varphi}{d_p}\left[\vec{U}\right]^f - 0.34\frac{1-\varphi}{\varphi}\frac{[\rho]^f \partial \left[\vec{U}\right]^f}{\partial t} \tag{4.3}$$

with d_p (m) as effective grain size diameter.

PorousInter uses the Volume of Fluid (VoF) approach. Consequently, multiple phases are treated as one fluid with changing properties (Hirt & Nichols, 1981). The indicator fraction α (-) varies between zero for the air phase and one for the water phase. The water-air interface is captured by a convective transport equation:

$$\varphi \frac{\partial [\alpha]^f}{\partial t} + \varphi \nabla \cdot ([\alpha]^f \left[\vec{U}\right]^f) = 0 \tag{4.4}$$

The dynamic viscosity and the density of each fluid are calculated according to their fraction as:

$$\mu = \alpha \mu_w + \mu_a (1-\alpha) \tag{4.5}$$

$$\rho = \alpha \rho_w + \rho_a (1-\alpha) \tag{4.6}$$

The subscripts ‘w’ and ‘a” denote the fluids water and air.

4.3.3 Turbulence

Turbulent properties have been captured by a large eddy simulation (LES) turbulence model (see also section 4.4.1). Eddies up to a certain size were consequently directly resolved, whereas

for small eddies a subgrid model is used. For the present study, the Smagorinski subgrid scale model (Smagorinsky, 1963) has been applied.

A measure $M(\vec{x},t)$ for the turbulence resolution was calculated after Pope (2004):

$$M(\vec{x},t) = \frac{k_r(\vec{x},t)}{K(\vec{x},t)+k_r(\vec{x},t)} \quad 4.7$$

where $K(\vec{x},t)$ defines the turbulent kinetic energy of the resolved motions by:

$$K(\vec{x},t) = \frac{1}{2}(\vec{U}-\vec{U}_{mean})(\vec{U}-\vec{U}_{mean}) \quad 4.8$$

and $k_r(\vec{x},t)$ defines the turbulent kinetic energy of the residual motions. The solver by Oxtoby et al. (2013) had to be adjusted to write $k_r(\vec{x},t)$ automatically. $K(\vec{x},t)$ and $k_r(\vec{x},t)$ were calculated and averaged for the whole running time. A measure $M(\vec{x},t) = 0.25$ corresponds to a resolution of 75% of the turbulent kinetic energy.

4.3.4 Boundary and initial conditions

Figure 4-2 shows the most important boundary conditions. The inlet of the boundary is divided into two fractions: for the air and for the water phase. The parameter α is fixed accordingly at the inlet. For the water phase the discharge is set to 0.5 m^3/s for case 1–5 and to 0.25 m^3/s for case 6, whereas for the air phase a total pressure condition is defined with a total pressure of 0 Pa. The total pressure condition specifies the given total pressure for outflow and the dynamic pressure subtracted from the total pressure for inflow. Next to the air phase at the inlet, the total pressure definition is applied for the upper boundary and at the outlet. The streambed is surrounded by walls. Consequently, the velocity is set to 0 m/s with a no flow condition.

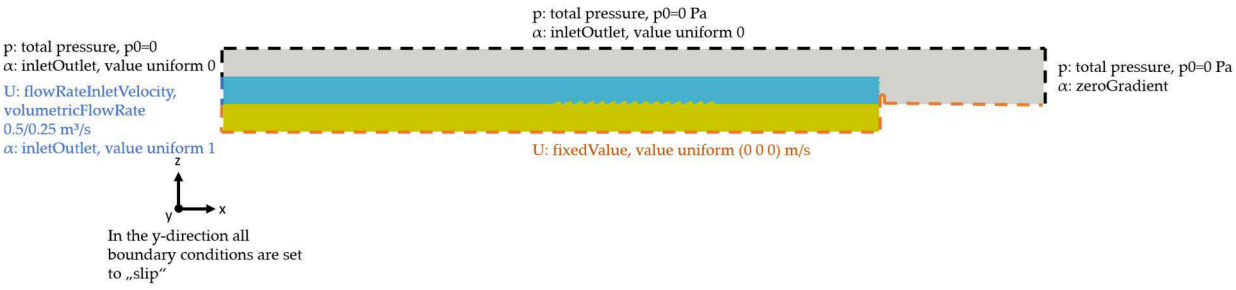

Figure 4-2: Boundary conditions.

In OpenFOAM a definition of a constant water level at the outlet is challenging (Thorenz & Strybny, 2012). Therefore, a weir structure is established as a barrier to keep a constant water level for our model. The water flows freely over the weir top. Behind the weir, the water level

decreases before it flows out of the model. This method is described e.g., in Bayon-Barrachina and Lopez-Jimenez (2015). For case 1–5 and case 6 different heights for the weir structure were chosen, since the water level is affected by the flow rate of the surface water. For the weir structure and at the whole bottom of the model, an impervious no slip condition is used. All boundary conditions in the third dimension contain slip conditions.

For the sediment, two materials are chosen: coarse sand with a grain size diameter of 2 mm and medium gravel with a grain size diameter of 1.5 cm. Both sediments have an effective porosity of 0.25 and are considered to be homogeneous. According to Freeze and Cherry (1979) coarse sand has a hydraulic conductivity of about 10^{-2} m/s and medium gravel of about 10^{-1} m/s. These values are only estimations and are not considered in our simulations. An initial water level of 1 m is set from the inlet up to the weir structure (see Figure 4-1).

4.3.5 Validation

To ensure reliable behavior of the integral model concerning the hydraulics for the interaction of groundwater and surface water, the solver was tested based on two applications. The seepages through dams with different water levels and dam geometries were compared with numerical and analytical solutions.

First, flow through a rectangular dam with a constant water level at both sides was investigated. The dam width amounts to 16 m and the dam height to 24 m. The dam height is equal to the water level at the left side of the dam. A median grain size diameter of 2 mm and a porosity of 0.25 were defined which correspond to a sandy dam filling. At the right hand, the water level is fixed to 4 m. The seepage through the dam was compared with two numerical solutions after Westbrook (1985) and Aitchison and Coulson (1972) and with a one-dimensional (Kobus & Keim, 2001) as well as with a two-dimensional analytical solution after Di Nucci (2015) (see Figure 4-3). The seepage calculated with the integral solver was in between the two-dimensional analytical solution after Di Nucci (2015) and the numerical solutions after Westbrook (1985) and Aitchison and Coulson (1972). A large deviation was recognized for the one-dimensional solution. Based on the two-dimensional velocities observed in the numerical simulation, an analytical one-dimensional solution is obviously not adequate.

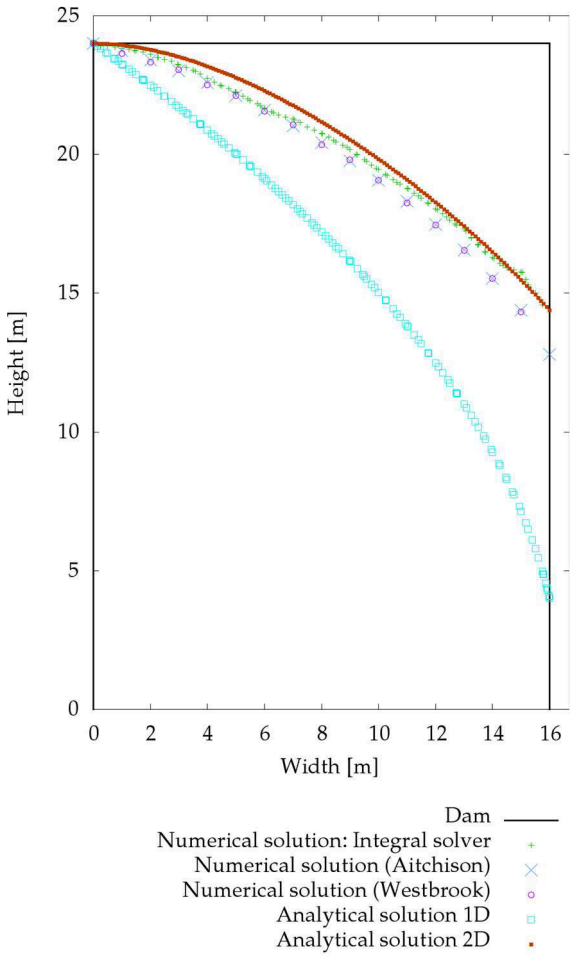

Figure 4-3: Seepage calculated with 1D and 2D analytical and numerical solutions for a rectangular dam.

For the second validation case, the seepage through a homogeneous dam with a constant water level of 1.9 m on the left side was compared with an analytical solution by Kozeny (Lattermann, 2010) and an analytical solution by Casagrande (1937). The latter is an improvement of the solution by Kozeny. The dam has a height of 2.2 m and a width of 8.7 m. The two-dimensional mesh consists of 750,000 rectangular elements with a width of 0.02 m in x-and y-direction. The dam material properties were the same as in the first validation case. A good agreement can be recognized for the simulated water levels with the calculated analytical data (see Figure 4-4). At the entrance and at the outlet, the results gained with the integral model were closer to the solution after Casagrande (1937) compared to the solution after Kozeny.

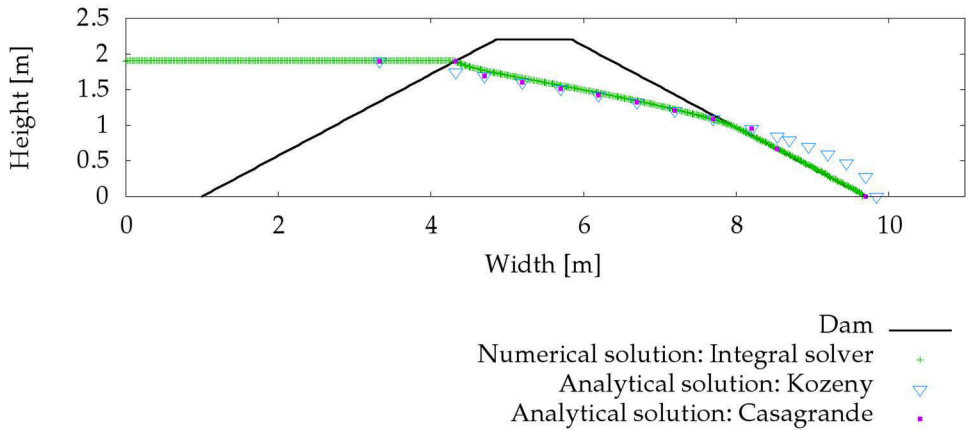

Figure 4-4: Seepage through a homogeneous dam after Kozeny (Kobus & Keim, 2001), Casagrande (1937) and calculated with the integral solver.

Our test simulations showed that the integral flow model can predict the interaction of surface and groundwater with reasonable accuracy compared to analytical and numerical solutions.

4.4 Results and discussion

In the following section, results for the reference case (see Table 4-1, case 1) will be presented for both sandy and gravel sediments. Based on these results, the influence of the different ripple parameters and surface water discharge on the flow field will be analyzed, including pressure and velocity distributions as well as hyporheic exchange fluxes after 5 min simulation time. For all cases we focused on a single ripple in the center of a series of ripples. For the quantification of the fluxes, fluxes through the cell faces at the investigated ripple are calculated at the intersections of surface water and sediment. The ripple is divided into an area left and right from the ripple crest (see Figure 4-5). In- as well as outflowing fluxes for both sides as well as the sum of these fluxes divided by the face area—defined as 'total flux"—are determined. The fluxes are averaged for the time frame of 60–300 s due to non-steady flow conditions.

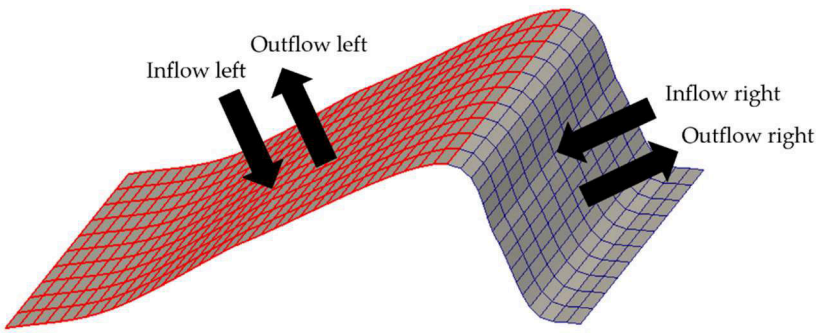

Figure 4-5: In- and outflowing fluxes at the left and right side of the ripple crest.

4.4.1 Reference case

For the reference case (see Table 4-1, case 1), the discharge amounts to 0.5 m^3/s, the ripple length to 20 cm and the height to 5.6 cm. Figure 4-6 shows the pressure distribution and velocity vectors at the investigated ripple (see Figure 4-1) for case 1 with a sandy and a gravel sediment. The solver solves the pressure term p_rgh as the static pressure minus the hydrostatic pressure (ρgz with z as coordinate vector). The highest pressure is observed at the last third of the upstream face of the ripple. Low pressure is present at the ripple crest and the first two-thirds of the upstream face as well as downstream the crest. As these pressure differences lead to hyporheic exchange, flow occurs in downstream and upstream directions from high to low pressure. The described flow paths fit well to the results by Fox et al. (2014), where the exchange of water between surface and subsurface was illustrated based on tracer experiments in the laboratory at a rippled sandy streambed. Also Thibodeaux and Boyle (1987), Elliott and Brooks (1997a) and Janssen et al. (2012) came to similar results from laboratory experiments with triangular bedforms. Fehlman (1985) and Shen et al. (1990) presented non-hydrostatic pressure distributions at triangular bed forms which were also similar to our results with pressure peaks at the middle of the stoss face, pressure minimum at the crest with low pressure remaining at the lee face until the pressure increases again at the stoss face of the following ripple. The description of the principal pressure pattern at the observed ripple in our simulations is valid for the sand as well as for the gravel, though the pressure values differ. Due to the higher resistance of the sand compared to gravel, higher pressure gradients are observed. Conversely, it behaves in terms of subsurface velocities: higher velocities are determined in the gravel sediment compared to the less permeable sand.

The applied LES turbulence model allows to resolve large parts of the turbulence at the streambed directly. Hence, between each ripple pair, eddies are identified. Comparing Figure 4-6 left and Figure 4-6 right, it is obvious, that the flow field in the surface water depends on the properties of the sediment: While in the sand, two eddies (clockwise as well as counterclockwise) can be recognized between the ripples, for the gravel only one eddy is apparent which flows in clockwise direction. This indicates, that a simple successively coupling via pressure distributions from surface water as a boundary condition for a groundwater model as for the example in Trauth et al. (2013); Trauth et al. (2014) is not adequate, since not only the surface water influences the subsurface, but also the subsurface affects the surface flow conditions. The feedback from the subsurface to the surface is consequently also important. The clockwise eddies are located in the area where surface water introduces into the ripple, while

the counterclockwise ripple is located in the area where the water within the ripple flows back to the surface water.

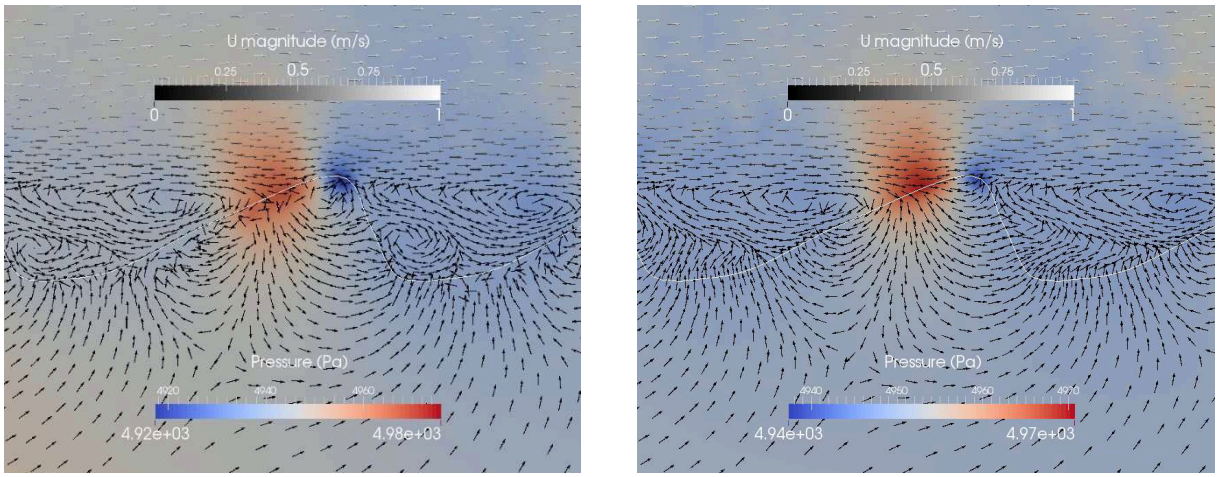

Figure 4-6: Pressure distribution and velocity vectors at a sandy (left) and gravel (right) ripple for case 1 (Table 4-1). The white line indicates the sediment-water interface. The colors indicate the pressure distribution. Please note that the scaling is different in the right and the left panel. The arrows indicate flow directions of the surface and the subsurface flow. To visualize the intensity of the flow U a grey is used.

Table 4-2 and Table 4-3 show the in- and outflowing fluxes for all cases as well as the total fluxes per ripple area for gravel and sand according to Figure 4-5. As described already above, in- as well as outflow are observed at the ripple lee while at the ripple stoss the outflow is dominant. The total flux is much higher for the gravel with 1.8×10^{-2} $m^3/s/m^2$ than for the sand with 2.7×10^{-3} $m^3/s/m^2$. This fits to the flume experiment results by Tonina and Buffington (2007), where larger hyporheic exchange was claimed for gravel compared to sandy sediments.

Table 4-2: Hyporheic fluxes of a single ripple in the center of a series of ripples for case 1–6 (sand). Right and left indicate the part of the ripple right and left of the ripple crest (compare Figure 4-5).

Case	Inflow Left (m^3/s)	Inflow Right (m^3/s)	Inflow Sum (m^3/s)	Outflow Left (m^3/s)	Outflow Right (m^3/s)	Outflow Sum (m^3/s)	Total Flux [1] ($m^3/s/m^2$)
1	2.9×10^{-4}	3.8×10^{-5}	3.3×10^{-4}	2.1×10^{-4}	1.2×10^{-4}	3.3×10^{-4}	2.7×10^{-3}
2	1.4×10^{-4}	6.3×10^{-6}	1.4×10^{-4}	3.7×10^{-5}	1.3×10^{-4}	1.6×10^{-4}	5.1×10^{-3}
3	6.6×10^{-4}	5.3×10^{-5}	7.2×10^{-4}	4.9×10^{-4}	2.4×10^{-4}	7.3×10^{-4}	3.0×10^{-3}
4	4.0×10^{-4}	6.1×10^{-5}	4.6×10^{-4}	3.3×10^{-4}	1.6×10^{-4}	4.9×10^{-4}	2.2×10^{-3}
5	4.2×10^{-4}	6.0×10^{-5}	4.8×10^{-4}	1.7×10^{-4}	2.9×10^{-4}	4.6×10^{-4}	3.9×10^{-3}
6	1.2×10^{-4}	2.0×10^{-5}	1.4×10^{-4}	9.6×10^{-5}	4.8×10^{-5}	1.4×10^{-4}	2.9×10^{-4}

[1] Total flux = (mag (inflow left) + mag (inflow right) + mag (outflow left) + mag (outflow right))/area.

Table 4-3: Hyporheic fluxes of a single ripple in the center of a series of ripples for case 1–6 (gravel). Right and left indicate the part of the ripple right and left of the ripple crest (compare Figure 4-5).

Case	Inflow Left (m^3/s)	Inflow Right (m^3/s)	Inflow Sum (m^3/s)	Outflow Left (m^3/s)	Outflow Right (m^3/s)	Outflow Sum (m^3/s)	Total Flux [1] ($m^3/s/m^2$)
1	2.2×10^{-3}	2.5×10^{-5}	2.2×10^{-3}	1.0×10^{-3}	1.2×10^{-3}	2.2×10^{-3}	1.8×10^{-2}
2	5.6×10^{-4}	2.9×10^{-5}	5.9×10^{-4}	1.6×10^{-4}	3.7×10^{-4}	5.2×10^{-4}	1.8×10^{-2}
3	4.5×10^{-3}	3.8×10^{-5}	4.6×10^{-3}	1.5×10^{-3}	2.1×10^{-3}	3.6×10^{-3}	1.7×10^{-2}
4	3.5×10^{-3}	0	3.5×10^{-3}	2.0×10^{-3}	1.9×10^{-3}	3.9×10^{-3}	1.7×10^{-2}
5	3.6×10^{-3}	0	3.6×10^{-3}	8.4×10^{-4}	2.2×10^{-3}	3.1×10^{-3}	2.7×10^{-2}
6	9.3×10^{-4}	1.4×10^{-5}	9.4×10^{-4}	4.6×10^{-4}	5.2×10^{-4}	9.8×10^{-4}	1.9×10^{-3}

[1] Total flux = (mag (inflow left) + mag (inflow right) + mag (outflow left) + mag (outflow right))/area.

Based on the overall high velocities within the sediment our simulations indicate, that non-Darcy-flow is present in the whole ripple nearly down to the bottom boundary for the gravel bed and to a part of the sandy bed (see Figure 4-7). At the near-surface area at the crest of the gravel ripple, Reynolds numbers up to 1770 were recognized, while for the sandy bed Reynolds numbers up to 330 were determined. For a better illustration of the non-Darcy-flow areas, Reynolds numbers up to 10 are illustrated in Figure 4-7. Consequently, dark red areas have a Reynolds number that equals or is higher than 10. Due to lower permeability, the flow velocities of the surface water influenced the sandy sediment less than the gravel bed with high

permeability. The explicit modelling of the hyporheic zone with Darcy's law is not possible in river beds with such coarse grain sizes since groundwater flow rates would be overestimated. Facing e.g., contaminant transport depending on residence time serious misperceptions could appear. The Reynolds number distribution of the following cases were similar to the reference case: for the whole gravel ripple down to the bottom non-Darcy-flow is apparent, while for the sand a small layer at the interface as well as the crest shows non-Darcy-flow areas. Only for case 5 with a distance of 20 cm between each ripple, there is even more non-Darcy-flow within the sandy ripple.

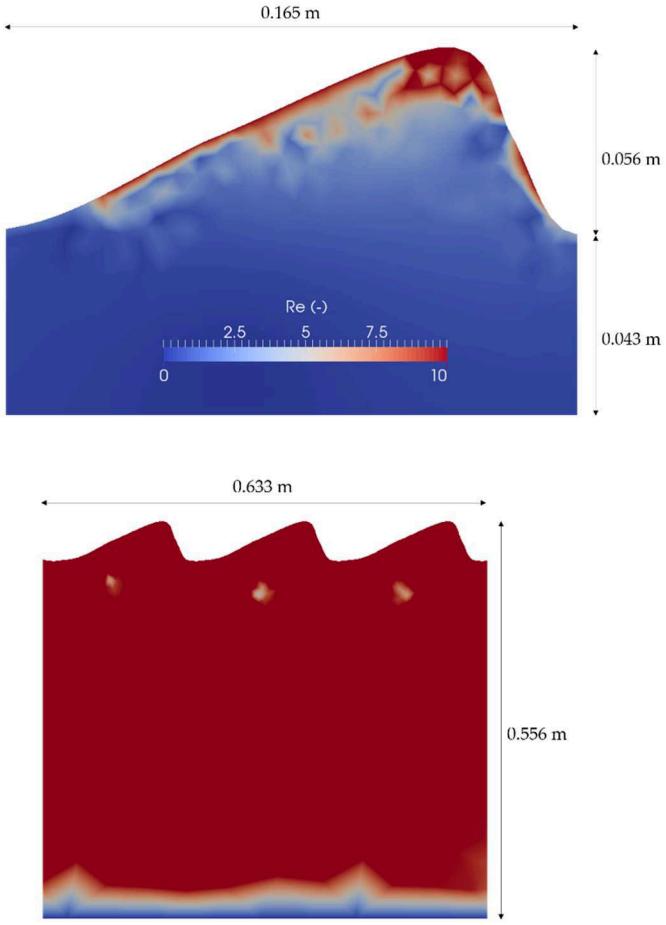

Figure 4-7: Reynolds numbers at a sandy (top) and gravel (bottom) ripple for case 1 (Table 4-1).

Janssen et al. (2012) stated that the largest discrepancies of most CFD simulations of flow over ripples and dunes occur in the eddy zone. Especially for Reynolds-averaged Navier–Stokes turbulence models this is a known weakness. Therefore, we have chosen a LES turbulence model. At the same time, we are aware of the computational limitation, which is additionally increased by the calculation of the three-dimensional Navier–Stokes equations in the sediment

in contrast to the commonly applied Darcy law. However, facing the growing availability of computational sources and the observed non-Darcy-flow areas in the investigated cases, we apply a promising tool for analyzing integral surface-subsurface flow processes with high-resolution.

4.4.2 Ripple dimension

For cases 2 and 3 the ripple length to height ratio is the same as for the reference case (see Table 4-1), but the ripple height and length are quartered for case 2 and doubled for case 3. Figure 4-8 shows the velocity and pressure distributions for the investigated ripples in the middle for case 2 for sand and gravel. The general pressure pattern for case 2 for sand and gravel as well as for the reference case are similar: the lowest pressure occurs at the crest and the highest pressure upstream of the crest. But the high-pressure area related to the ripple size is much higher for case 2 than for the reference case. Related to the ripple face area at the interface, we consequently expect higher inflow rates compared to the reference case, which can be seen in Table 4-2 and Table 4-3. The total flux per area is higher for case 2 with 5.1×10^{-3} $m^3/s/m^2$ and 1.81×10^{-2} $m^3/s/m^2$ than for the reference case with 2.7×10^{-3} $m^3/s/m^2$ and 1.84×10^{-2} $m^3/s/m^2$.

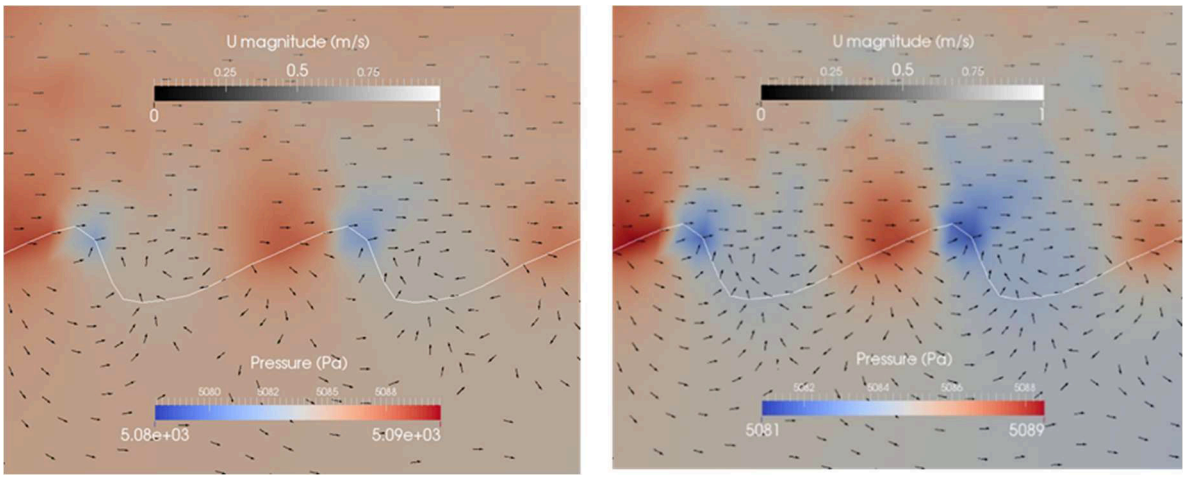

Figure 4-8: Pressure distribution and velocity vectors at a sandy (left) and gravel (right) ripple for case 2 (Table 4-1). The white line indicates the sediment-water interface. The colors indicate the pressure distribution. Please note that the scaling is different in the right and the left panel. The arrows indicate flow directions of the surface and the subsurface flow. To visualize the intensity of the flow U a grey is used.

The flow field within the ripple is again directed upstream and downstream from the point of highest pressure. For both simulations (case 2 sand and gravel) only one eddy was recognized in a clockwise direction. For case 3 high turbulence was recognized between

the ripples with up to five eddies (see Figure 4-9). Significantly high- and low-pressure areas are recognized in the turbulent phase of the surface area especially for the simulation with sandy sediment. For this simulation two instead of one inflow area can be recognized at the upstream face of the ripple. Between these inflow areas, there is an outflow area. Another outflow area is located upstream of the lower inflow area, but the main outflow occurs downstream of the ripple crest. In the simulation of the gravel ripple, less eddies are observed than for the simulation with the sand. For the gravel ripple only one inflow area is present. The outflow is located similar to case 1 and 2: upstream from the inflow area and downstream from the crest.

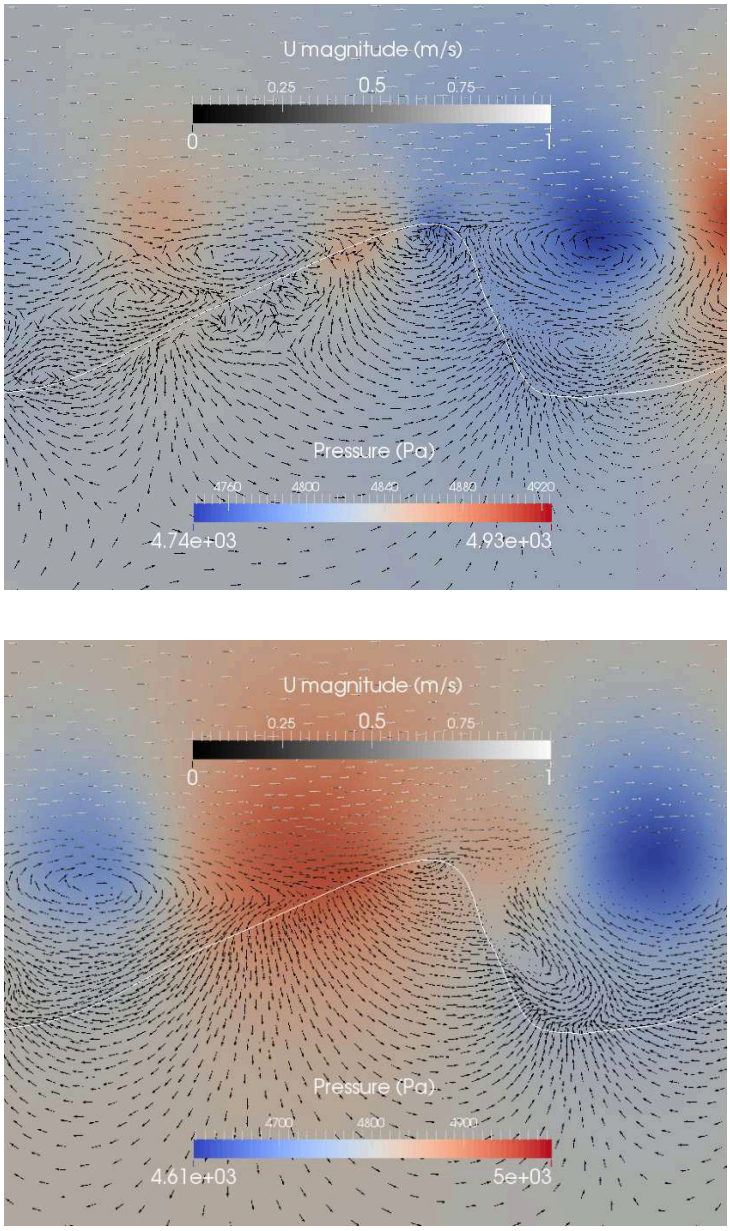

Figure 4-9: Pressure distribution and velocity vectors at a sandy (top) and gravel (bottom) ripple for case 3 (Table 4-1). The white line indicates the sediment-water interface. The colors indicate

the pressure distribution. Please note that the scaling is different in the right and the left panel. The arrows indicate flow directions of the surface and the subsurface flow. To visualize the intensity of the flow U a grey is used.

The total fluxes per area are bigger for case 3 with sand (3.0×10^{-3} $m^3/s/m^2$) compared to the reference case (case 1) with sand (2.7×10^{-3} $m^3/s/m^2$). For the gravel the opposite is true (case 3: 1.7×10^{-2} $m^3/s/m^2$ and case 1: 1.8×10^{-2} $m^3/s/m^2$). The extremely high turbulence between the ripples for the sand could be an explanation for that. The results for cases 2 and 3 with gravel and sand show, that a general statement about the influence of the ripple size is not possible, as there is a complex relation between the size and the material leading to different turbulence and pressure distributions, where also a threshold can be conceivable. Tonina and Buffington (2007) presented results from a laboratory experiment with a pool-riffle channel and came to the same conclusion that hyporheic exchange does not necessarily decrease with lower bed form amplitudes. Closer investigations with more simulations including additional ripple size variations would be necessary for a more profound interpretation.

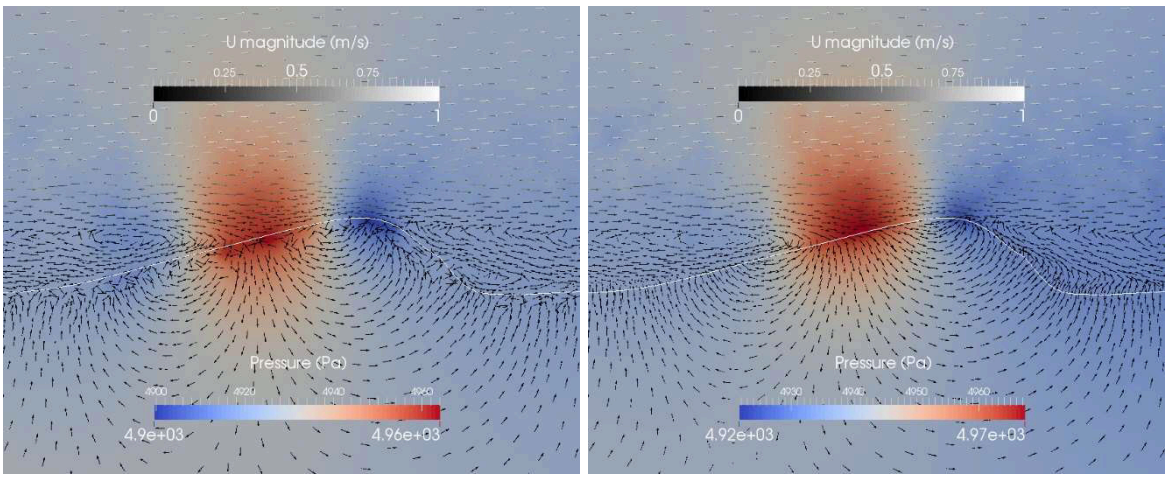

Figure 4-10: Pressure distribution and velocity vectors at a sandy (left) and gravel (right) ripple for case 4 (Table 4-1). The white line indicates the sediment-water interface. The colors indicate the pressure distribution. Please note that the scaling is different in the right and the left panel. The arrows indicate flow directions of the surface and the subsurface flow. To visualize the intensity of the flow U a grey is used.

4.4.3 Ripple length

For case 4 the ripple height equals the reference case, but the ripple length is doubled with 40 cm. This leads to less turbulence between the ripples (compare Figure 4-6 and Figure 4-10). The bigger area leads to higher fluxes per ripple, but the total flux per area is smaller compared to the reference case for sand as well as for gravel (case 4: 2.2×10^{-3} $m^3/s/m^2$ and 1.7×10^{-2} $m^3/s/m^2$, case 1: 2.7×10^{-3} $m^3/s/m^2$ and 1.8×10^{-2} $m^3/s/m^2$). The pressure distribution is very similar to the reference case (case 1). The decisive difference is probably again the turbulence, which is higher for large height-to-length-ratios as already described by Broecker et al. (2018).

4.4.4 Ripple distance

Figure 4-11 shows the velocity and pressure distributions for case 5 with the same ripple geometry as for the reference case, but with a distance between the ripples of 20 cm. This distance leads to higher pressure gradients for gravel and sand compared to the reference case. The flow fields within the ripples are similar to the reference case. But for this case there are also in- and outflow areas at the flat streambed between the ripples for both simulations. Eddies occur between the investigated ripples, but due to the distance, they are more elongated than for the reference case (case 1). Since the pressure gradients are higher for case 5 compared to the reference case and the area is the same for both cases, (the area is only the ripple area, not the flat part between the ripples) the total flux is higher for gravel as well as for sand compared to the reference case with both sediments (case 5: 3.9×10^{-3} $m^3/s/m^2$ and 2.7×10^{-2} $m^3/s/m^2$, case 1: 2.7×10^{-3} $m^3/s/m^2$ and 1.8×10^{-2} $m^3/s/m^2$). Broecker et al. (2018) already presumed higher hyporheic exchange for this case compared to the reference case, based on the higher pressure gradients. To our knowledge, distances between the ripples were never investigated so far for hyporheic zone processes, apart from Broecker et al. (2018) where only a surface water model was used.

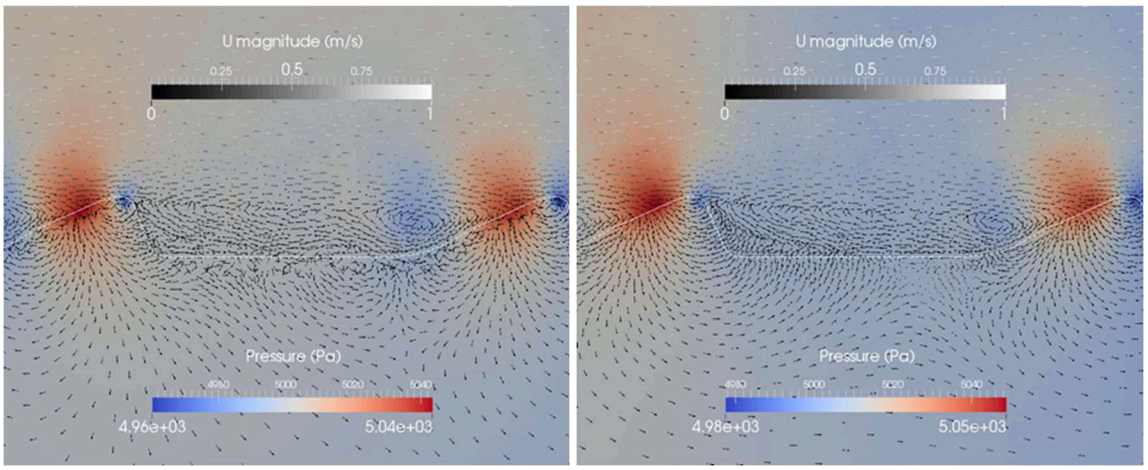

Figure 4-11: Pressure distribution and velocity vectors at a sandy (left) and gravel (right) ripple for case 5 (Table 4-1). The white line indicates the sediment-water interface. The colors indicate the pressure distribution. Please note that the scaling is different in the right and the left panel. The arrows indicate flow directions of the surface and the subsurface flow. To visualize the intensity of the flow U a grey is used.

Compared to the investigated sandy ripples described above, the non-Darcy-flow areas of case 5 are significantly larger (compare Figure 4-7 and Figure 4-12). Due to the distance between the ripples, higher velocities reach the ripple stoss which influence the velocities within the ripple.

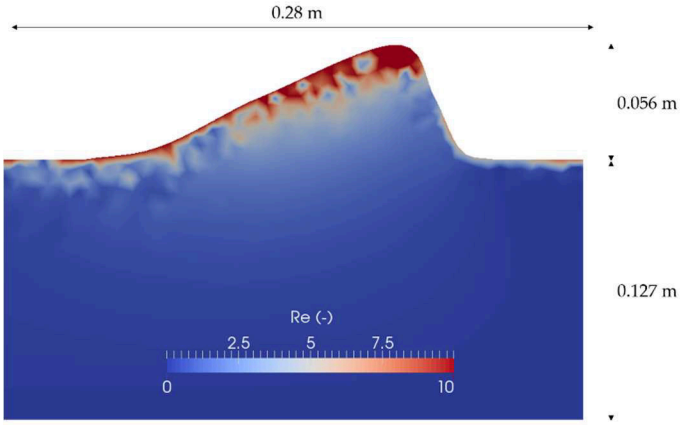

Figure 4-12: Reynolds numbers at a sandy ripple for case 5.

4.4.5 Flow rate

For case 6 the discharge was set to 0.25 m^3/s (for case 1–5 the discharge was 0.5 m^3/s). The ripple geometry is the same as for the reference case (case 1). Comparing the reference case with case 6, it is obvious that both flow discharges show qualitatively similar flow fields. The flow velocities within the ripples decrease due to lower surface water velocities. Nevertheless, there is still a layer with Reynolds numbers higher than 10, which is slightly smaller than for the reference case (see Figure 4-13). The hyporheic fluxes are decreased compared to the reference case (case 6: 2.9×10^{-4} $m^3/s/m^2$ and 1.9×10^{-3} $m^3/s/m^2$, case 1: 2.7×10^{-3} $m^3/s/m^2$ and 1.8×10^{-2} $m^3/s/m^2$). This fits with laboratory observations e.g., by Marion et al. (2002) and Elliott and Brooks (1997a).

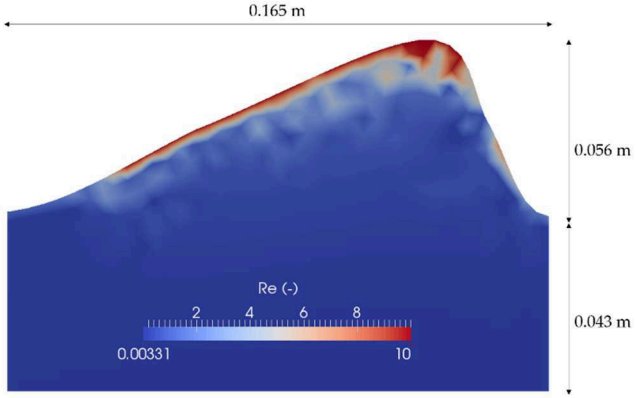

Figure 4-13: Reynolds numbers at a sandy ripple for case 6.

4.5 Conclusions

CFD simulations were designed to simultaneously examine both surface and subsurface flow processes with an extended version of the three-dimensional Navier–Stokes equations. Based on two simulations for seepages through dams, it was shown that the applied model can describe the interaction of groundwater and surface water. The validated CFD model was applied to investigate the impact of bed form structures, grain sizes and surface flow discharges on hyporheic exchange processes. The examined ripple structures changed the streambed pressure and created in- and outflowing fluxes at the interface which were calculated for each case study for a representative ripple in the middle and play a significant role in biogeochemical processes within the hyporheic zone. It was shown that not only the surface water influences the flow within the sediment, but also the sediment properties lead to a change of the flow field within the surface water. Consequently, we claim, that a simple coupling of surface water with a closed boundary at the streambed, which is commonly used, is not appropriate at least for coarse

sediments. Moreover, non-Darcy-flow areas were observed for all cases within the sediment. For the sandy sediment, the non-Darcy-flow areas are restricted to the upper layer and the crest of the investigated ripples. For the gravel non-Darcy-flow was observed almost down to the bottom of the model. The application of the Darcy law in these areas would lead to an overestimation of flow rates. For equations that can be applied in non-Darcy-flow areas in the subsurface such as the Darcy-Brinkmann-equation, additional parameters such as the effective viscosity have to be determined.

Comparing the extended Navier–Stokes equations with the commonly used coupling of surface water with a Darcy-law-model, the integral model is definitely more time consuming than the coupled models. The model shows direct feedbacks from surface to subsurface and vice versa, is applicable also in non-Darcy-flow areas and provides high-resolution results. The applied LES turbulence model gives additional insights about the turbulence at the interface which has a high impact on hyporheic exchange.

The general flow paths were the same for almost all simulations. Upstream of the crest, in high pressure areas, surface water flows into the ripple. Subsurface water flows out of the ripple towards the crest as well as upstream of the inflow area. Only for the ripple with the highest dimension multiple inflow areas were recognized upstream of the crest. Higher turbulences were generally observed for sandy ripples compared to gravel ripples. Gravel ripples always showed higher hyporheic exchange fluxes compared to sand ripples. Three ripple dimensions with the same height to length ratios were examined, but no clear relationship to exchange fluxes was found. For longer ripples, the exchange was slightly smaller due to less turbulence, while distances between the ripples increased the hyporheic exchange fluxes drastically. Also, in the flat streambed sections exchange was observed. Decreasing flow rates lead to decreasing exchange fluxes.

Numerous of the observations of our simulations were already seen in laboratory experiments. Our simulations allowed to get a deeper understanding of the present velocity and pressure distribution at the interface and to determine in- and outflowing fluxes, which can be important for the understanding and prediction of hydrological, chemical, and biological processes. In contrast to other coupled models, it is applicable in non-Darcy-flow areas and allows to simultaneously simulate the surface and subsurface with one system of equation for surface and groundwater. We can develop upscaling approaches where we quantify the exchange rates depending on the ripple geometry and other variables with the high-resolution three-dimensional integral model to serve as sink/source terms in one- or two-dimensional shallow water flow models. The shallow water equations are based on vertical averaged velocities (not

discretizing the vertical dimension) and are generally applied on coarser scales. In a next step, also transport equations will be included in the presented integral model.

Funding: The funding provided by the German Research Foundation (DFG) within the Research Training Group ‘Urban Water Interfaces’ (GRK 2032) is gratefully acknowledged.

Acknowledgments: Parts of the simulations were computed on the supercomputers of Norddeutscher Verbund für Hoch- und Höchstleistungsrechnen in Berlin.

5. Transport simulations for groundwater-surface water interactions under neutral, losing and gaining flow conditions

This study was published in Groundwater as:

Broecker, T., Sobhi Gollo, V., Fox, A., Lewandowski, J., Nützmann, G., Arnon, S. & Hinkelmann, R. (2021). High Resolution Integrated Transport Model for Studying Surface Water–Groundwater Interaction, Groundwater, https://doi.org/10.1111/gwat.13071.

This is the postprint version of the article.

The test cases' setups are listed in Appendix B (B8 One-dimensional tracer transport in surface water and groundwater, B9 Transport simulations for groundwater-surface water interactions at rippled streambeds).

5.1 Abstract

Transport processes that lead to exchange of mass between surface water and groundwater play a significant role for the ecological functioning of aquatic systems, for hydrological processes and for biogeochemical transformations. In this study, we present a novel integral modeling approach for flow and transport at the sediment-water interface. The model allows us to simultaneously simulate turbulent surface and subsurface flow and transport with the same conceptual approach. For this purpose, a conservative transport equation was implemented to an existing approach that uses an extended version of the Navier-Stokes equations. Based on previous flume studies which investigated the spreading of a dye tracer under neutral, losing and gaining flow conditions the new solver is validated. Tracer distributions of the experiments are in close agreement with the simulations. The simulated flow paths are significantly affected by in- and outflowing groundwater flow. The highest velocities within the sediment are found for losing condition, which leads to shorter residence times compared to neutral and gaining conditions. The largest extent of the hyporheic exchange flow is observed under neutral

condition. The new solver can be used for further examinations of cases that are not suitable for the conventional coupled models, for example, if Reynolds numbers are larger than 10. Moreover, results gained with the integral solver provide high resolution information on pressure and velocity distributions at the rippled streambed, which can be used to improve flow predictions. This includes the extent of hyporheic exchange under varying ambient groundwater flow conditions.

5.2 Introduction

Stream water can enter the streambed, mix with groundwater and return after traveling some distance to the overlying water body. The zone of the streambed where at least 10% of the pore water is stream water is called “hyporheic zone” (Harvey & Bencala, 1993). The hyporheic zone plays a fundamental role for the transport and transformation of pollutants and natural solutes as well as habitat and refugium for aquatic organisms (Boulton et al., 2010; Hester & Gooseff, 2010; Krause et al., 2013; Lewandowski et al., 2019; Sophocleous, 2002). Hyporheic exchange can be generated by streambed morphologies such as meanders, bars, ripples, or other obstacles (Bencala & Walters, 1983; Cardenas, 2009; Elliott & Brooks, 1997a; Packman et al., 2004; Tonina & Buffington, 2007). The exchange depends on the sediment permeability and head gradients (Bardini et al., 2012; Buffington & Tonina, 2009; Cardenas, 2009; Dent et al., 2007; Ruehl et al., 2009; Wu et al., 2018). Solutes are exchanged with groundwater and stream water, too. Thereby, contaminants can be transported from surface water to groundwater and vice versa (Engelhardt et al., 2014; Lewandowski et al., 2011b; van der Molen et al., 1998). As a result, on the one hand a spreading of contamination is possible; on the other hand, the water quality can also be improved, for example, by nutrient turnover or the retention and/or transformation of trace organic compounds in the hyporheic zone (Botter et al., 2010; Brunke & Gonser, 1997; Heberer et al., 2008; Huntscha et al., 2012; Lawrence et al., 2013; Regnery et al., 2015; Schaper et al., 2019; Schaper et al., 2018). Important parameters for the solute exchange and biogeochemical reactions within the hyporheic zone are hyporheic exchange flux, residence times within the sediment and the biogeochemical milieu (Arnon et al., 2013; Bardini et al., 2012; Gomez et al., 2012; Marzadri et al., 2012; Trauth et al., 2015; Zarnetske et al., 2011).

Due to increasing interest on hyporheic zones, many studies rely on field and laboratory experiments and investigated the magnitude and direction of water exchange (Gariglio et al., 2013; Kasahara & Wondzell, 2003; Lewandowski et al., 2019; Peterson & Sickbert, 2006). While for real case observations of hyporheic exchange processes, field studies are preferred,

detailed process understanding and generalizations are more difficult to derive from such studies. Compared to field studies, flumes studies allow to control various factors such as permeability, water levels, or discharges. For a deeper understanding of physical principles of the complex dynamics at the sedimen-water interface, modeling studies have the advantage to contribute a high-resolution process understanding, both spatially and temporally. This is particularly important for groundwater, where measurements providing high spatial resolution are challenging. Moreover, information about variables that are difficult to measure such as turnover rates can be determined with modeling approaches. However, especially for the validation of these models, experimental data are still needed.

Numerical simulations of flow in the hyporheic zone usually couple a surface water flow model to a flow model of the porous sediment - considering different time scales. Often, a one-way sequential coupling method is applied, where pressure distributions from the surface water are used as a boundary condition for the groundwater model with no feedback from groundwater to surface water (Cardenas & Wilson, 2007b, 2007d; Jin et al., 2011; Trauth et al., 2013; Trauth et al., 2014). But also, some coupled models with feedback from the subsurface to the surface and vice versa (e.g. Nützmann and Mey (2007)) and fully coupled models such as the integrated hydrology model (VanderKwaak, 1999) or HydroGeoSphere have already been applied for the exchange of groundwater and surface water (Alaghmand et al., 2014; Brunner et al., 2009; Brunner & Simmons, 2012). For these models the two-dimensional diffusion-wave approximation of the St. Venant equations is applied for surface water and the three-dimensional Richards equation is used for the subsurface. To simultaneously solve one system of equations, exchange flux terms are applied in these models. Li et al. (2020) presented a fully coupled model for the hyporheic zone using Open Source Field Operation and Manipulation (OpenFOAM). The Navier-Stokes equations used for surface water are coupled with the Darcy equation by flux boundary conditions at the interface through an iterative algorithm. In the present study, an extended version of the three-dimensional Navier-Stokes equations is used for the whole system. The integral solver for surface water and groundwater was developed by Oxtoby et al. (2013) and was already validated and applied for the hyporheic zone in Broecker et al. (2019). The solver allows to investigate feedbacks from surface to subsurface and vice versa directly with one time step in the whole domain and is applicable also in non-Darcy-flow areas with Reynolds numbers higher than 10 (Broecker et al., 2019).

The impact of gaining and losing flow conditions on hyporheic exchange was previously simulated by Cardenas and Wilson (2007b); (2007d) and Trauth et al. (2013), but only with one-way sequential coupled models with no feedback to surface water. Li et al. (2020)

emphasized the necessity of fully coupled models and stated that for conservative solute transport in closed systems, the sequential model shows incorrect results. The difference between the results of one-way coupled and fully coupled models depends on permeability. Especially for increasing permeabilities, one-way sequential coupling is not sufficient (Li et al., 2020). To our knowledge, up to now there is no integral modeling approach that comprises turbulent flow and transport over and within dunes or ripples. Our integral model can also show turbulent effects that penetrate into the sediment, which is especially significant for bigger grain sizes. This penetration of turbulence into the sediment can directly control the interfacial exchange (Roche et al., 2018). Moreover, the feedback from groundwater to surface water can be important for intense up- or downward groundwater flow that affects the turbulent boundary layer (Cheng & Chiew, 1998; Prinos, 1995).

For the present study an additional transport equation is added to the existing integral modeling approach by Oxtoby et al. (2013) to investigate next to flow processes the transport of a conservative tracer. The correct description of the extended solver will be investigated with the help of flume experiments after Fox et al. (2014). Within these experiments, effects of neutral conditions (no in- or outflowing subsurface flow), outflowing subsurface flow (losing condition) and inflowing subsurface flow (gaining condition) on hyporheic exchange fluxes were analyzed with a laboratory flume system. We compare the simulated transport of a dye tracer with photographs taken during the experiments after Fox et al. (2014) and provide insights into flow processes at the rippled streambed for the conducted laboratory experiments with high-resolution results gained with the integral solver.

5.3 Materials and methods

5.3.1 Geometry and mesh

The geometry of the numerical model is based on the flume experiments of Fox et al. (2014). To reduce the computing time, the length of the 6.4 m long flume is shortened to approximately 1.75 m in the two-dimensional model. The shortened numerical model is a cut of the original flume. Only one phase which considers the surface water as well as the water in the sediment is taken into account. According to the water level used in the flume experiment the model has a height of 0.17 m. The dune-shaped sediment is located downstream of a ramp with a height of 0.08 m and a length of 0.93 m. The model geometry for the neutral case can be seen in Figure 5-1. For losing and gaining conditions the ripple geometries were adjusted slightly according to the photographs of the experiments. For this purpose, the meshes were modified manually.

The average length of the bed form structures amounts to 15 cm, the height to 2 cm. The bed form geometry used in the experiments is commonly found in sandy streambeds (Harvey et al., 2013; Lewandowski et al., 2011a; Stofleth et al., 2008).

The mesh generator gmsh (Geuzaine & Remacle, 2009) was used to discretize the two-dimensional mesh. About 77,000 unstructured elements were chosen to depict the dune shaped profiles. The exact number varies slightly for the different morphologies, while similar mesh conditions were chosen for the three meshes with similar element sizes in surface water, in the sediment and at the interface. Small element sizes at the interface of surface water and subsurface were used to account for the steep velocity gradients at the interface. The minimum element area of the applied mesh amounts to 1.93×10^{-7} m² and is located at the interface, while the maximum area amounts to 0.0033 m² and is located within the surface water.

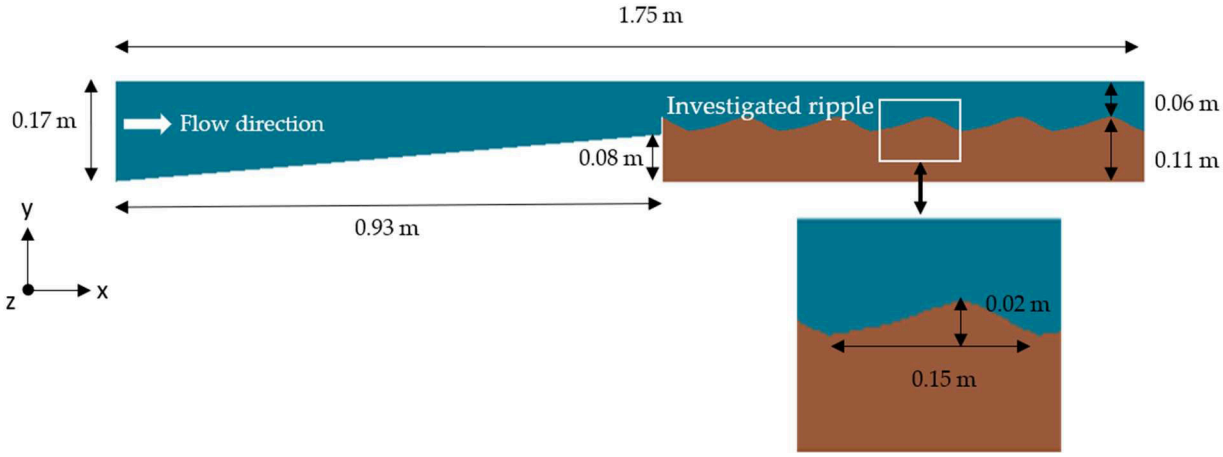

Figure 5-1: Model geometry for neutral conditions (sediment: brown, water: blue).

5.3.2 Numerical model

The open-source computational fluid dynamics (CFD) package OpenFOAM version 2.4.0 was used to simulate the dye spreading at the rippled streambed. The solver applied is based on the "porousInter" solver by Oxtoby et al. (2013). This solver uses the Navier-Stokes equations in surface water and in the sediment without any additional parameters. Solvers within the standard OpenFOAM library determining the interaction of surface water and groundwater - as porousInterFoam - apply resistance source terms for which such additional parameters as Darcy-Forchheimer coefficients are needed. For this reason, we decided to use the porousInter solver by Oxtoby et al. (2013). Since this solver only considers flow processes, we extended this solver for the investigation of transport processes. Flow processes are still determined using the equations available in the porousInter solver. PorousInter is based on the interFoam solver of OpenFOAM and is a multiphase solver for immiscible fluids (such as water and air) which extends the three-dimensional Navier-Stokes equations by the consideration of soil porosity

and effective grain size diameter. All values represented by $[\ ]^f$ are averaged over the pore space volume. The equations for the conservation of mass and momentum are defined after Oxtoby et al. (2013):

Mass conservation

$$\varphi\nabla\cdot\left[\vec{U}\right]^f = 0 \tag{5.1}$$

Momentum conservation

$$\varphi\left(\frac{\partial[\rho]^f\left[\vec{U}\right]^f}{\partial t}+\left[\vec{U}\right]^f\cdot\nabla([\rho]^f\left[\vec{U}\right]^f)\right) = -\varphi\nabla[p]^f+\varphi[\mu]^f\nabla^2\left[\vec{U}\right]^f+\varphi[\rho]^f\vec{g}+D \tag{5.2}$$

with φ representing the soil porosity (-); $\vec{U}$ the velocity (m/s); ρ the density (kg/m^3); t the time (s); p the pressure (Pa); μ the dynamic viscosity (Ns/m^2), g the gravitational acceleration (m/s^2) and D as an additional drag term (kg/(m^{2}s^2)).

The drag term is defined after Oxtoby et al. (2013) to account for the momentum loss by means of fluid friction with the porous medium after Ergun (1952) and for flow recirculation after van Gent (1995):

$$D= -\left(150\frac{1-\varphi}{d_p\varphi}[\mu]^f+1.75[\rho]^f\left[\vec{U}\right]^f\right)\frac{1-\varphi}{d_p}\left[\vec{U}\right]^f-0.34\frac{1-\varphi}{\varphi}\frac{[\rho]^f\partial\left[\vec{U}\right]^f}{\partial t} \tag{5.3}$$

with d_p (m) as effective grain size diameter.

An advection-diffusion equation for a passive tracer with a concentration C was implemented into the porousInter-solver. According to Burnett et al. (2003), Huettel et al. (2003), Jones and Mulholland (2000) and Mermillod-Blondin et al. (2000), advection dominates at the sediment-water interface. This observation is consistent with our results and no dispersion in groundwater was included. Consequently, the only transport parameter for this approach is the molecular diffusion coefficient D_{mol} (m²/s) and no calibration of transport parameters is needed. Due to the small cell sizes numerical diffusion is subordinate. The transport equation is defined as:

$$\frac{\partial C}{\partial t}+\nabla\cdot\left(C\vec{U}\right)+\nabla\cdot\left(D_{mol}\right)\nabla C= 0 \tag{5.4}$$

The standard k-epsilon turbulence model, which is based on the Reynolds averaged Navier-Stokes equations (RANS), is applied. Using the RANS turbulence model, not all scales of turbulence are directly resolved, instead they are modeled through different approaches. The

turbulent flow is divided into an average and a fluctuating velocity and leads to a Reynolds stress tensor in the Navier-Stokes equations which is often computed with the help of two-equation models. Two extra transport equations represent the turbulent flow properties. Commonly, the transported variables are either k for turbulent kinetic energy and ϵ for the turbulent dissipation within the k-ϵ turbulence model or k and ω (specific dissipation) within the k-ω turbulence model. In contrast to more advanced turbulence models, such as Large Eddy Simulations (LES) or direct numerical simulations (DNS), much less computation time is needed for the RANS turbulence models. For DNS even the smallest turbulences are resolved, while for LES the large-scale eddies are resolved and the small-scale eddies are taken into account with a subgrid scale model. Already with the standard k-epsilon turbulence model, the computation time of 1-min simulation for the reduced two-dimensional geometry amounts to ∼5 h on 100 parallel processors using the high-performance computing clusters of the Technische Universität Berlin with a MPP system. For LES, the cell sizes need to be decreased drastically and generally three, instead of two dimensions have to be considered. With the application of the RANS turbulence model an accurate description of tracer spreading is demonstrated compared to laboratory observations, which allows us to maintain the applied turbulence model with less computational effort.

5.3.3 Validation with one-dimensional analytical results

Two different cases were used for a first validation of the implemented transport application of the integral solver. The simulated results were compared to analytical one-dimensional results for a continuous and for a pulse injection after Kinzelbach (1992). For the validation of the flow processes we refer to Broecker et al. (2019).

For the first case, a 10-m long one-dimensional domain was separated in two equal parts - the first half consists of water (porosity of 1), the second consists of soil with a porosity of 0.3 and an effective grain size diameter of 1 cm (Figure 5-2a). A conservative tracer with a molecular diffusion coefficient of 10^{-9} m²/s flowed continuously into the water phase at the inlet (Figure 5-2b). The flow velocity at the inlet was fixed to 0.01 m/s. For the second case, the setup was very similar, but instead of a continuous injection, a pulse injection was assumed. At the beginning, the tracer was placed into a line of 2 m to 2.01 m (Figure 5-2c). Afterwards, no further tracer injection was assumed and only the spreading of this tracer mass was observed.

The simulated tracer breakthrough curves for the constant and the pulse injection were compared with analytical results and showed a good agreement for the transport of a conservative tracer in surface water and the subsurface as it can be seen in Figure 5-3.

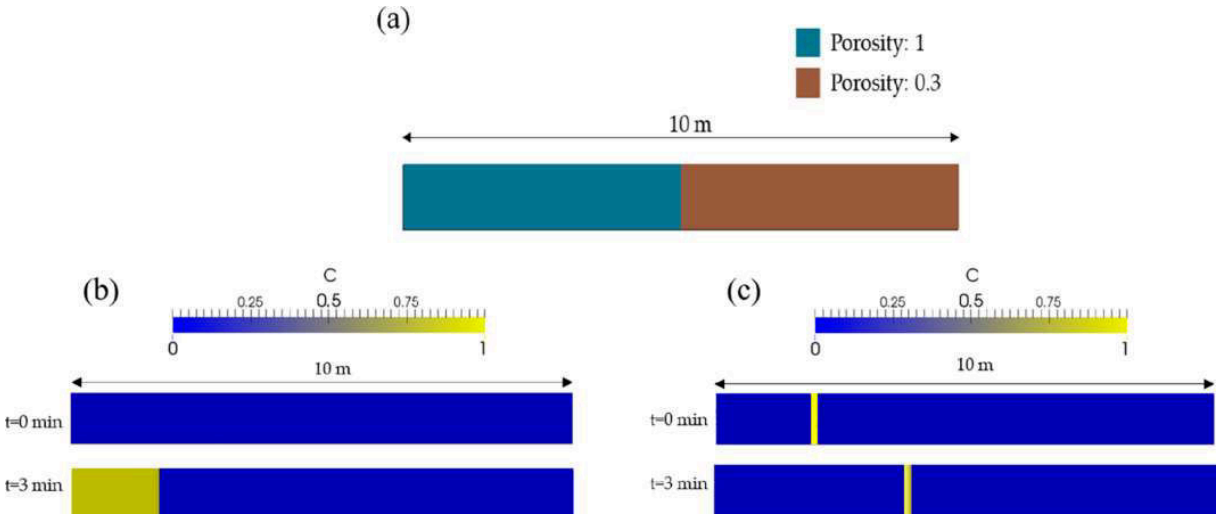

Figure 5-2: Model geometry (a) and tracer distribution at t = 0 min and at t = 3 min for a constant injection (b) and for a pulse injection (c).

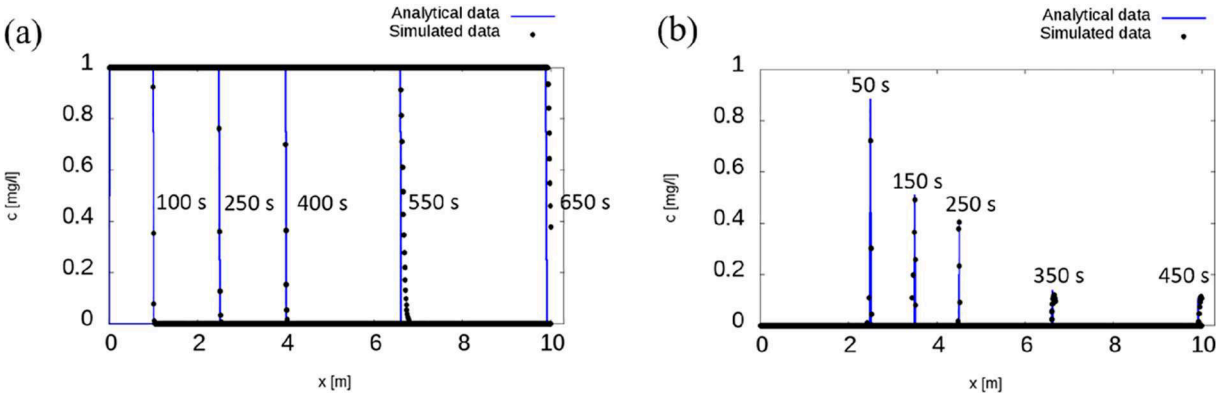

Figure 5-3: Comparison of simulated and analytically calculated concentrations for a constant injection (a) and for a pulse injection (b).

5.3.4 Boundary and initial conditions

The examined sandy sediment has a medium grain size of 0.384 mm and a porosity of 0.33. The most relevant boundary conditions can be seen in Figure 5-4 . At the inlet, surface water enters the domain with a fixed discharge of 0.0025 m^3/s and a velocity of 0.0507 m/s. Because of the shallower depth of the water column above sediment the flow velocity on the right side of the domain shown in Figure 5-1 is higher. In Fox et al. (2014) the velocity of the surface water above the sediment was 0.123 m/s for a mean water level of 0.07 m and a flume width of 0.29 m. The spatial dimensions of our model domain are identical except for the reduced flume length. The discharge and the velocity at the inlet were calculated accordingly. All boundary conditions at the top contain slip conditions. We decided to apply a one-phase model to reduce the computational effort under the assumption that the water level fluctuations are negligible. Within the flume experiment, the water depth was kept constant also for losing and gaining

conditions. All boundary conditions in the third dimension are set to “empty” which is a boundary condition implemented in OpenFOAM to describe sidewalls of two-dimensional geometries. At the left and at the right side of the sediment and at the ramp, walls with no-slip condition are defined. The wall at the right side of the sediment was also placed in the original flume, however not after 1.75 m, but after 6.4 m. Moreover, the original flume was recirculating while we defined the surface water to flow out of the domain. The outflowing discharge of the water equals the inflowing discharge. For the neutral conditions the bottom of the sediment is also a wall, while for the gaining and losing conditions the flux is fixed at the bottom of the sediment. The flowrates of $\pm 1.35 \times 10{-}6$ m^3/s were calculated according to the inflow area at the bottom (0.29 m × 0.82 m) and the velocities of $\pm 5.67 \times 10{-}6$ m/s for gaining and losing conditions in the y-direction corresponding to Fox et al. (2014), who applied velocities of ±49 cm/d at the bottom of the flume for losing and gaining conditions. A fixed pressure of 0 Pa is defined at the outlet. For the gaining and losing conditions, the pressure at the bottom of the sediment is set to “fixedFluxPressure” to adjust the pressure gradient according to the fluxes at the boundary.

To quickly reach the quasi-steady state, adequate initial conditions are specified in analogy to measurements of Fox et al. (2014). The surface water velocity was set to 0.123 m/s in x-direction and the pore water velocity at the bottom of the sediment domain was set to 0 m/s for neutral conditions and to $\pm 5.67 \times 10^{-6}$ m/s in the y-direction for the gaining and losing cases. Since there is exchange across the sediment-water interface the values are only valid for the lower boundary of the sediment.

All cases run for 5 min without a tracer to approach steady state condition. Afterwards, a tracer with a molecular diffusion coefficient D_{mol} of 10^{-9} m^2/s enters with a concentration of 1 from the inlet into the domain. For gaining and losing conditions the incoming concentration at the bottom of the sediment is fixed to 0.

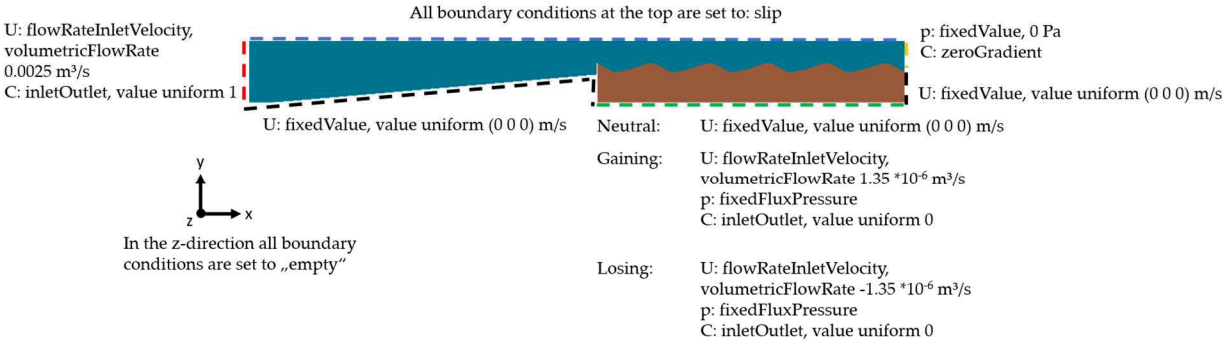

Figure 5-4: Boundary conditions (blue - overlying water; brown - sediment; U - velocity; C - tracer concentration; p - pressure; different colours of dashed lines indicate the different boundaries for the specified boundary conditions).

All cases run for 5 minutes without a tracer to approach steady state condition. Afterwards, a tracer with a molecular diffusion coefficient D_{mol} of 10^{-9} m²/s enters with a concentration of 1 from the inlet into the domain. For gaining and losing conditions the incoming concentration at the bottom of the sediment is fixed to 0.

5.4 Results and discussion

In the following we investigate the spreading of a conservative tracer with the novel integral modeling approach and compare the results with experimental observations of Fox et al. (2014) who used the dye tracer Brilliant Blue FCF to visualize the penetration of surface water into the sediment. For the comparison we use photo series of three experiments that is, neutral, losing, and gaining condition. The photographs were taken every minute through the flume's glass walls. We compare photographs after every 10 min for the first hour of each experiment. The dyed area for the simulations as well as for the experiments were calculated using the software “ImageJ” for scientific image analysis and can be seen in Table 5-1. A threshold adjustment for RGB colours is applied to calculate the pixel area coverage. The propagation speeds of the tracer fronts in the sediments show a reasonable agreement (see Table 5-1). Next to the comparison of the tracer transport, we provide a closer understanding of the prevailing processes within the hyporheic zone through calculated velocity and pressure distributions.

Table 5-1: Comparison of dyed areas for the experiments and the simulations at the investigated ripple calculated with an image analysis software.

	Neutral		**Losing**		**Gaining**	
	Experiment	**Simulation**	**Experiment**	**Simulation**	**Experiment**	**Simulation**
10 min	6.163	6.685	21.732	20.082	4.083	4.011
30 min	20.654	20.705	51.105	51.900	7.765	7.861
60 min	27.695	32.439	85.483	90.691	9.906	9.888
Root mean square error	2.76		3.19		0.07	

5.4.1 Neutral conditions

For neutral conditions, an impermeable wall is set at the bottom of the sediment. For all of our investigations we focused on the ripple in the middle of the flume (Figure 5-1). However, the flow processes are similar for all ripples (except for the first and the last ripple) as it can be seen in Figure 5-5a. Higher velocities within the surface water are observed above the ripple crests while lower velocities occur in the troughs. Within the sediment, the highest velocities can be seen at a small layer directly at the interface between the stream and the sediment as well as at the ripple crest (Figure 5-5b). The maximum Reynolds number in the sediment is 3.84, which means that Darcy's law is applicable.

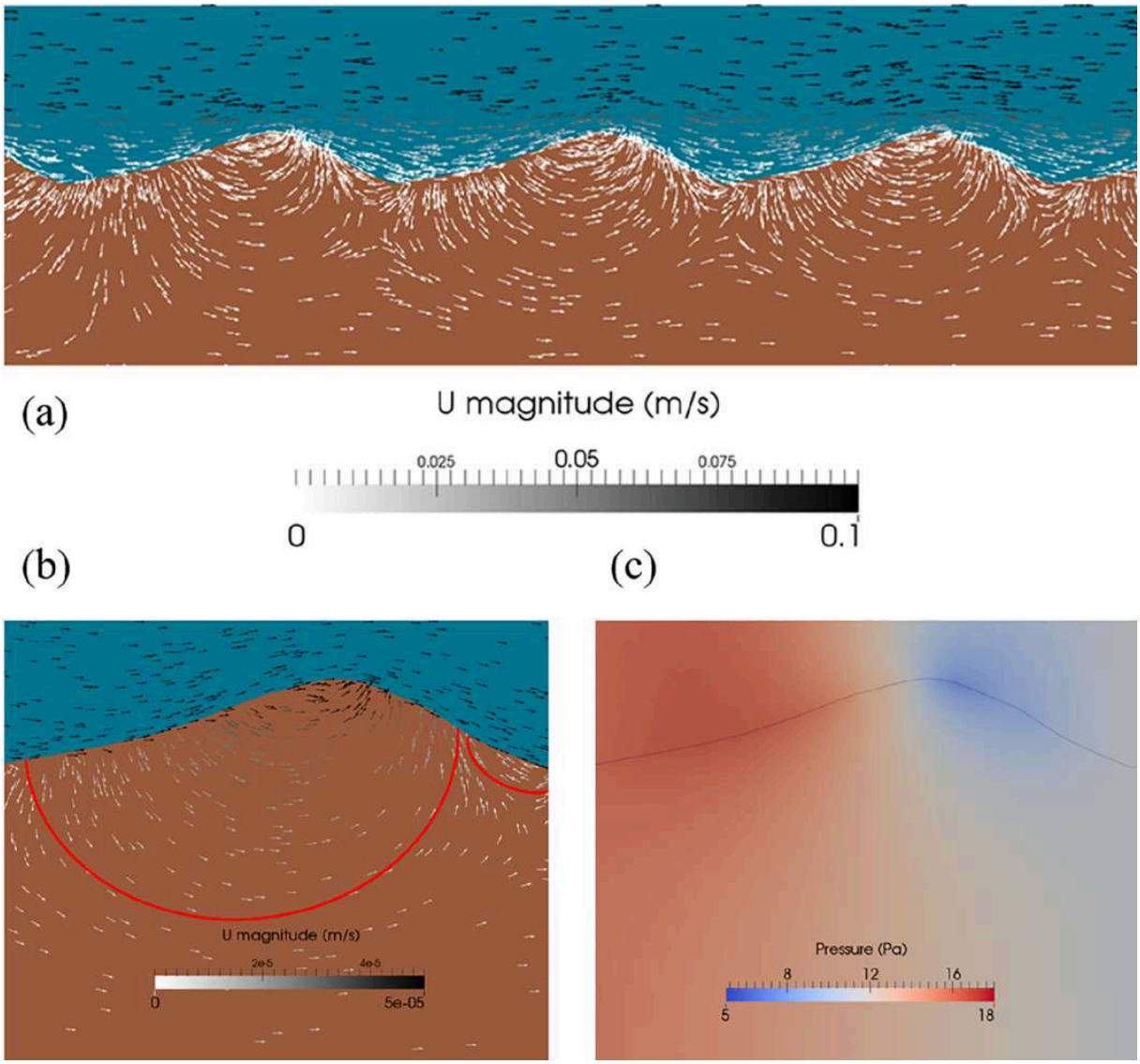

Figure 5-5: Velocity distribution of the neutral case at the rippled sediment (a) and velocity (b) and pressure distribution (c) at the investigated ripple. The red lines indicate the hyporheic flow cells.

Figure 5-5c shows the pressure distribution at the interface of surface and subsurface flow at the investigated ripple. The applied solver uses a specific formulation for the pressure where the pressure term p_rgh is used to avoid the occurrence of steep pressure gradients caused by hydrostatic effects. p_rgh is defined as the static pressure minus the hydrostatic pressure (prgh = p − ρgy with y as coordinate vector). The highest pressure is observed upstream of the crest. Lower pressure is determined downstream of the crest. Accordingly, the main flow within the sediment is from upstream of the crest to downstream - from high to low pressure. Additional flow occurs at the last third of the investigated ripple's lee face (Figure 5-5a and Figure 5-5b). Consequently, two “hyporheic flow cells” with paths downwelling from surface water and returning to the water column within relatively short distances (Hester et al., 2013) are recognized for the neutral case at each ripple as also shown in three dimensions by Trauth et al. (2013) for pool riffle morphologies and earlier by Cardenas and Wilson (2007a) for ripples.

The two flow cells can also be seen in the tracer concentrations even though the second zone is still very thin after 1 h and hardly visible (Figure 5-6). Figure 5-6 shows the simulated tracer concentrations at the investigated ripple as well as the observed tracer spreading during the laboratory experiment for the first hour. A good agreement can be recognized with a root mean square error of 2.76 cm^2 (see Table 5-1), though a slightly faster spreading is observed within the simulations. A reason for this might be the shortened flume for the CFD simulation compared to the original flume length. Another reason might be that in the simulation the spread toward the edge of the plume can be seen with high-resolution results, while in the experiment lower concentrations are not visible in the pictures. Moreover, laboratory experiments cannot guarantee absolutely homogeneous sediment, which is assumed for our simulations. This means, that for example the grain size, the bulk density, and consequently also the porosity of the sediment can vary slightly and/or small deviations of neighbouring ripple geometries can occur during the installation or during the experiment. Small-scale inhomogeneities can also be seen in the photographs, which show a slightly uneven course in the lower area of the tracer penetration. Since the simulation was only based on photos of the investigated ripple, all neighbouring ripples are considered to have exactly the same geometry as the investigated ripple in our simulations.

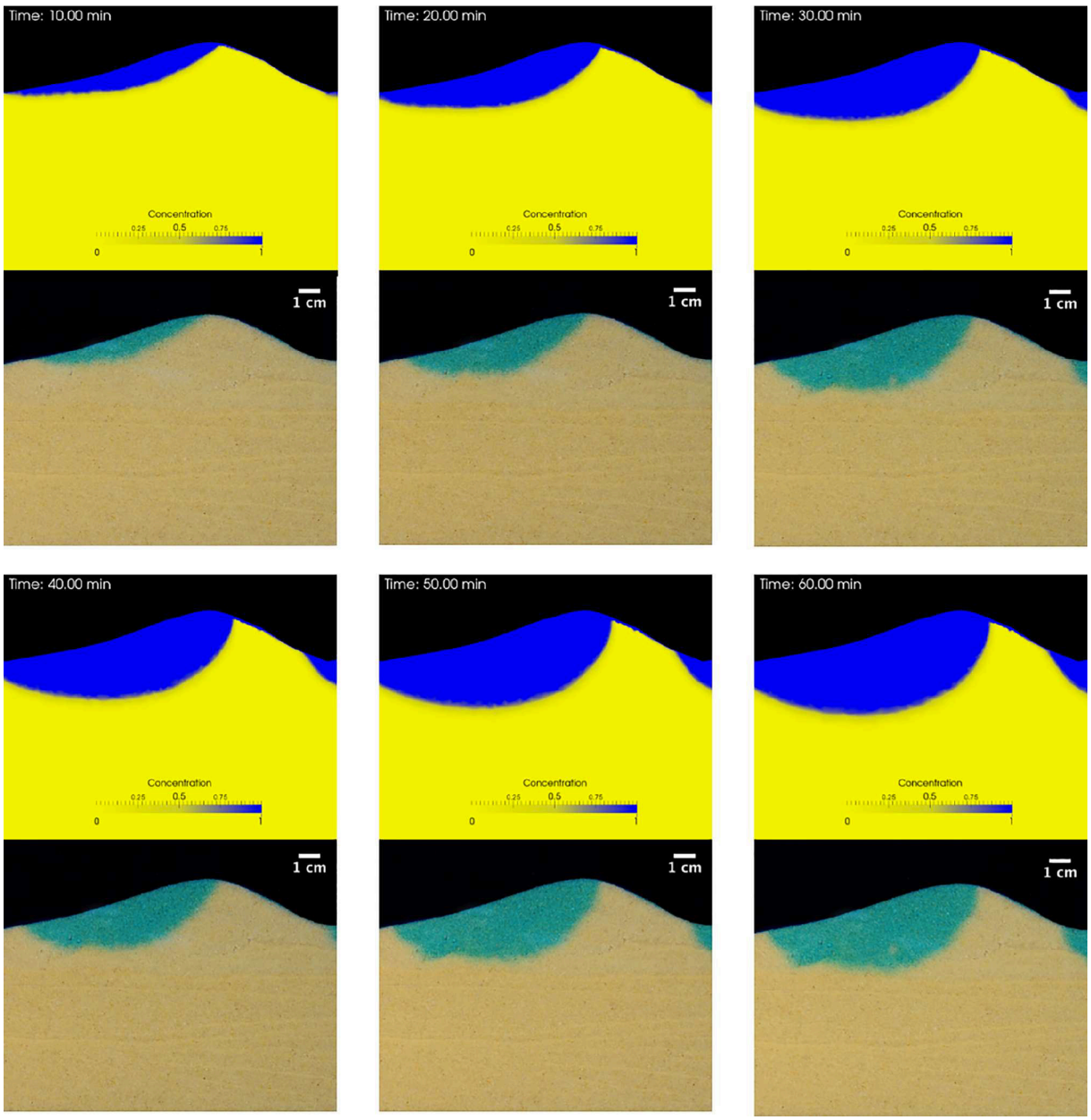

Figure 5-6: Simulated tracer concentrations (yellow blue images) and photos of laboratory experiments (beige-turquoise) after Fox et al. (2014) for 10-60 min under neutral conditions.

5.4.2 Losing conditions

The outflowing velocity at the bottom of the sediment is 5.67×10^{-6} m/s for losing conditions, which corresponds to the bottom flux used in the experiment by Fox et al. (2014). Compared to the neutral case the velocity distribution in the sediment changes drastically even though the surface water velocity is the same (compare Figure 5-5 and Figure 5-7). The main flow direction within the sediment is downwards which can also be seen in the pressure distribution: low pressure occurs not only at and downstream of the ripple crest, but also toward the bottom of the sediment (Figure 5-7c). Still, most of the surface water that enters the sediment flows into

the ripple at the stoss side, where the highest pressure is observed (Figure 5-7b and Figure 5-7c). However, a further fraction comes from the last third of the lee side of the ripple and flows (except of a small layer at the interface to the surface water) in upstream direction. These different flow cells that are pointing in upstream as well as in downstream directions for infiltrating stream water were also observed in several studies investigating losing conditions (Boano et al., 2008; Cardenas & Wilson, 2007b; Trauth et al., 2013).

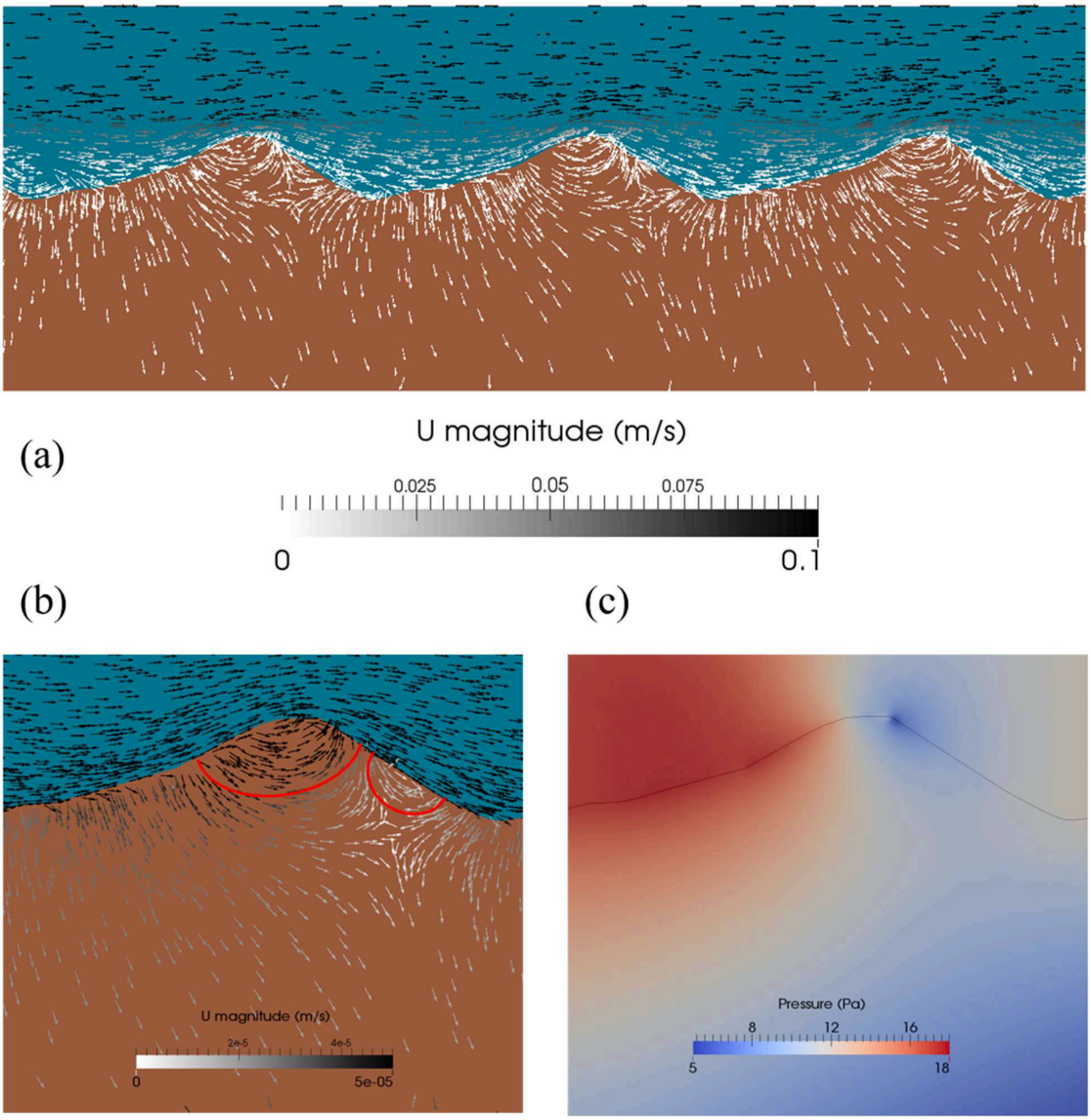

Figure 5-7: Velocity distribution for losing conditions at the rippled sediment (a) and velocity (b) and pressure distribution (c) at the investigated ripple. The red lines indicate the hyporheic flow cells.

The flow entering the ripple is divided into a part that gets back to the surface water and another part that flows toward the bottom of the sediment domain. Hyporheic exchange flow, that is, flow paths beginning and ending at the sediment-water interface, is centred around the ripple crest and at a shallow area at the lee side. Compared to neutral conditions, a larger area with high velocities is observed in the sediment especially around the ripple crest, but also at the stoss side (compare Figure 5-5b and Figure 5-7b) which was also seen in Trauth et al. (2013). For losing conditions in this case the Reynolds numbers increase slightly with a maximum of 4.23 compared to the neutral conditions. However, the Darcy law is still applicable. Cardenas and Wilson (2007d) stated that large temperature variations of the water column penetrate deep into the subsurface for losing conditions and that with increasing downwelling the temperature signal penetrates deeper into the sediment - especially at the stoss side of ripples and at a narrow upwelling zone below the crest. These observations coincide qualitatively with our simulation and the observations by Fox et al. (2014).

Figure 5-8 shows the tracer spreading for losing conditions during the flume experiment compared with simulated tracer concentrations. In the first 20 min the tracer concentrations downstream of the ripple crest are slightly lower for the simulations compared to the photos of the experiment. This can be based on small variations of the sediment parameters during the experiments or due to slight variations of the ripple geometry from the simulations compared to the experiment. Moreover, the ripple geometries of the neighbouring ripples can influence the spreading. But overall, a good agreement between the experimental observations and the simulations is observed with a root mean square error of 3.19 cm^2. Especially the most important structures of losing conditions compared to neutral and gaining conditions can be well recognized. Due to the higher velocities in the sediment under losing conditions compared to neutral conditions (Figure 5-7b) the tracer penetrates much faster into the sediment compared to neutral conditions (Figure 5-6). Moreover, in the velocity field we can see that the surface water infiltrates almost at the whole lee side of the ripple directly into the sediment, while under neutral conditions the tracer flows in upstream direction and colours the ripple toe only through hyporheic exchange. Under neutral conditions the tracer flows into the ripple and then back to the surface water; under losing conditions most of the tracer mass that enters the ripple flows

toward the bottom of the model (Figure 5-7a). Therefore, the infiltrated area increases constantly during the experiment (and consequently also during the simulation).

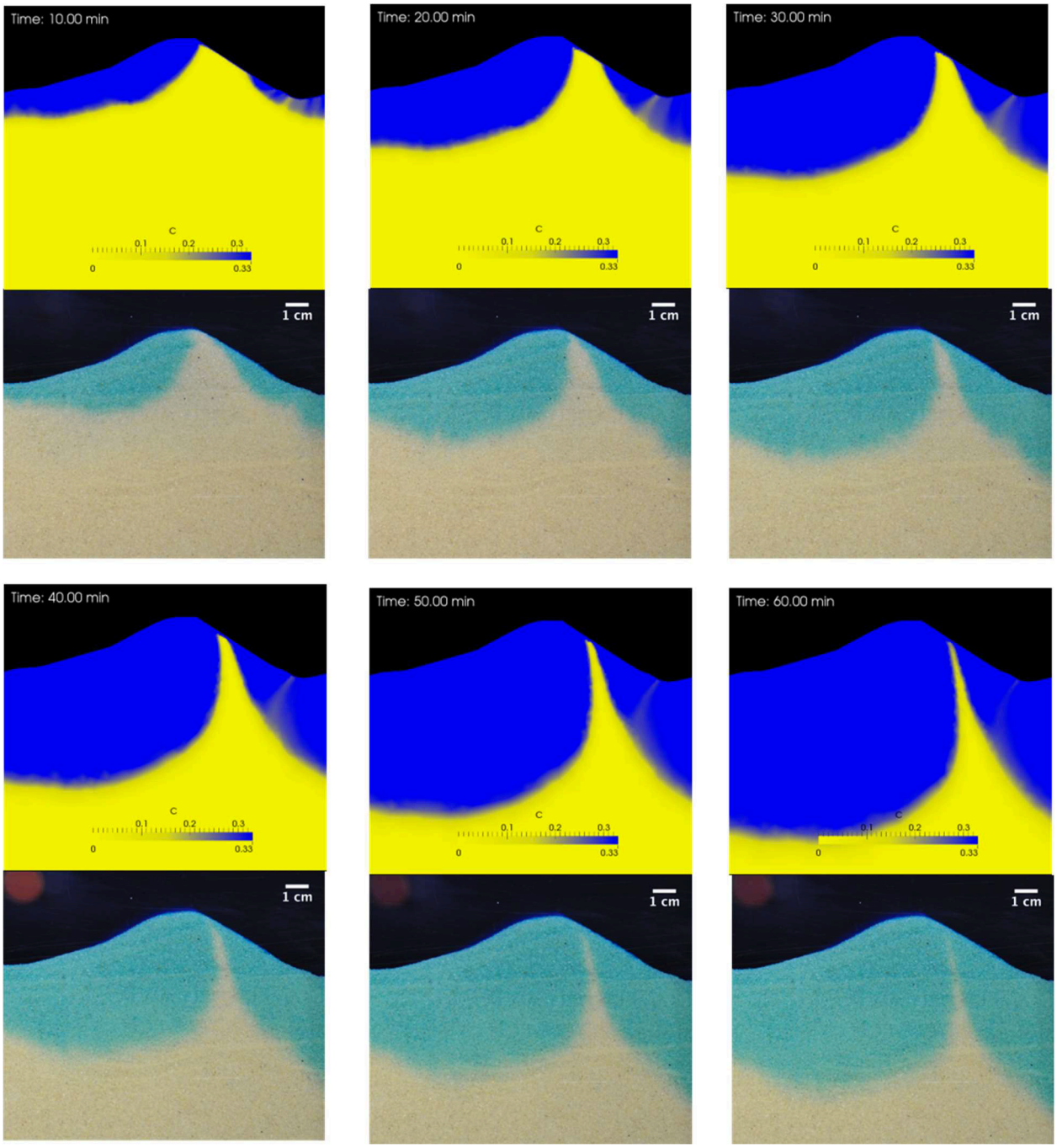

Figure 5-8: Simulated tracer concentrations (yellow blue images) and photos of laboratory experiments (beige-turquoise) after Fox et al. (2014) for 10-60 min under losing conditions.

5.4.3 Gaining conditions

For gaining conditions we use the same flow velocity at the bottom of the sediment domain as for losing conditions but in opposite direction. Accordingly, the flow field within the sediment changes from downward to upward (Figure 5-9a and Figure 5-9b). Surface water enters the

sediment only at the stoss side of ripples which is consistent with Trauth et al. (2013). Cardenas and Wilson (2007b) also stated that the geometry of hyporheic flow cells is different for gaining and losing conditions even if the depth of the hyporheic flow cells is similar for gaining and losing condition. Hyporheic exchange flow, that is, flow paths beginning and ending at the sediment-water interface, is centred at the stoss side of ripples for gaining condition. In contrast to neutral and losing conditions, under gaining conditions outflowing subsurface flow is not only observed at the lee side of the ripple but also at the beginning of the stoss side (Figure 5-9b). Trauth et al. (2013) observed upstream and downstream directed hyporheic flow cells for gaining conditions. In the present modeling study upstream directed flow originates from deeper pore water (groundwater) while hyporheic exchange flow is only directed downstream. As also indicated by the pressure field (Figure 5-9c) and velocity distribution (Figure 5-9a and Figure 5-9b), flow occurs from high pressure in the first section of the stoss side of the ripple toward the second section of the stoss side and from the high pressure zone at the bottom of the sediment domain to the low pressure zone at the lee side of the ripple. The same main flow directions for gaining conditions were also observed by (Cardenas & Wilson, 2007b).

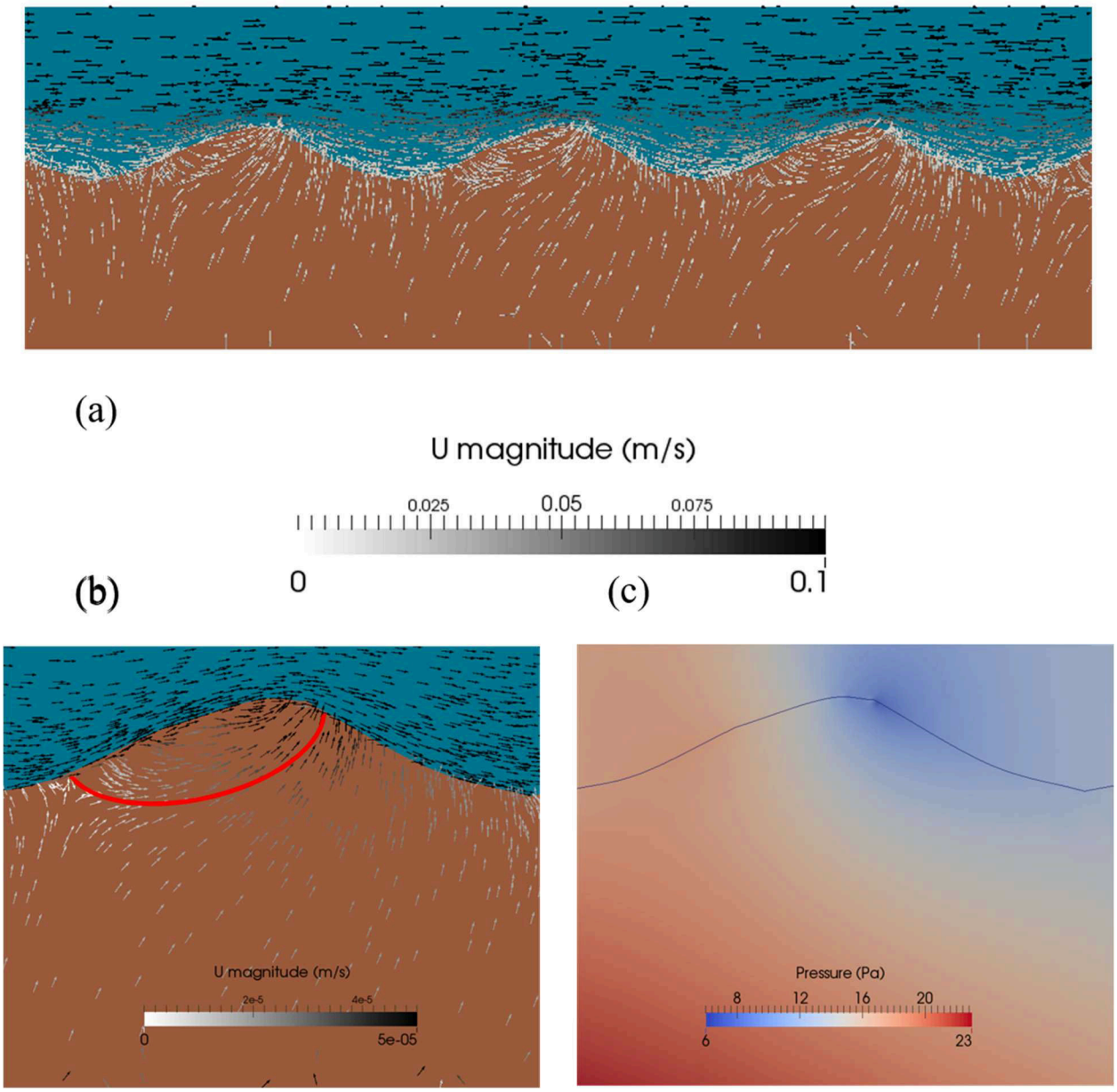

Figure 5-9: Velocity distribution for gaining conditions at the rippled sediment (a) and velocity (b) and pressure distribution (c) at the investigated ripple. The red line indicates the hyporheic flow cell.

Comparing the hyporheic flow fields of gaining and losing conditions, we conclude that faster hyporheic flow and thus shorter residence times occur under losing conditions. This supports results of Trauth et al. (2013). Shorter residence times can significantly affect biogeochemical processes (Zarnetske et al., 2011).

In contrast to neutral and losing conditions, only one hyporheic flow cell occurs under gaining conditions. This single flow cell is also reflected in the transport of the dye tracer (Figure 5-10). Moreover, there is less tracer mass transported into the sediment compared to neutral and losing conditions due to the upward directed flow of the groundwater (compare Figure 5-6, Figure 5-8

and Figure 5-10). This was also seen in Fox et al. (2014) and there is a good agreement between their laboratory observations and the modeled tracer concentrations of the present study with a root mean square error of 0.07 cm². Even after 4 h, the tracer spreading observed by Fox et al. (2014) did not vary much since the coloured area is only caused by hyporheic flow cells.

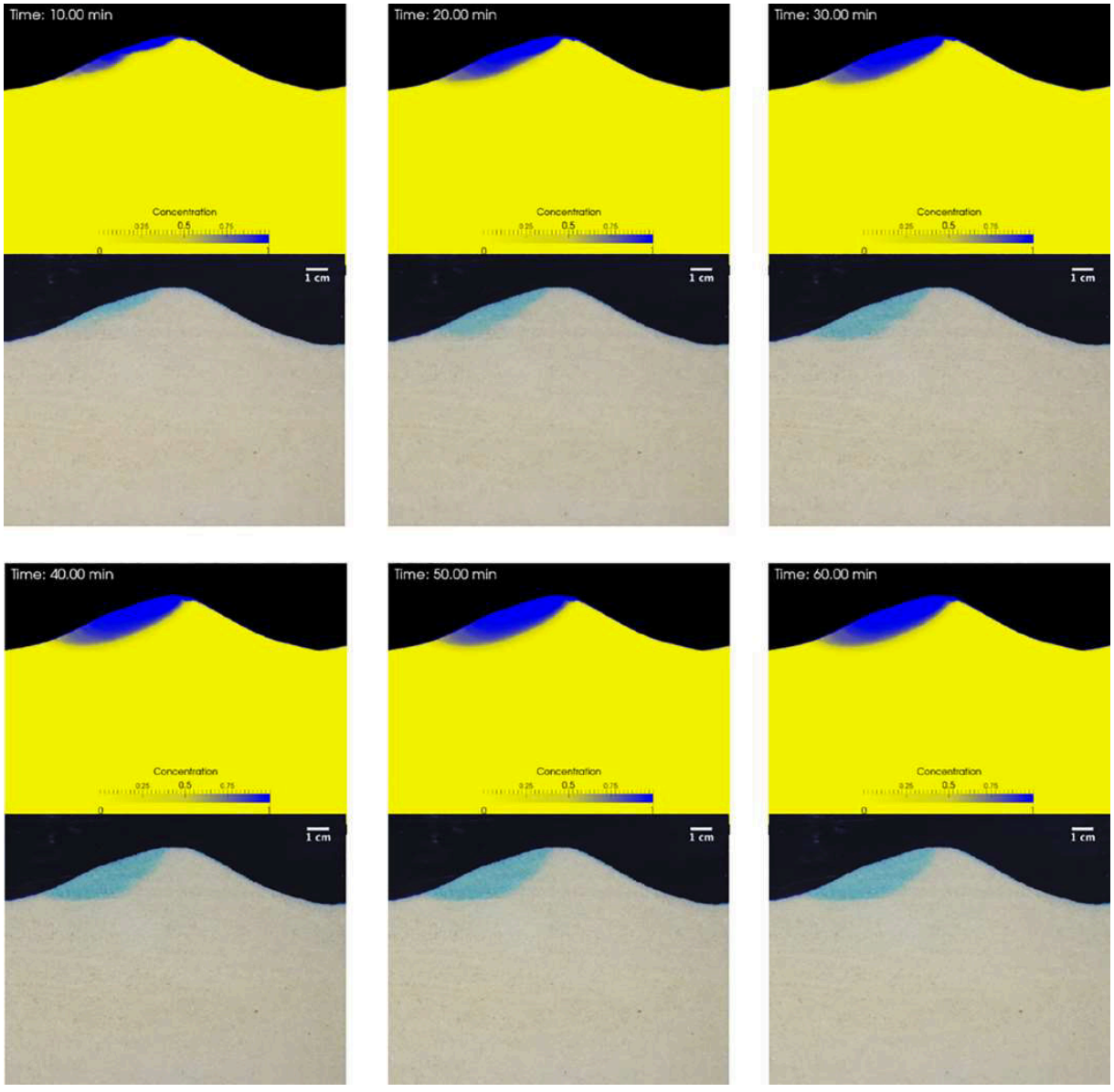

Figure 5-10: Simulated tracer concentrations (yellow blue images) and photos of laboratory experiments (beige-turquoise) after Fox et al. (2014) for 10-60 min under gaining conditions.

5.4.4 Conceptual and computational consideration

Regarding the general application of Computational Fluid Dynamics software, we want to point out, that a lot of decisions have to be made to find the right model for each investigation. The user can, for example, decide whether water level fluctuations are important and thus a two-phase model has to be chosen or if a one phase model is sufficient. Also, it has to be decided

whether one-, two-, or three dimensions are investigated. These decisions affect the quality of the results as well as the computational effort and depend on the aim of the investigation. Also, the boundary and initial conditions as well as the mesh quality influence the results significantly. As a consequence, even though we do not have one or various parameters to calibrate, it is not always easy to find the right model settings. These points are independent of the presented integral modeling approach and are also applicable for other CFD approaches. As mentioned in the introduction, various studies investigated flow and transport processes in the hyporheic zone using coupled modeling approaches. In the present study, we present and validate an integral model which has some advantages and disadvantages compared to the coupled approaches. For the coupled approaches usually a surface water model is applied and subsequently the corresponding pressure distribution is used as an input for the calculation with a groundwater model. Commonly, different time steps are used for the groundwater and the surface water model in the coupled approach while for the integral model the time step is the same for the whole model domain. On the one hand, a direct feedback from the subsurface to the surface and vice versa is possible for every time step in the coupled approach. On the other hand, a high computational effort is needed. The direct feedback can be important, for example, for unsteady flow conditions, which can have a significant impact on biogeochemical processes in the hyporheic zone (Galloway et al., 2019). In contrast to coupled approaches, variations of velocity or tracer concentration within both surface water and sediment and their effects on flow and transport processes can be directly observed at the same time in the whole domain with the integral model. Especially compared to one-way sequentially coupled approaches the integral approach is more appropriate if, for example, a contamination of the groundwater that spreads into the surface water is considered.

Also turbulent structures that can penetrate from the surface water into the sediment can be simulated, which is not possible with coupled approaches that use the Darcy law to describe flow processes within the sediment. An accurate description of all turbulent structures is only possible by directly resolving them (i.e. using DNS approaches). But facing the computational effort, we decided to use a RANS turbulence model for this study as the turbulent structures can still be depicted qualitatively well. The k-epsilon turbulence model was applied as it showed better results than the k-omega model, used, for example, by Cardenas and Wilson (2007b); (2007d). This is probably based on the fact that we did not set a wall at the interface of surface and subsurface water in contrast to Cardenas and Wilson (2007b); (2007d). The k-omega turbulence model has the advantage compared to the k-epsilon model to show better results close to walls. Also three-dimensional investigations using advanced turbulence models such

as LES are generally possible with the integral solver as applied by Broecker et al. (2019). However, this turbulence model causes again considerably more computational effort.

In the present study, we validated the new integral model for transport processes at the hyporheic zone with previously performed flume experiments. Compared to one-way coupled approaches the integral model is definitely more time consuming. However, the integral solver is applicable where commonly used coupled approaches cannot be applied as, for example, for Reynolds numbers higher than 10 and where the Darcy law would consequently lead to overestimated flow rates. In the present study the maximum Reynolds number was lower than 5 which means that a coupled model has probably similar results. But Broecker et al. (2019) showed that already coarser sand can lead to significantly higher Reynolds numbers in the sediment close to the interface. For these sediments with bigger grain sizes which lead to non-Darcy flow areas, the integral model is still applicable and additionally the calculation time is considerably smaller than for fine sediments.

5.5 Conclusions

In this study we present and validate an integral solver which was extended for tracer transport at the interface of surface water and groundwater. Similar observations were stated in previously presented modeling approaches that coupled a surface water model with a groundwater model. However, the integral model can also be used for unsteady conditions in groundwater or surface water and can show direct feedbacks from the surface water to the groundwater and vice versa. It is also applicable in non-Darcy flow layers as an extended version of the Navier-Stokes equations is solved in the stream as well as in the sediment, which is especially important for bigger grain sizes.

The results demonstrate the reliability of our modeling study and provide further insights into a laboratory experiment for the transport of a dye tracer. With the integral solver it is possible to depict complex hydraulics and their effects on tracer transport at the interface of groundwater and the stream. Results like the thin top layer for the neutral case with inflowing surface water on the lee side (depicted within the simulations as well as during the experiments) would look completely different with a one-way coupled model. A detailed comparison between one way coupled and the integral model is planned. In future, the integral solver can also be applied to heterogeneous sediments (with different grain size diameters and porosities) but a validation for heterogeneous sediments is still needed. As a basis for the validation of the integral model for heterogeneous sediments, a further experiment of Fox et al. (2016) conducted in the same

flume system but with different sediment can be used. For examinations over long periods of time or for larger investigation areas upscaling methods are required.

Acknowledgments: We would like to acknowledge the time and effort by Jan H. Fleckenstein to improve the quality of this paper. The funding provided by the German Research Foundation (DFG) within the Research Training Group "Urban Water Interfaces" (GRK 2032) and the grant from the Technische Universität Berlin, Germany, are gratefully acknowledged. Data archiving for all simulations and analytical results are underway and will be available in the repository of the Technische Universität Berlin "DepositOnce." Datasets of the experimental results used for this research are included in this paper.

6. Supplementary contributions

6.1 Applications of mass transfer phenomena across the water-air interface

This study was published as:

Teuber, K., Broecker, T., Bentzen, T.R., Stephan, D., Nützmann, G. & Hinkelmann, R. (2019). Using computational fluid dynamics to describe H2S mass transfer across the water-air interface in sewers, Water Science and Technology, 79 (10), 1934-1946, https://doi.org/10.2166/wst.2019.193.

This is the abstract of the article (postprint).

Abstract

For the past 70 years, researchers have dealt with the investigation of odour in sewer systems caused by hydrogen sulphide formations and the development of approaches to describe it. The state-of-the-art models are one-dimensional. At the same time, flow and transport phenomena in sewers can be three-dimensional, for example the air flow velocities in circular pipes or flow velocities of water and air in the reach of drop structures. Within the past years, increasing computational capabilities enabled the development of more complex models. This paper uses a three-dimensional two-phase Computational Fluid Dynamics model to describe mass transfer phenomena between the two phases: water and air. The solver has been extended to be capable to account for temperature dependency, the influence of pH value and a conversion to describe simulated air phase concentrations as partial pressure. Its capabilities are being explored in different application examples and its advantages compared to existing models are demonstrated in a highly complex three-dimensional test case. The resulting interH2SFoam solver is a significant step in the direction of describing and analysing H2S emissions in sewers.

6.2 High-resolution modelling of free-surface flows in closed conduits

This study was published as:

Teuber, K., Broecker, T., Bayón, A., Nützmann, G. & Hinkelmann, R. (2019). CFD-modelling of free-surface flows in closed conduits, Progress in Computational Fluid Dynamics 19 (6), 368-380, https://doi.org/10.1504/PCFD.2019.103266.

This is the abstract of the article (postprint).

Abstract

Computational Fluid Dynamics (CFD) is gaining an increasing importance in the field of hydraulic engineering. This publication presents different application examples of a two-phase approach as implemented in the open source software OpenFOAM. The chosen approach is based on the Volume of Fluid method focusing on the simulation of flow in closed conduits. Three examples are presented: single-phase flow over a ground sill and free surface flow over a hill as well as complex free surface flow in a sewer model. The first example compares the results of different RANS turbulence models with experimental results. The results of the second example are compared with an analytical solution. In the last example the behaviour of the free surface flow is compared with the results of a model test and existing simulations using a simplified, open channel geometry for the closed conduit. For the examples analysed, the two-phase approach provides stable and reliable results.

6.3 Relevance of the hyporheic zone

This study was published as:

Lewandowski, J.; Arnon, S.; Banks, E.; Batelaan, O.; Betterle, A.; Broecker, T.; Coll, C.; Drummond, J.D.; Gaona Garcia, J.; Galloway, J.; Gomez-Velez, J.; Grabowski, R.C.; Herzog, S.P.; Hinkelmann, R.; Höhne, A.; Hollender, J.; Horn, M.A.; Jaeger, A.; Krause, S.; Löchner Prats, A.; Magliozzi, C.; Meinikmann, K.; Mojarrad, B.B.; Mueller, B.M.; Peralta-Maraver, I.; Popp, A.L.; Posselt, M.; Putschew, A.; Radke, M.; Raza, M.; Riml, J.; Robertson, A.; Rutere, C.; Schaper, J.L.; Schirmer, M.; Schulz, H.; Shanafield, M.; Singh, T.; Ward, A.S.; Wolke, P.; Wörman, A.; Wu, L.. (2019). Is the Hyporheic Zone Relevant beyond the Scientific Community? Water, 11(11), 2230, https://doi.org/10.3390/w11112230.

This is the abstract of the article (postprint).

Abstract

Rivers are important ecosystems under continuous anthropogenic stresses. The hyporheic zone is a ubiquitous, reactive interface between the main channel and its surrounding sediments along the river network. We elaborate on the main physical, biological, and biogeochemical drivers and processes within the hyporheic zone that have been studied by multiple scientific disciplines for almost half a century. These previous efforts have shown that the hyporheic zone is a modulator for most metabolic stream processes and serves as a refuge and habitat for a diverse range of aquatic organisms. It also exerts a major control on river water quality by increasing the contact time with reactive environments, which in turn results in retention and transformation of nutrients, trace organic compounds, fine suspended particles, and microplastics, among others. The paper showcases the critical importance of hyporheic zones, both from a scientific and an applied perspective, and their role in ecosystem services to answer the question of the manuscript title. It identifies major research gaps in our understanding of hyporheic processes. In conclusion, we highlight the potential of hyporheic restoration to efficiently manage and reactivate ecosystem functions and services in river corridors.

7. Synthesis

7.1 Summary and conclusions

Understanding exchange processes of groundwater and surface water is important for a sustainable water management that includes quantitative calculations of water exchange, consideration of water quality and the impact on the ecology. The present thesis is based on a numerical model that uses the CFD software OpenFOAM. Through numerical models, it is possible to gain knowledge of complex processes at the interface of groundwater and surface water with high-resolution. Next to investigations of flow processes, information of transport processes as retention and dilution of contaminated water can be received. But even though the relevance of the exchange is widely accepted, numerical modelling applications focusing on groundwater-surface water interactions mainly use coupled approaches. For both domains various coupling strategies can be applied which were presented in section 1.3. Contrary to these applications, the focus of this thesis is the validation, application and extension of an integral modelling approach for groundwater and surface water with the same conceptual model for both domains with high resolution in space and time. The integral model solves an extended version of the three-dimensional Navier-Stokes equations including a porosity and a drag term to account for the porous medium and is capable to simulate high-resolution turbulent free surface flow and transport processes including their interactions and exchanges with the near bed groundwater.

7.1.1 General outcomes

Before addressing the specific outcomes of interactions of groundwater and surface water concerning hydrodynamics and transport, some general conclusions can be summarized:

- It is possible to describe groundwater-surface water flow and transport processes with the same model concept, called integral in the following. It is based on a three-dimensional two-phase model using the Volume of Fluid (VoF) method and an approach by Oxtoby et al. (2013) to account for the flow processes in the porous media.
- To get accurate results with the CFD model, detailed knowledge about streambed geometries, sediment properties (grain size diameters, porosities), flow conditions in the sediment and in surface water and information about the model boundaries are needed. Moreover, high-resolution meshes are required especially at the interface, where steep velocity gradients between surface water and groundwater occur. Obstacles at the interface can have a high impact on the turbulence and in turn also on the exchange of

groundwater and surface water and consequently, the choice of turbulence model is important for the model results.

- The integral solver provides high-resolution information of pressure and velocity distributions at the groundwater-surface water interaction space. However, the application leads to significantly higher computation times compared to coupled approaches. Therefore, high performance computers are necessary for insights into the local flow and transport processes with high-resolution results in space and time.
- The Urban Water Interfaces Research Training Group (UWI), focuses on natural and technical interfaces in different interdisciplinary topics. One of these common topic group concerns surface water – groundwater interactions from lakes as well as from lotic systems. The hyporheic zone as well as bank filtration were examined with the help of laboratory and field experiments as well as with modelling approaches on different scales. Although the focus of each project lies on different aspects, profits can be achieved through the collaboration. Due to the integral modelling approach e.g. flow paths and exchange rates can be indicated which are important for biogeochemical processes addressed in a further project. Moreover, detailed insights could and can help to design future experiments. Results of laboratory, flume or field experiments from other projects within UWI could and can be used for further validation of the integral solver, which are addressed in section 7.3. A first step of the collaboration was initiated with the common topic group. The second cohort of the Research Training Group UWI has formed to a common topic group called ‘Hyporheic Zones”, which will carry out further cooperation on the basis of the surface water-groundwater interactions group.

7.1.2 Outcomes of flow and tracer retention modelling over rippled streambeds

Three-dimensional free surface flow solving the Navier-Stokes equations with a LES turbulence model and the retention of a tracer pulse over idealized ripples with varying geometries and flow rates were analysed with high-resolution. For a precise description of the prevailing processes non-hydrostatic pressure distributions and two-phase flow (water and air) for the consideration of water level variations were used. The effect of ripple spacing, that was not studied so far, was examined. Similar to commonly applied coupled models, pressure distributions at rippled streambeds were used to locate the exchange of stream and groundwater, while pressure gradients draw conclusions about the amount of exchange. The model was validated based on two experiments for an accurate representation of the flow characteristics at rippled streambeds. The existing two-phase OpenFOAM solver interFoam was extended by an

advection-diffusion equation for the investigation of transport processes. With the help of analytical solutions, the correct description of the transport of a conservative tracer was examined for a constant as well as for a pulse injection. For all simulations at the rippled streambed, the main transport occurred above the ripples with high flow velocities. The tracer was retained between the ripples due to comparatively small velocities and due to recirculation zones. No recirculation zones were observed for the highest ripple length to height ratio. While the pressure gradient – and consequently also the expected amount of water exchange – was the same for ripples with the same height and distance, the tracer disappeared very fast for longer ripples. This led to the assumption, that turbulence has a significant influence on residence times at streambeds. The highest ripple dimension caused waves at the surface with high pressure gradients at the streambed and significantly reduced tracer retention. For smaller ripples, pressure gradients and tracer retention decreased compared to the reference case. For larger distances between the ripples more tracer mass reached the streambed. Although the recirculation zones increased according to the distances, less retention was observed for bigger distances. For lower discharges, pressure gradients decreased, while tracer retention increased. The research showed, that small scale ripples can have a high impact on the amount of water and solute exchange between groundwater and surface water. Ripple geometries and spacing as well as flow discharges decide how long compounds from the surface can be stored within surface water dead zones. The gained results of this research can be important with regard to the hyporheic zone for the movement of compounds like oxygen, carbon, nitrogen-species or contaminants that can be found in surface water and introduce into the sediment. Detailed information can be found in section 3

7.1.3 Outcomes of stream flow modelling for groundwater-surface water interactions

In a next step the sediment was added to the examinations. First of all, the integral solver that extends the three-dimensional Navier-Stokes equations by including the porosity and grain size of the sediment within an additional drag term was validated. For the validation of the description of groundwater-surface water interactions, two cases for seepages through homogeneous dams with different water levels and different dam geometries were examined. The modelled high-resolution results were compared with analytical solutions as well as with other numerical approaches and showed a good agreement. The first study for free surface flow at rippled streambeds using the LES turbulence model was extended for the consideration of the sediment, while the ripple geometries and discharges of the surface water were maintained. Grain sizes that correspond to medium gravel and coarse sand were chosen for the

investigations. For each case study, in- and outflowing fluxes for a representative ripple at the interface were calculated. These fluxes can be important for biogeochemical processes. The sandy ripples showed for all cases lower exchange rates as for the gravel ripples. For the ripple height no clear dependency of the exchange rates on ripple geometry was found, while for ripple spacing and higher flow rates the exchange increased significantly. The simulations showed that not only the surface water flow affected the flow processes in the sediment, but also the sediment properties lead to a change of the surface water flow field compared to the previous study without the sediment. In contrast to the widely used one-way sequential coupling methods, the integral solver is able to consider these interactions in both directions. Non-Darcy-flow areas were observed for sand at a small layer of the interface as well as at the crest. For the gravel higher turbulences were found and non-Darcy-flow areas were depicted almost down to several decimetres. Common coupled approaches apply the Darcy law in the sediment. In contrast to the integral model, the application of the Darcy law for these examinations with higher Reynolds number would lead to an overestimation of flow rates within the sediment. While the Darcy-Brinkmann equation could be used also in non-Darcy-flow areas, an additional parameter has to be determined for this approach. No additional parameters for the interface have to be determined for the applied modelling approach. Investigations of the fluxes, velocities and pressure distributions for all cases were presented in detail in section 4.

7.1.4 Outcomes of transport modelling for surface water-groundwater interactions

In a further step the integral solver was extended for conservative transport with an advection-diffusion equation. First of all, the solver was validated with analytical solutions for a constant and for a pulse injection - similar to the validation of conservative transport in surface water, but with the additional consideration of the sediment. Again, a good agreement with the analytical results was observed. Afterwards, the spreading of a dye tracer, injected into surface water, was simulated for sandy, rippled streambeds under neutral, losing and gaining flow conditions for one hour. In contrast to the previous studies, two-dimensional simulations in combination with a k-ε turbulence model were conducted to reduce the computational effort. Based on photographs of previous flume experiments by Fox et al. (2014), the accurate description of the tracer spreading in the sediment was proven. Moreover, high-resolution results for pressure and velocity distributions at the interface were presented and gave additional insights to the findings of the laboratory experiments. The flow distributions show, that the hyporheic exchange decreased with ambient groundwater flow for losing and for gaining conditions. Consequently, the ambient groundwater flow significantly influenced the velocity

directions and also the tracer spreading within the sediment as the losing and gaining conditions became the dominant mechanisms for water and tracer exchange. Various of the finding for losing and gaining conditions were already seen in other modelling studies. However, the novel integral model for flow and transport is able – in contrast to previous one-way coupled approaches – to consider feedbacks from surface water to groundwater and vice versa. At the same time the model is also applicable for higher Reynolds numbers within the sediment. As described in section 4, this is preferably important for bigger grain sizes, but can also occur at the interface for sandy sediments as seen in section 4. With this study, we proved the correct description of the novel integral solver for transport processes at the interface of surface water and groundwater not only with analytical results, but also with observations of flume experiments. Details of this study can be found in section 5.

7.1.5 Final notes

The main outcome of this thesis is the validation and extension of an integral solver for the understanding of flow and transport processes at the interface of groundwater and surface water. As described in the first section, this understanding of flow paths and tracer transport is important for various disciplines examining exchange processes at the interface, e.g. for biogeochemical processes. The results of the approach show the impact of streambed geometries, surface hydraulics, ambient groundwater and sediment grain sizes on the exchange of water and solute at the interface. The Volume of Fluid approach was used for two-phase water-air flow, to account for water level fluctuations that can have an impact on the non-hydrostatic pressure distribution at the interface and hence also on the exchange of water and solutes. Changes of flow or transport conditions of both domains as e.g. flow velocities, water elevations or changes in tracer concentrations can be resolved during the simulation with the integral model, since the solver is fully coupled in space and time. With one-way coupled approaches it is difficult to consider all these interactions. With the integral solver, three-dimensional investigations using advanced turbulence models like LES can be applied, but also two-dimensional models using the k-ε turbulence model showed good results as the comparison with laboratory observations showed. Turbulent structures that can penetrate from surface water into the sediment can be considered, which is not possible for common applied coupled models. Due to the application of the extended Navier-Stokes equations in groundwater and surface water, non-Darcy flow areas can be considered without the need of additional parameters.

Modelling the interactions of groundwater and surface water can be important for many fields of research with different emphasis and on different scales. Understanding prevailing processes

at the interface or predict processes based on future scenarios - as the impact of climate or demographic changes - can be essential e.g. for hydrological, biological or chemical researches. But not always precise small-scale results are needed. According to the focus of each investigation, adequate modelling strategies have to be applied. In the following sections, the limitations of the present model and future research for improvements are addressed.

7.2 Limitations of the modelling approach

The present integral model is able, to show high-resolution results at the interface of groundwater and surface water with one conceptual model that considers groundwater and surface water with the same time step. This leads on the one hand to a high accuracy but also to the main limitation of the solver: the significant high computation effort. Next to the effort due to the high-resolution in time and space, the computational effort is even increased in the presented research studies due to the applied sophisticated turbulence models, which were relevant for the suitable description of the exchange processes across the interface. Therefore, the solver is mainly recommended for the application on supercomputers, especially if small grain sizes are considered. The model is definitely more appropriate for larger grain sizes with non-Darcy flow areas in the sediment since the calculations for these cases run faster and at the same time the integral solver shows a clear advantage compared to the commonly applied coupled approaches. The sediment with the smallest grain size applied in this thesis was medium sand.

The modelling approach in the current form is recommended if detailed understanding of small-scale processes from several 10 meters or less is required. In the current form it is not applicable for large scales. Also larger time scales – as usually considered for groundwater processes - take too much time with the presented integral solver. A computation time of already ~5 hours on 100 parallel processors is needed for 1-minute simulation of the small scale transport model presented in section 5. The main application area of the integral solver lies consequently at processes close to the interface of groundwater and surface water at small time frames. Larger scales – especially for the consideration of groundwater flow - should be examined with the help of a coupled model.

Many aspects, that are not considered in this thesis - as heterogeneity, sediment transport or reactive transport - can be included in the future (see section 7.3). However, for all supplementary implementations the additional computational effort must always be considered.

7.3 Outlook

The present model was validated based on analytical results and on laboratory experiments under controlled conditions. In a next step, the integral solver for flow and transport will be tested for further cases, geometries and scales, which also should include field site studies. In this context, it is especially important to consult a detailed comparison of the integral solver to a coupled model, in order to depict the advantages and disadvantages of both models more accurately. Afterwards, the functionality can be expanded for reactive transport in collaboration with other UWI projects. However, the investigated reaction processes should be selected carefully - especially with regards to expected computing times. A reactive transport model called 'BioChemFOAM" that also solves the three-dimensional Navier-Stokes equations for the consideration of flow processes was already developed and could be used as a basis for the integral model (Hernandez Murcia, 2014). This model considers algae, organic carbon, phosphorus, nitrogen and dissolved oxygen, that are very important components for groundwater-surface water interactions.

The study showed, that variations of small-scale structures in streams can have a high impact on the exchange rates at the interface. Hence, sediment transport could be added to the modelling approach in the future to simulate morphological changes of the river bed. A sediment transport application called 'SedFoam" was already implemented into OpenFOAM and is based on the twoPhaseEulerFoam solver (Chauchat et al., 2017).

So far, all applications in this thesis, assume quasi steady state flow conditions, although transient flow generally has a significant effect on solute transport and the exchange of groundwater and surface water. Therefore, examining the effect of transient flow conditions could be addressed in further studies – the application is already possible with the present solver.

In addition to the previous studies with homogenous sediments, processes under heterogeneous conditions should be examined. For this purpose, a further experiment with the same flume as presented in section 5 could be used as first test case (Fox et al., 2016), changing mainly the grain sizes and porosities for the sediment in the modelling approach. Since studies, focusing on the impact of heterogeneity on exchange processes came to contradictory conclusions, a systematic analysis of the effect of heterogeneity for different scenarios in a realistic range could be approached. In general, the solver is already able to account for different soil types, but a validation for heterogeneous sediments is still needed.

The presented simulations offer the benefit of detailed insights into local flow and transport processes. To account for effects on larger scales, upscaling approaches have to be developed in the future. Depending on ripple geometries, flow velocities and other variables, exchange rates could be quantified for a one- or two-dimensional shallow water models through sink or source terms. Thereby, coarser meshes can be applied resulting in lower computation times for larger scales, while impacts of small-scale structures could conceptually be accounted for.

To expand the area of application, further surface water-porous media interactions can be examined with the integral solver considering, for example flow through breakwater or simultaneous flow over or through dikes.

Appendix A: Solver extensions

A1 File structure

New solvers, solver extensions or modifications of the official OpenFOAM solvers are usually stored in a user directory. While the official solvers can be found in the directory $WM_PROJECT_DIR, custom solvers can be called via $WM_PROJECT_USER_DIR.

In this thesis, the interFoam solver is used for flow simulations in surface waters and a modified interFoam solver called passiveScalarInterFoam for the transport simulations, which additionally solves an included advection-diffusion transport equation. To use the passiveScalarInterFoam, the official file containing the interFoam solver has to be copied into a subdirectory of $WM_PROJECT_USER_DIR under /applications/solvers/multiphase.

Modifications in the files createFields.H, interFoam.C and in a subfolder called Make have to be executed. The subfolders of other derived solvers (interMixingFoam, LTSInterFoam and porousInterFoam) can be deleted.

The files of the interFoam and the passiveScalarInterFoam solver are presented in Figure A 1 and Figure A 2. The files which have to be modified are highlighted in red. The file interFoam.C has to be renamed to passiveScalarInterFoam.C.

In a similar way as for the passiveScalarInterFoam solver, an advection-diffusion transport equation was integrated into the porousInter solver which was developed by Oxtoby et al. (2013). The porousInter solver considers - in contrast to the interFoam solver - surface water as well as porous media flow. The file structure of the porousInter and the passiveScalarPorousInter solver are listed in Figure A 3 and Figure A 4. The files in the porousInter folder that have to be modified are highlighted in red.

The modifications and extensions within the files are presented in the following sections.

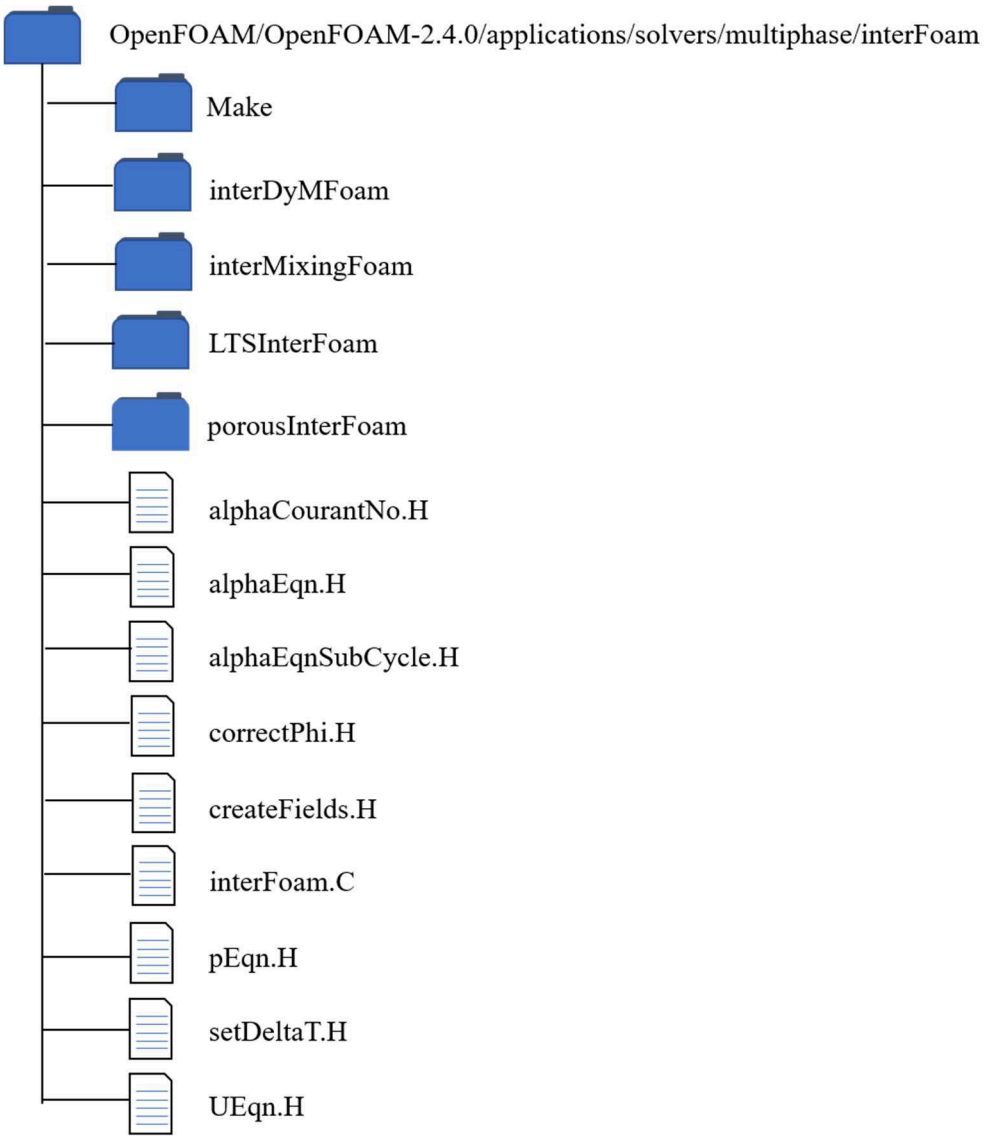

Figure A 1: File structure of interFoam.

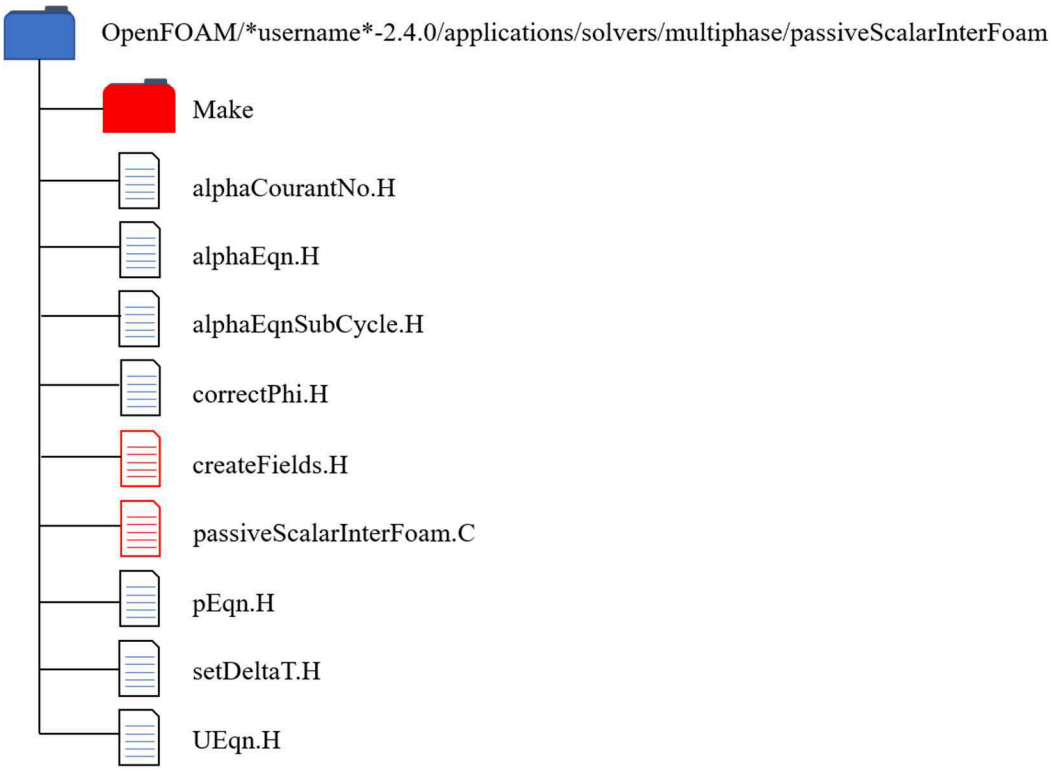

Figure A 2: File structure of passiveScalarInterFoam (files to be modified shown in red).

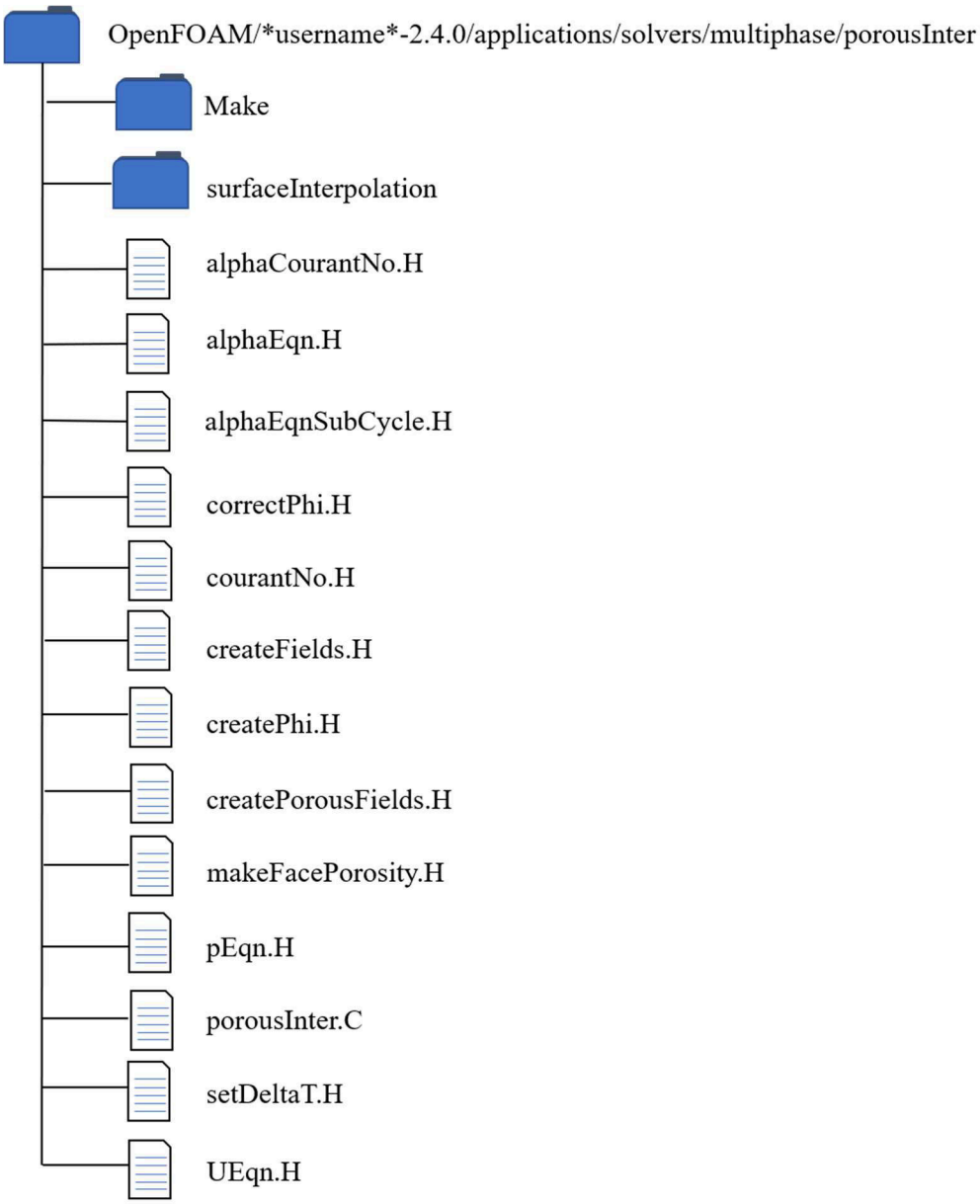

Figure A 3: File structure of porousInter.

Figure A 4: File structure of passiveScalarPorousInter (files to be modified shown in red).

A2 Make/files

First of all, the files within the Make directory have to be modified for a correct initialization of the solver. The content of the file Make/files is illustrated for the passiveScalarInterFoam in Listing A 1. The modifications are made accordingly for the passiveScalarPorousInter solver.

```
passiveScalarInterFoam.C
EXE = $(FOAM_USER_APPBIN)/passiveScalarInterFoam
```

Listing A 1: Modifications in Make/files

A3 createFields.H

All relevant variables of the passiveScalarInterFoam solver are defined within the file createFields.H. The extensions within this file compared to the interFoam solver are illustrated in Listing A 2. The diffusion coefficient is defined as dimensionedScalar D and the turbulent Schmidt number by dimensionedScalar Schmidtnumber. Both variables are user defined and are read from the case directory. The tracer is defined as volScalarField C.

```
dimensionedScalar D
(
        transportProperties.lookup("D")
);

dimensionedScalar Schmidtnumber
(
        transportProperties.lookup("Schmidtnumber")
);

Info<< "Reading field C\n" << endl;
volScalarField C
(
IOobject
   (
   "C",
   runTime.timeName(),
   mesh,
   IOobject::MUST_READ_IF_MODIFIED,
   IOobject::AUTO_WRITE
   ),
   mesh
);
```

Listing A 2: Extensions in createFields.H

A4 passiveScalarInterFoam.C

The transport is described within the file passiveScalarInterFoam.C and is displayed in Listing A 3. The turbulent viscosity is stored in a volScalarField nut.

```
volScalarField nut("nut", turbulence->nut());


fvScalarMatrix CEqn
(
fvm::ddt(C)
+ fvm::div(phi, C)
- fvm::laplacian(D, C)
- fvm::laplacian((nut/Schmidtnumber), C)
);
CEqn.solve();
```

Listing A 3: Modifications of the interFoam solver in passiveScalarInterFoam.C to account for transport

A5 passiveScalarPorousInter.C

Similar, to the mentioned steps before, the porousInter folder has to be modified to account for transport processes. The solver has to be renamed to passiveScalarPorousInter and resetted with wclean. The file Make/files has to be modified similarly to Listing A 1 but with the new solver name passiveScalarPorousInter. The dimensionedScalar D for the diffusion and the volScalarField C for the tracer concentrations have to be initialized in createFields.H according to Listing A 2. The file porousInter.C has to be renamed to passiveScalarPorousInter.C and modifications according to Listing A 4 are needed to solve the advection-diffusion transport equation. Finally, the modified solver has to be recompiled using wmake.

```
surfaceScalarField phi2=phi/(linearInterpolate(porosity));


fvScalarMatrix CEqn
(
fvm::ddt(C)
+fvm::div(phi2, C)
- fvm::laplacian(Dmol, C)
);
CEqn.solve();
```

Listing A 4: Modifications of the porousInter solver in passiveScalarPorousInter.C to account for transport

.

Appendix B: Test case overview

B1 Seepage through a homogeneous dam with an impervious foundation compared with analytical solutions after Casagrande and Kozeny

Table B 1: Model setup for test case B1 (seepage through a homogeneous dam with an impervious foundation compared with analytical solutions after Casagrande and Kozeny).

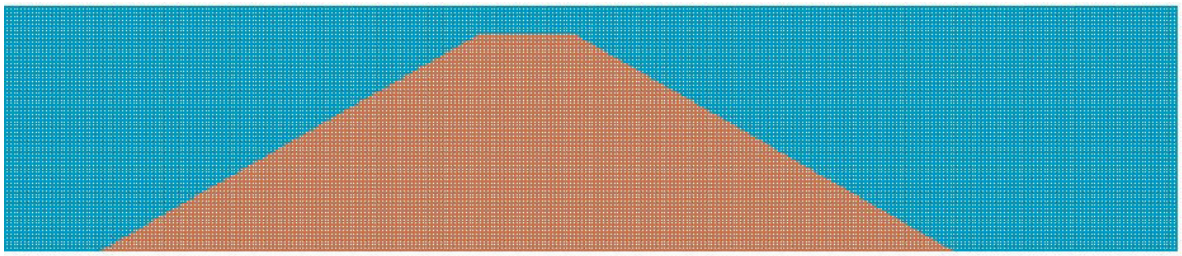

General	
Referred to in chapters	2.1.3.2, 4.3.5
References	Casagrande (1937), Lattermann (2010)
Published in	Broecker et al. (2017); Broecker et al. (2019)
Domain discretization	
Dimensions	two-dimensional (length: 120 m/1.2 m, height: 25 m/2.5 m)
Mesh generator	blockMesh
Number of cells	75000
Turbulence model	laminar
Hydrodynamic simulations	
Solver	porousInter
Time step	variable
Simulation time	9000 s
Transport simulations	Not performed

Table B 2: Boundary conditions for test case B1.

	alpha.water (-)	p_rgh (kg/(ms²))	U (m/s)	effPackingRadius (m)	porosity (-)
inlet_water	inletOutlet inletValue: uniform 1 value: uniform 1	fixedValue value uniform 186390/18639	zeroGradient	zeroGradient	zeroGradient
inlet_air	inletOutlet inletValue: uniform 0 value: uniform 0	totalPressure p0: uniform 0 value: uniform 0	zeroGradient	zeroGradient	zeroGradient
outlet	zeroGradient	totalPressure p0: uniform 0 value: uniform 0	zeroGradient	zeroGradient	zeroGradient
atmosphere	inletOutlet inletValue: uniform 0 value: uniform 0	totalPressure p0: uniform 0 value: uniform 0	pressureInletOutletVelocity value uniform (0 0 0)	zeroGradient	zeroGradient
ground	zeroGradient	fixedFluxPressure value uniform 0	fixedValue value: uniform (0 0 0)	zeroGradient	zeroGradient
sidewalls	empty	empty	empty	empty	empty
initial conditions	uniform 0 define initial water level of 19 m/1.9 m the first 100 m /10 m using boxToCell in setFields (volScalarFieldValue alpha.water 1)	uniform 0 define initial water level of 19 m/1.9 m the first 100 m/10 m using boxToCell in setFields (volScalarFieldValue p_rgh 186390/18639)	uniform (0 0 0)	uniform 0.0159/0.002	uniform 0 in the sediment 0.25 defined by setFields

B2 Seepage through a homogeneous, rectangular dam with an impervious foundation

Table B 3: Model setup for test case B2 (Seepage through a homogeneous, rectangular dam with an impervious foundation).

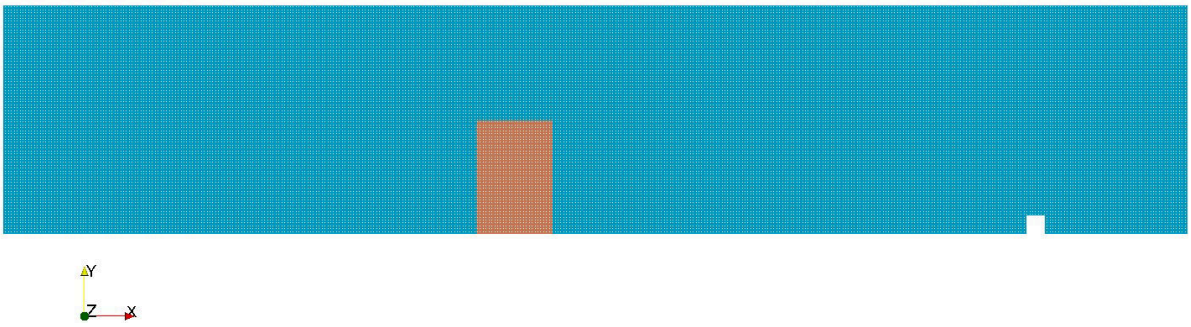

General	
Referred to in chapters	2.1.3.2, 4.3.5
References	Westbrook (1985), Aitchison and Coulson (1972), Kobus and Keim (2001), Di Nucci (2015)
Published in	Broecker et al. (2017); Broecker et al. (2019)
Domain discretization	
Dimensions	two-dimensional (length: 250 m, height: 48 m)
Mesh generator	blockMesh
Number of cells	191744
Turbulence model	laminar
Hydrodynamic simulations	
Solver	porousInter
Time step	variable
Simulation time	9000 s
Transport simulations	Not performed

Table B 4: Boundary conditions for test case B2.

	alpha.water (-)	p_rgh (kg/(ms²))	U (m/s)	effPackingRadius (m)	porosity (-)
inlet_water	inletOutlet inletValue: uniform 1 value: uniform 1	fixedValue value uniform 235440	zeroGradient	zeroGradient	zeroGradient
inlet_air	inletOutlet inletValue: uniform 0 value: uniform 0	totalPressure p0: uniform 0 value: uniform 0	zeroGradient	zeroGradient	zeroGradient
outlet	zeroGradient	totalPressure p0: uniform 0 value: uniform 0	zeroGradient	zeroGradient	zeroGradient
atmosphere	inletOutlet inletValue: uniform 0 value: uniform 0	totalPressure p0: uniform 0 value: uniform 0	pressureInletOutletVelocity value uniform (0 0 0)	zeroGradient	zeroGradient
ground	zeroGradient	fixedFlusPressure value uniform 0	fixedValue value: uniform (0 0 0)	zeroGradient	zeroGradient
sidewalls	empty	empty	empty	empty	empty
initial conditions	uniform 0 define initial water level of 24 m at the left side of the dam, to 4 m at the right side and stepwise from 24 to 4 m inside the dam using boxToCell in setFields (volScalarFieldValue alpha.water 1)	uniform 0 define pressure according to initial water level using boxToCell in setFields	uniform (0 0 0)	uniform 0.0159/0.002	uniform 0 in the sediment 0.25 defined by setFields

B3 One-phase channel flow over a single ripple

Table B 5: Model setup for test case B3 (One-phase channel flow over a single ripple).

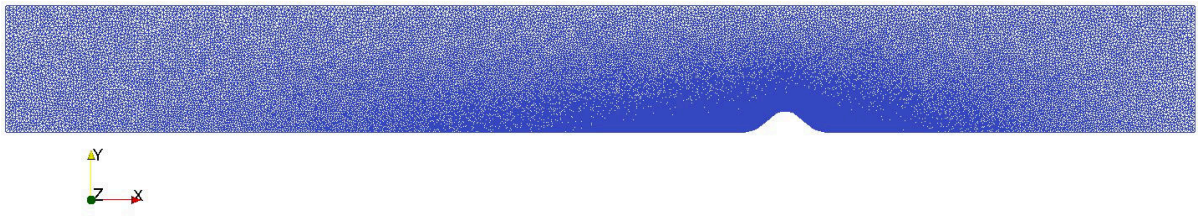

General	
Referred to in chapters	3.4
References	Almeida et al. (1990)
Published in	Broecker et al. (2018)
Domain discretization	
Dimensions	two-dimensional (length: 1.608 m, height: 0.17 m (max))
Mesh generator	gmsh
Number of cells	63806
Turbulence model	Standard k-ε, Standard k-ω, k-ω SST, LES
Hydrodynamic simulations	
Solver	interFoam
Time step	variable
Simulation time	10 s
Transport simulations	Not performed

Table B 6:Boundary conditions for test case B3.

	alpha.water (-)	p_rgh (kg/(ms²))	U (m/s)	k (m²/s²)	ε (m²/s³)/ω (1/s)
inlet	inletOutlet inletValue: uniform 1 value: uniform 1	zeroGradient	fixedValue value: parabolic function following experimental results, applied using funkySetBoundary	turbulentIntensity-kineticEnergyInlet intensity: 0.03 value: uniform 0.00622	ε: turbulentMixingLength-DissipationRateInlet mixingLength: 0.0119 value: uniform 0.00371 ω: turbulentMixingLengthFrequencyInlet mixingLength: 0.0119 value: 6.629
outlet	zeroGradient	fixedValue value: uniform 1668	zeroGradient	zeroGradient	zeroGradient
upper wall	zeroGradient	zeroGradient	fixedValue value: uniform (0 0 0)	kqRWallFunction value: uniform 0.00622	ε: epsilonWallFunction value: uniform 0.00371 ω: omegaWallFunction value: 6.629
ground	zeroGradient	zeroGradient	fixedValue value: uniform (0 0 0)	kqRWallFunction value: uniform 0.00622	ε: epsilonWallFunction value: uniform 0.00371 ω: omegaWallFunction value: 6.629
sidewalls	empty	empty	empty	empty	empty
initial conditions	uniform 1	uniform 1668	uniform (0 0 0)	uniform 0.00622	ε: uniform 0.00371 ω: uniform 6.62906

B4 Two-phase flow over triangular ripples

Table B 7: Model setup for test case B4 (Two-phase flow over triangular ripples).

General	
Referred to in chapters	3.4
References	Fehlman (1985)
Published in	Broecker et al. (2018)
Domain discretization	
Dimensions	two-dimensional (length: 18.288 m, height: 0.762 m (max))
Mesh generator	gmsh
Number of cells	624360/677610
Turbulence model	LES
Hydrodynamic simulations	
Solver	interFoam
Time step	variable
Simulation time	600 s/1000 s
Transport simulations	Not performed

Table B 8: Boundary conditions for test case B4.

	alpha.water (-)	p_rgh (kg/(ms²))	U (m/s)
inlet_water	inletOutlet inletValue: uniform 1 value: uniform 1	fixedFluxPressure value: uniform 0	flowRateInletVelocity volumetricFlowRate 0.039671902/0.079343804 value: uniform (0 0 0)
inlet_air	inletOutlet inletValue: uniform 0 value: uniform 0	totalPressure p0: uniform 0 value: uniform 0	zeroGradient
outlet	zeroGradient	totalPressure p0: uniform 0 value: uniform 0	zeroGradient
atmosphere	inletOutlet inletValue: uniform 0 value: uniform 0	totalPressure p0: uniform 0 value: uniform 0	pressureInletOutletVelocity value: uniform (0 0 0)
walls	zeroGradient	fixedFluxPressure value: uniform 0	fixedValue value: uniform (0 0 0)
initial conditions	uniform 0 define initial water level of 0.2723 m using boxToCell in setFields (volScalarFieldValue alpha.water 1)	uniform 0	uniform (0 0 0) volVectorFieldValue (0.2944368/0.5886 0 0) for initial water level of 0.2723 m

B5 One-dimensional tracer transport in surface water

Table B 9: Model setup for test case B5 (One-dimensional tracer transport in surface water).

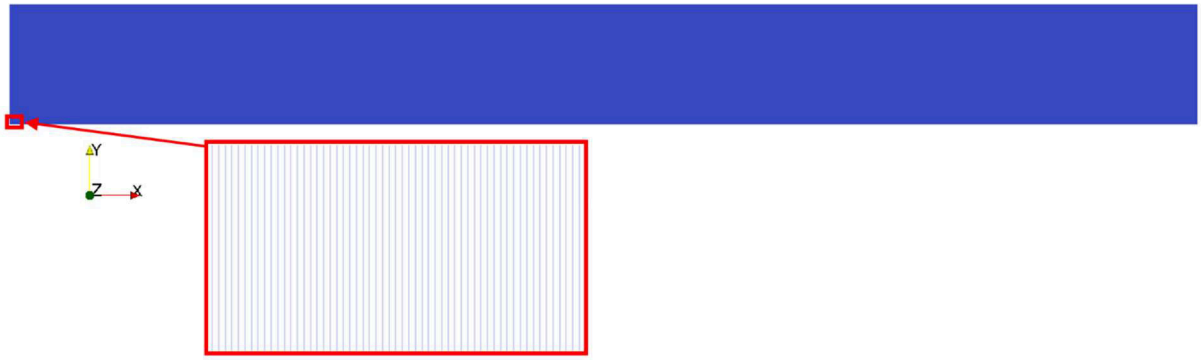

General	
Referred to in chapters	3.4
References	Kinzelbach (1992)
Published in	Broecker et al. (2018)
Domain discretization	
Dimensions	one-dimensional (length: 10 m, height: 1 m)
Mesh generator	blockMesh
Number of cells	10000
Turbulence model	laminar
Hydrodynamic simulations	Not performed
Transport simulations	
Solver	passiveScalarInterFoam
Time step	variable
Simulation time	8 s
Tracer diffusivity	0.1 m^2/s and 10^{-9} m^2/s (a high diffusivity was chosen to check the implementation of the diffusion term)

Table B 10: Boundary conditions for test case B5.

	alpha.water (-)	p_rgh (kg/(ms²))	U (m/s)	C (kg/m³)
inlet	inletOutlet inletValue: uniform 1 value: uniform 1	zeroGradient	fixedValue value: uniform (1 0 0)	fixedValue value: uniform 1/uniform 0
outlet	zeroGradient	fixedValue value: uniform 0	zeroGradient	zeroGradient
Upper, lower and sidewalls	empty	empty	empty	empty
initial conditions	uniform 1	uniform 0	uniform (1 0 0)	uniform 0/ define initial tracer concentration of uniform 1 for x = 2 m to x = 2.01 m using boxToCell in setFields for pulse injection

B6 Two-phase flow and tracer transport over rippled streambeds

Table B 11: Model setup for test case B6 (Two-phase flow and tracer transport over rippled streambeds).

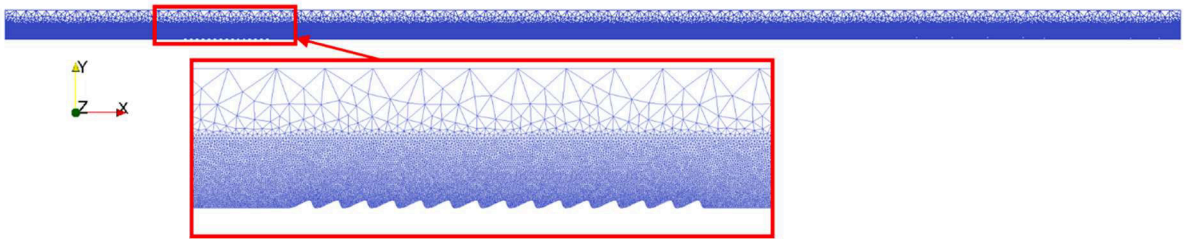

General	
Referred to in chapters	3.5
References	-
Published in	Broecker et al. (2018)
Domain discretization	
Dimensions	three-dimensional (length: 40 m, height: 1 m (max), depth: 1 m)
Mesh generator	gmsh
Number of cells	1236910-2104910
Turbulence model	LES
Hydrodynamic simulations	
Solver	interFoam
Time step	variable
Simulation time	100 s
Transport simulations	
Solver	passiveScalarInterFoam
Time step	variable
Simulation time	100 s
Tracer diffusivity	10^{-9} m^2/s

Table B 12: Boundary conditions for test case B6.

	alpha.water (-)	p_rgh (kg/(ms²))	U (m/s)	C (kg/m³)
inlet_water	inletOutlet inletValue: uniform 1 value: uniform 1	fixedFluxPressure value: uniform 0	flowRateInletVelocity volumetricFlowRate 0.5/0.25 value: uniform (1 0 0)/(0.5 0 0)	fixedValue value: uniform 0
inlet_air	inletOutlet inletValue: uniform 0 value: uniform 0	totalPressure p0: uniform 0 value: uniform 0	zeroGradient	fixedValue value uniform 0
outlet	zeroGradient	fixedFluxPressure value: uniform 0	outletPhaseMeanVelocity Umean 1.0/0.5 alpha alpha.water value: uniform (1 0 0)/(0.5 0 0)	zeroGradient
atmosphere	zeroGradient	totalPressure p0: uniform 0 value: uniform 0	pressureInletOutletVelocity value: uniform (0 0 0)	fixedValue value: uniform 0
ground	zeroGradient	fixedFluxPressure value: uniform 0	fixedValue value: uniform (0 0 0)	zeroGradient
sidewalls	slip	slip	slip	slip
initial conditions	uniform 0 define initial water level of 0.5 m using boxToCell in setFields (volScalarFieldValue alpha.water 1)	uniform 0	uniform (1 0 0)/(0.5 0 0)	uniform 0 define initial tracer concentration from x = 0 m to 0.5 m and y = 0 m to y = 0.5 m and z = 0 m to 1 m using boxToCell in setFields (volScalarFieldValue C 1)

B7 Flow simulations for groundwater-surface water interactions at rippled streambeds

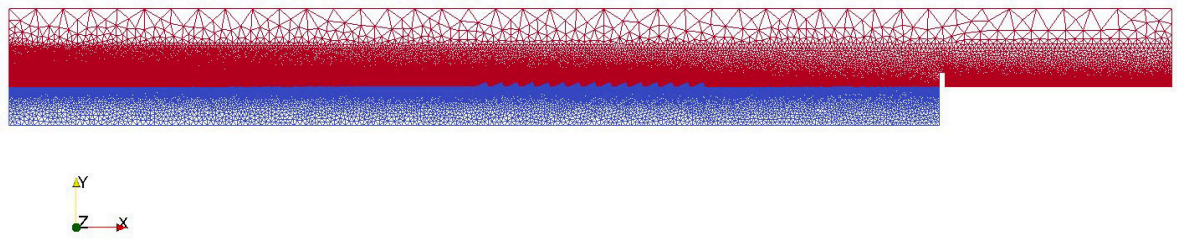

Table B 13: Model setup for test case B7 (Flow simulations for groundwater-surface water interactions at rippled streambeds).

General	
Referred to in chapters	4.3, 4.4
References	-
Published in	Broecker et al. (2019)
Domain discretization	
Dimensions	three-dimensional (length: 15 m, height: 1.5 m (max), depth: 1 m)
Mesh generator	gmsh
Number of cells	1653080-1806450
Turbulence model	LES
Hydrodynamic simulations	
Solver	porousInter
Time step	variable
Simulation time	300 s
Transport simulations	Not performed

Table B 14: Boundary conditions for test case B7.

	alpha.water (-)	p_rgh (kg/(ms²))	U (m/s)	effPackingRadius (m)	porosity (-)
inlet_water	inletOutlet inletValue: uniform 1 value: uniform 1	fixedFluxPressure value: uniform 0	flowRateInletVelocity volumetricFlowRate 0.5/0.25 value: uniform (1 0 0)/(0.5 0 0)	zeroGradient	zeroGradient
inlet_air	inletOutlet inletValue: uniform 0 value: uniform 0	totalPressure p0: uniform 0 value: uniform 0	zeroGradient	zeroGradient	zeroGradient
outlet	zeroGradient	totalPressure p0: uniform 0 value: uniform 0	zeroGradient	zeroGradient	zeroGradient
atmosphere	inletOutlet inletValue: uniform 0 value: uniform 0	totalPressure p0: uniform 0 value: uniform 0	pressureInletOutletVelocity value: uniform (0 0 0)	zeroGradient	zeroGradient
walls	zeroGradient	fixedFluxPressure value: uniform 0	fixedValue value uniform (0 0 0)	zeroGradient	zeroGradient
side	slip	slip	slip	slip	slip
initial conditions	uniform 0 define initial water level from x = 0 m to x = 12 m and y = -0.5 m to 0.5 m and z = 0 m to z = 1 m using boxToCell in setFields (volScalarFieldValue alpha.water 1)	uniform 0	uniform (0 0 0)	uniform 0.015/0.002	uniform 0 in the sediment 0.25 defined by setFields

B8 One-dimensional tracer transport in surface water and groundwater

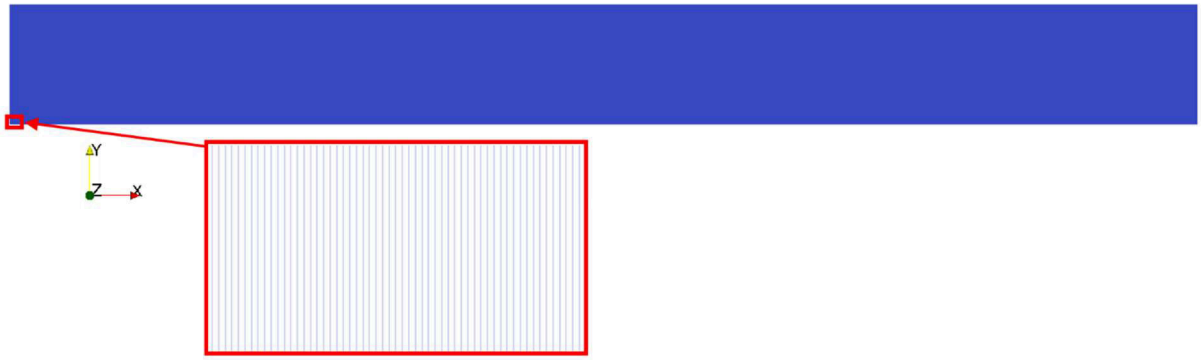

Table B 15: Model setup for test case B8 (One-dimensional tracer transport in surface water and groundwater).

General	
Referred to in chapters	5.3.3
References	Kinzelbach (1992)
Published in	Broecker et al. (submitted)
Domain discretization	
Dimensions	one-dimensional (length: 10 m, height: 1 m)
Mesh generator	blockMesh
Number of cells	10000
Turbulence model	laminar
Hydrodynamic simulations	Not performed
Transport simulations	
Solver	passiveScalarPorousInter
Time step	variable
Simulation time	1000 s
Tracer diffusivity	10^{-9} m^2/s

Table B 16: Boundary conditions for test case B8.

	alpha.water (-)	p_rgh (kg/(ms²))	U (m/s)	C (kg/m³)	effPackingRadius (m)	porosity (-)
inlet	inletOutlet inletValue: uniform 1 value: uniform 1	zeroGradient	fixedValue value: uniform (0.01 0 0)	fixedValue value: uniform 1/uniform 0	zeroGradient	zeroGradient
outlet	zeroGradient	fixedValue value: uniform 0	zeroGradient	zeroGradient	zeroGradient	zeroGradient
Upper, lower and sidewalls	empty	empty	empty	empty	zeroGradient	zeroGradient
initial conditions	uniform 1	uniform 0	uniform (0.01 0 0)	uniform 0/ define initial tracer concentration of uniform 1 for x = 2 m to x = 2.01 m using boxToCell in setFields for pulse injection	uniform 0.01t	Define sediment from x = 5 m to x=10 m and y = 0 m to 1 m and z = 0 m to z = 1 m using boxToCell in setFields (volScalarFieldValue porosity 0.3)

B9 Transport simulations for groundwater-surface water interactions at rippled streambeds

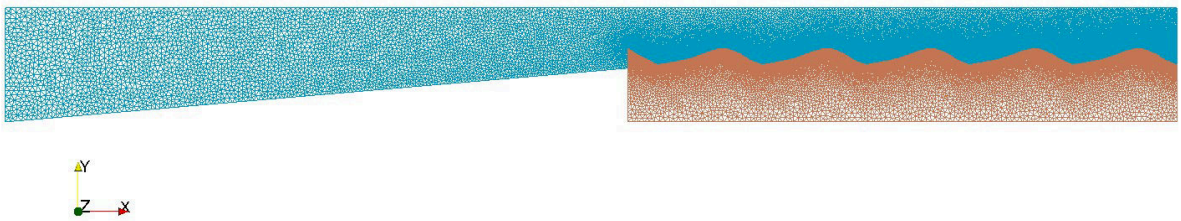

Table B 17: Model setup for test case (B9 Transport simulations for groundwater-surface water interactions at rippled streambeds).

General	
Referred to in chapters	5.3, 5.4
References	Fox et al. (2014)
Published in	Broecker et al. (submitted)
Domain discretization	
Dimensions	two-dimensional (length: 1.75 - 1.755 m, height: 0.17 m)
Mesh generator	gmsh
Number of cells	76743-77148
Turbulence model	k-ε
Hydrodynamic simulations	
Solver	porousInter
Time step	variable
Simulation time	3900 s
Transport simulations	
Solver	passiveScalarPorousInter
Time step	variable
Simulation time	3900 s
Tracer diffusivity	10^{-9} m^2/s

Table B 18: Boundary conditions for test case B9.

	alpha.water (-)	p_rgh (kg/(ms²))	U (m/s)	C (kg/m³)	k (m²/s²)	ε (m²/s³)	effPackingRadius (m)	porosity (-)
inlet	fixedValue value: uniform 1	zeroGradient	flowRateInletVelocity volumetricFlowRate 0.0025 value: uniform (0.0507099 0 0)	inletOutlet inletValue: uniform 1 value: uniform 1	fixedValue value $internalField	fixedValue value $internalField	zeroGradient	zeroGradient
outlet	inletOutlet inletValue: uniform 1 value: uniform 1	fixedValue value: uniform 0	zeroGradient	zeroGradient	inletOutlet inletValue $internalField value $internalField	inletOutlet inletValue $internalField value $internalField	zeroGradient	zeroGradient
atmosphere	slip	slip	slip	slip	inletOutlet inletValue $internalField value $internalField	inletOutlet inletValue $internalField value $internalField	zeroGradient	zeroGradient
lower walls	zeroGradient	zeroGradient	fixedValue value: uniform (0 0 0)	zeroGradient	kqRWallFunction value $internalField	epsilonWallFunction value $internalField	zeroGradient	zeroGradient
sidewalls	empty	empty	empty	empty	empty	empty	empty	empty

groundwater inflow (for gaining and losing conditions)	fixedValue value: uniform 1	fixedFluxPressure	flowRateInletVelocity volumetricFlowRate 0.000001349 value: uniform (0 0.0000056713 0)	inletOutlet inletValue: uniform 1 value: uniform 1	fixedValue value uniform 0.001	fixedValue value uniform 0.002	zeroGradient	zeroGradient
initial conditions	uniform 1	uniform 0	for surface water: uniform (0.123 0 0), for the sediment: uniform (0 0 0) for neutral conditions, uniform (0 +/-0.0000056713 0) for gaining and losing conditions defined by setFields	uniform 0	uniform 0.0000567	uniform 0.00000785	uniform 0.000384	uniform 0, in the sediment uniform 0.33 defined by setFields

Bibliography

Aitchison, J. & Coulson, C. A. (1972). Numerical treatment of a singularity in a free boundary problem. *Proceedings of the Royal Society of London A: Mathematical and Physical Sciences, 330*(1583), 573-580, doi:10.1098/rspa.1972.0160.

Alaghmand, S., Beecham, S., Jolly, I. D., Holland, K. L., Woods, J. A. & Hassanli, A. (2014). Modelling the impacts of river stage manipulation on a complex river-floodplain system in a semi-arid region. *Environmental Modelling & Software, 59*, 109-126, doi:10.1016/j.envsoft.2014.05.013.

Almeida, G. P., Durao, D. F. G., Simoes, J. P. & Heitor, M. V. (1990). *Laser-Doppler measurements of fully developed turbulent channel flow.* Paper presented at the 5th International symposia on applications of laser techniques to fluid mechanics.

Alvarez, D. & Nicieza, A. G. (2005). Compensatory response 'defends' energy levels but not growth trajectories in brown trout, Salmo trutta L. *Proceedings of the Royal Society B: Biological Sciences, 272*(1563), 601-607, doi:10.1098/rspb.2004.2991.

Anderson, M. P. (2005). Heat as a Ground Water Tracer. *Groundwater, 43*(6), 951-968, doi:10.1111/j.1745-6584.2005.00052.x.

Arnon, S., Yanuka, K. & Nejidat, A. (2013). Impact of overlying water velocity on ammonium uptake by benthic biofilms. *Hydrological Processes, 27*(4), 570-578, doi:10.1002/hyp.9239.

Badarch, A. (2017). *Application of macro and mesoscopic numerical models to hydraulic problems with solid substances.*

Bardini, L., Boano, F., Cardenas, M. B., Revelli, R. & Ridolfi, L. (2012). Nutrient cycling in bedform induced hyporheic zones. *Geochimica et Cosmochimica Acta, 84*, 47-61, doi:10.1016/j.gca.2012.01.025.

Baumgarten, B. (2013). *Entfernung von Sulfamethoxazol in der Bodenpassage.* (Doctoral Thesis), Technische Universität Berlin Berlin.

Bayani Cardenas, M. & Wilson, J. L. (2006). The influence of ambient groundwater discharge on exchange zones induced by current–bedform interactions. *Journal of Hydrology, 331*(1), 103-109, doi:10.1016/j.jhydrol.2006.05.012.

Bayon-Barrachina, A. & Lopez-Jimenez, P. A. (2015). Numerical analysis of hydraulic jumps using OpenFOAM. *Journal of Hydroinformatics, 17*(4), 662-678, doi:10.2166/hydro.2015.041.

Bear, J. (1972). *Dynamics of Fluids In Porous Media*: American Elsevier Publishing Company.

Beavers, G. S. & Joseph, D. D. (1967). Boundary conditions at a naturally permeable wall. *Journal of Fluid Mechanics, 30*(1), 197-207, doi:10.1017/S0022112067001375.

Becker, M. W., Georgian, T., Ambrose, H., Siniscalchi, J. & Fredrick, K. (2004). Estimating flow and flux of ground water discharge using water temperature and velocity. *Journal of Hydrology, 296*(1), 221-233, doi:10.1016/j.jhydrol.2004.03.025.

Bencala, K. E. (2000). Hyporheic zone hydrological processes. *Hydrological Processes, 14*(15), 2797-2798, doi:10.1002/1099-1085(20001030)14:15<2797::Aid-hyp402>3.0.Co;2-6.

Bencala, K. E. & Walters, R. A. (1983). Simulation of solute transport in a mountain pool-and-riffle stream: A transient storage model. *Water Resources Research, 19*(3), 718-724, doi:10.1029/WR019i003p00718.

Birgand, F., Skaggs, R. W., Chescheir, G. M. & Gilliam, J. W. (2007). Nitrogen Removal in Streams of Agricultural Catchments—A Literature Review. *Critical Reviews in Environmental Science and Technology, 37*(5), 381-487, doi:10.1080/10643380600966426.

Blois, G., Best, J. L., Sambrook Smith, G. H. & Hardy, R. J. (2014). Effect of bed permeability and hyporheic flow on turbulent flow over bed forms. *Geophysical Research Letters, 41*(18), 6435-6442, doi:10.1002/2014gl060906.

Boano, F., Camporeale, C., Revelli, R. & Ridolfi, L. (2006). Sinuosity-driven hyporheic exchange in meandering rivers. *Geophysical Research Letters, 33*(18), doi:10.1029/2006gl027630.

Boano, F., Harvey, J. W., Marion, A., Packman, A. I., Revelli, R., Ridolfi, L. & Wörman, A. (2014). Hyporheic flow and transport processes: Mechanisms, models and biogeochemical implications. *Reviews of Geophysics, 52*(4), 603-679, doi:10.1002/2012rg000417.

Boano, F., Revelli, R. & Ridolfi, L. (2007). Bedform-induced hyporheic exchange with unsteady flows. *Adv. Water Resour., 30*(1), 148-156.

Boano, F., Revelli, R. & Ridolfi, L. (2008). Reduction of the hyporheic zone volume due to the stream-aquifer interaction. *Geophysical Research Letters, 35*(9), doi:10.1029/2008gl033554.

Boisneau, C., Moatar, F., Bodin, M. & Boisneau, P. (2008). Does global warming impact on migration patterns and recruitment of Allis shad (Alosa alosa L.) young of the year in the Loire River, France? In S. Dufour, E. Prévost, E. Rochard, & P. Williot (Eds.), *Fish and Diadromy in Europe (ecology, management, conservation): Proceedings of the symposium held 29 March – 1 April 2005, Bordeaux, France* (pp. 179-186). Dordrecht: Springer Netherlands.

Borch, T., Kretzschmar, R., Kappler, A., Cappellen, P. V., Ginder-Vogel, M., Voegelin, A. & Campbell, K. (2010). Biogeochemical Redox Processes and their Impact on Contaminant Dynamics. *Environmental Science & Technology, 44*(1), 15-23, doi:10.1021/es9026248.

Boscarino, B. T., Rudstam, L. G., Mata, S., Gal, G., Johannsson, O. E. & Mills, E. L. (2007). The effects of temperature and predator—prey interactions on the migration behavior and vertical distribution of Mysis relicta. *Limnology and Oceanography, 52*(4), 1599-1613, doi:10.4319/lo.2007.52.4.1599.

Botter, G., Basu, N. B., Zanardo, S., Rao, P. S. C. & Rinaldo, A. (2010). Stochastic modeling of nutrient losses in streams: Interactions of climatic, hydrologic and biogeochemical controls. *Water Resources Research, 46*(8), doi:10.1029/2009wr008758.

Boulton, A., Datry, T., Kasahara, T., Mutz, M. & Stanford, J. (2010). Ecology and management of the hyporheic zone: Stream-groundwater interactions of running waters and their floodplains. *Journal of the North American Benthological Society, 29*, 26-40, doi:10.1899/08-017.1.

Boulton, A., Findlay, S., Marmonier, P., Stanley, E. H. & Valett, H. M. (1998). The functional significance of the hyporheic zone in streams and rivers. *Annual Review of Ecology and Systematics, 29*(1), 59-81, doi:10.1146/annurev.ecolsys.29.1.59.

Boutron, O., Margoum, C., Chovelon, J.-M., Guillemain, C. & Gouy, V. (2011). Effect of the submergence, the bed form geometry, and the speed of the surface water flow on the mitigation of pesticides in agricultural ditches. *Water Resources Research, 47*(8), doi:10.1029/2011wr010378.

Brinkman, H. C. (1949). A calculation of the viscous force exerted by a flowing fluid on a dense swarm of particles. *Flow, Turbulence and Combustion, 1*(1), 27, doi:10.1007/BF02120313.

Broecker, T., Elsesser, W., Teuber, K., Özgen, I., Nützmann, G. & Hinkelmann, R. (2018). High-resolution simulation of free-surface flow and tracer retention over streambeds with ripples. *Limnologica, 68*, 46-58, doi:10.1016/j.limno.2017.06.005.

Broecker, T., Schaper, J., El-Athman, F., Gillefalk, M., Hilt, S. & Hinkelmann, R. (2017). *Surface water-groundwater interactions.* Paper presented at the 37th IAHR

(International Association for Hydro-Environment Engineering and Research) World Congress, Kuala Lumpur, Malaysia.

Broecker, T., Teuber, K., Sobhi Gollo, V., Nützmann, G., Lewandowski, J. & Hinkelmann, R. (2019). Integral Flow Modelling Approach for Surface Water-Groundwater Interactions along a Rippled Streambed. *Water, 11*(7), 1517.

Brunke, M. (2001). Wechselwirkungen zwischen Fließgewässer und Grundwasser: Bedeutung für aquatische Biodiversität, Stoffhaushalt und Lebensraumstrukturen. *Wasserwirtschaft, 90*, 32-37.

Brunke, M. & Gonser, T. (1997). The ecological significance of exchange processes between rivers and groundwater. *Freshwater Biology, 37*(1), 1-33, doi:10.1046/j.1365-2427.1997.00143.x.

Brunner, P., Cook, P. G. & Simmons, C. T. (2009). Hydrogeologic controls on disconnection between surface water and groundwater. *Water Resources Research, 45*(1), doi:10.1029/2008wr006953.

Brunner, P. & Simmons, C. (2011). *HydroGeoSphere: A Fully Integrated, Physically Based Hydrological Model* (Vol. 50).

Brunner, P. & Simmons, C. T. (2012). HydroGeoSphere: A Fully Integrated, Physically Based Hydrological Model. *Groundwater, 50*(2), 170-176, doi:10.1111/j.1745-6584.2011.00882.x.

Buffington, J. M. & Tonina, D. (2009). Hyporheic exchange in mountain rivers II: Effects of channel morphology on mechanics, scales, and rates of exchange. *Geography Compass, 3*(3), 1038-1062, doi:10.1111/j.1749-8198.2009.00225.x.

Burnett, W. C., Bokuniewicz, H., Huettel, M., Moore, W. S. & Taniguchi, M. (2003). Groundwater and pore water inputs to the coastal zone. *Biogeochemistry, 66*(1), 3-33, doi:10.1023/B:BIOG.0000006066.21240.53.

Buss, S., Cai, Z., Cardenas, B., Fleckenstein, J., Hannah, D., Heppell, K., Hulme, P., Ibrahim, T., Kaeser, D., Krause, S., Lawler, D., Lerner, D., Mant, J., Malcolm, I., Old, G., Parkin, G., Pickup, R., Pinay, G., Porter, J., Rhodes, G., Richie, A., Riley, J., Robertson, A., Sear, D., Shields, B., Smith, J., Tellam, J. & Wood, P. (2009). *The Hyporheic Handbook - A handbook on the groundwater–surface water interface and hyporheic zone for environment managers*: Environment Agency.

Cardenas, M. B. (2008). The effect of river bend morphology on flow and timescales of surface water groundwater exchange across pointbars. *J. Hydrol., 362*(1-2), 134-141.

Cardenas, M. B. (2009). Stream-aquifer interactions and hyporheic exchange in gaining and losing sinuous streams. *Water Resources Research, 45*(6), doi:10.1029/2008wr007651.

Cardenas, M. B. (2015). Hyporheic zone hydrologic science: A historical account of its emergence and a prospectus. *Water Resources Research, 51*(5), 3601-3616, doi:10.1002/2015wr017028.

Cardenas, M. B., Cook, P. L. M., Jiang, H. & Traykovski, P. (2008). Constraining denitrification in permeable wave-influenced marine sediment using linked hydrodynamic and biogeochemical modeling. *Earth Planet. Sci. Lett., 275*(1-2), 127–137.

Cardenas, M. B. & Wilson, J. L. (2007a). Dunes, turbulent eddies, and interfacial exchange with permeable sediments. *Water Resources Research, 43*(8), doi:10.1029/2006wr005787.

Cardenas, M. B. & Wilson, J. L. (2007b). Exchange across a sediment–water interface with ambient groundwater discharge. *Journal of Hydrology, 346*, 69-80, doi:10.1016/j.jhydrol.2007.08.019.

Cardenas, M. B. & Wilson, J. L. (2007c). Hydrodynamics of coupled flow above and below a sediment-water interface with triangular bedforms. *Adv. Water Resour., 30*(3), 301-313.

Cardenas, M. B. & Wilson, J. L. (2007d). Thermal regime of dune-covered sediments under gaining and losing water bodies. *Journal of Geophysical Research: Biogeosciences, 112*(G4), doi:10.1029/2007jg000485.

Caretto, L. S., Gosman, A. D., Patankar, S. V. & Spalding, D. B. (1973, 1973//). *Two calculation procedures for steady, three-dimensional flows with recirculation.* Paper presented at the Proceedings of the Third International Conference on Numerical Methods in Fluid Mechanics, Berlin, Heidelberg.

Casagrande, A. (1937). *Seepage Through Dams*: Harvard University Graduate School of Engineering.

Chanson, H. & Montes, J. S. (1995). Characteristics of undular hydraulic jumps: Experimental apparatus and flow patterns. *J. Hydraul. Eng., 121*(2), 129-144.

Chauchat, J., Cheng, Z., Nagel, T., Bonamy, C. & Hsu, T. J. (2017). SedFoam-2.0: a 3-D two-phase flow numerical model for sediment transport. *Geosci. Model Dev., 10*(12), 4367-4392, doi:10.5194/gmd-10-4367-2017.

Chen, X., Cardenas, M. B. & Chen, L. (2015). Three-dimensional versus two-dimensional bed form-induced hyporheic exchange. *Water Resources Research, 51*(4), 2923-2936, doi:10.1002/2014wr016848.

Chen, X., Cardenas, M. B. & Chen, L. (2018). Hyporheic Exchange Driven by Three-Dimensional Sandy Bed Forms: Sensitivity to and Prediction from Bed Form Geometry. *Water Resources Research, 54*(6), 4131-4149, doi:10.1029/2018wr022663.

Cheng, N.-S. & Chiew, Y.-M. (1998). Modified Logarithmic Law for Velocity Distribution Subjected to Upward Seepage. *Journal of Hydraulic Engineering, 124*(12), 1235-1241, doi:10.1061/(ASCE)0733-9429(1998)124:12(1235).

Cole, J. J., Caraco, N. F., Kling, G. W. & Kratz, T. K. (1994). Carbon Dioxide Supersaturation in the Surface Waters of Lakes. *Science, 265*(5178), 1568-1570, doi:10.1126/science.265.5178.1568.

Cook, P. G. (2015). Quantifying river gain and loss at regional scales. *Journal of Hydrology, 531*, 749-758, doi:10.1016/j.jhydrol.2015.10.052.

Dahm, C. N., Grimm, N. B., Marmonier, P., Valett, H. M. & Vervier, P. (1998). Nutrient dynamics at the interface between surface waters and groundwaters. *Freshwater Biology, 40*(3), 427-451, doi:10.1046/j.1365-2427.1998.00367.x.

Darcy, H. P. G. (1856). Les fontaines publiques de la ville de DijonVictor Dalmon. In H. R. a. S. Inc (Ed.), *History of Hydraulics* (pp. 169-177).

Dent, C. L., Grimm, N. B., Martí, E., Edmonds, J. W., Henry, J. C. & Welter, J. R. (2007). Variability in surface-subsurface hydrologic interactions and implications for nutrient retention in an arid-land stream. *Journal of Geophysical Research: Biogeosciences, 112*(G4), doi:10.1029/2007jg000467.

Di Nucci, C. (2015). *A free boundary problem for fluid flow through porous media*.

Doyle, M. W. (2005). Incorporating hydrologic variability into nutrient spiraling. *Journal of Geophysical Research: Biogeosciences, 110*(G1), doi:10.1029/2005jg000015.

Drews, A., Klahm, T., Renk, B., Saygili, M., Baumgarten, G. & Kraume, M. (2003). Nanofiltration of CIP waters from iodine X-ray contrast media production: process design and modelling. *Desalination, 159*(2), 119-129, doi:10.1016/S0011-9164(03)90064-6.

Duff, J., Hendricks, S., Jackman, A. & Triska, F. (2001). The effect of Elodea canadensis beds on porewater chemistry, microbial respiration, and nutrient retention in the Shingobee River, Minnesota, North America. *SIL Proceedings, 1922-2010, 28*, 214-222, doi:10.1080/03680770.2001.11902575.

DWA. (2013). *Wechselwirkungen zwischen Grund- und Oberflächenwasser: DWA-Themen T 2/2013*: Deutsche Vereinigung für Wasserwirtschaft, Abwasser und Abfall.

Ebert, I., Konradi, S., Hein, A. & Amato, R. (2014). Arzneimittel in der Umwelt - vermeiden, reduzieren, überwachen. Retrieved from https://www.umweltbundesamt.de/sites/default/files/medien/378/publikationen/01.08.2014_hintergrundpapier_arzneimittel_final_.pdf

Elliott, A. H. & Brooks, N. H. (1997a). Transfer of nonsorbing solutes to a streambed with bed forms: Laboratory experiments. *Water Resources Research, 33*(1), 137-151, doi:10.1029/96wr02783.

Elliott, A. H. & Brooks, N. H. (1997b). Transfer of nonsorbing solutes to a streambed with bed forms: Theory. *Water Resources Research, 33*(1), 123-136, doi:10.1029/96wr02784.

Engelhardt, I., Barth, J. A. C., Bol, R., Schulz, M., Ternes, T. A., Schüth, C. & van Geldern, R. (2014). Quantification of long-term wastewater fluxes at the surface water/groundwater-interface: An integrative model perspective using stable isotopes and acesulfame. *Science of The Total Environment, 466-467*, 16-25, doi:10.1016/j.scitotenv.2013.06.092.

Ergun, S. (1952). Fluid Flow Through Packed Column. *Chemical Engineering Progress, 48*, 89-94.

Fehlman, H. M. (1985). *Resistance Components and Velocity Distributions of Open Channel Flows Over Bedforms*: Colorado State University.

Feris, K., Ramsey, P., Frazar, C., Moore, J. N., Gannon, J. E. & Holben, W. E. (2003a). Differences in Hyporheic-Zone Microbial Community Structure along a Heavy-Metal Contamination Gradient. *Applied and Environmental Microbiology, 69*(9), 5563-5573, doi:10.1128/aem.69.9.5563-5573.2003.

Feris, K., Ramsey, P., Frazar, C., Rillig, M. C., Gannon, J. E. & Holben, W. E. (2003b). Structure and seasonal dynamics of hyporheic zone microbial communities in free-stone rivers of the estern United States. *Microbial Ecology, 46*(2), 200-215, doi:10.1007/BF03036883.

Findlay, S. (1995). Importance of surface-subsurface exchange in stream ecosystems: The hyporheic zone. *Limnology and Oceanography, 40*(1), 159-164, doi:10.4319/lo.1995.40.1.0159.

Fischer, H., Kloep, F., Wilzcek, S. & Pusch, M. T. (2005). A River's Liver – Microbial Processes within the Hyporheic Zone of a Large Lowland River. *Biogeochemistry, 76*(2), 349-371, doi:10.1007/s10533-005-6896-y.

Fleckenstein, J. H., Niswonger, R. G. & Fogg, G. E. (2006). River-Aquifer Interactions, Geologic Heterogeneity, and Low-Flow Management. *Groundwater, 44*(6), 837-852, doi:10.1111/j.1745-6584.2006.00190.x.

Fleckenstein, J. H. & Schmidt, C. (2009). Themenheft: Grundwasser-Oberflächenwasser-Interaktionen. *Grundwasser, 14*(3), 161-162, doi:10.1007/s00767-009-0115-z.

Fox, A., Boano, F. & Arnon, S. (2014). Impact of losing and gaining streamflow conditions on hyporheic exchange fluxes induced by dune-shaped bed forms. *Water Resources Research, 50*(3), 1895-1907, doi:10.1002/2013wr014668.

Fox, A., Laube, G., Schmidt, C., Fleckenstein, J. H. & Arnon, S. (2016). The effect of losing and gaining flow conditions on hyporheic exchange in heterogeneous streambeds. *Water Resources Research, 52*(9), 7460-7477, doi:10.1002/2016wr018677.

Freeze, R. A. & Cherry, J. A. (1979). *Groundwater*: Prentice-Hall.

Galloway, J., Fox, A., Lewandowski, J. & Arnon, S. (2019). The effect of unsteady streamflow and stream-groundwater interactions on oxygen consumption in a sandy streambed. *Scientific Reports, 9*(1), 19735, doi:10.1038/s41598-019-56289-y.

Gariglio, F. P., Tonina, D. & Luce, C. H. (2013). Spatiotemporal variability of hyporheic exchange through a pool-riffle-pool sequence. *Water Resources Research, 49*(11), 7185-7204, doi:10.1002/wrcr.20419.

Gessner, M. O., Hinkelmann, R., Nützmann, G., Jekel, M., Singer, G., Lewandowski, J., Nehls, T. & Barjenbruch, M. (2014). Urban water interfaces. *Journal of Hydrology, 514*, 226-232, doi:10.1016/j.jhydrol.2014.04.021.

Geuzaine, C. & Remacle, J.-F. (2009). Gmsh: A 3-D finite element mesh generator with built-in pre- and post-processing facilities. *International Journal for Numerical Methods in Engineering, 79*(11), 1309-1331, doi:10.1002/nme.2579.

Gomez-Velez, J. D., Harvey, J. W., Cardenas, M. B. & Kiel, B. (2015). Denitrification in the Mississippi River network controlled by flow through river bedforms. *Nature Geoscience, 8*, 941, doi:10.1038/ngeo2567.

Gomez, J. D., Wilson, J. L. & Cardenas, M. B. (2012). Residence time distributions in sinuosity-driven hyporheic zones and their biogeochemical effects. *Water Resources Research, 48*(9), doi:10.1029/2012wr012180.

Gooseff, M. N. (2010). Defining Hyporheic Zones – Advancing Our Conceptual and Operational Definitions of Where Stream Water and Groundwater Meet. *Geography Compass, 4*(8), 945-955, doi:10.1111/j.1749-8198.2010.00364.x.

Gordon, R. P., Lautz, L. K., Briggs, M. A. & McKenzie, J. M. (2012). Automated calculation of vertical pore-water flux from field temperature time series using the VFLUX method and computer program. *Journal of Hydrology, 420-421*, 142-158, doi:10.1016/j.jhydrol.2011.11.053.

Greenshields, C. (2010). OpenFOAM 1.7.0 Released. Retrieved from http://openfoam.org/release/1-7-0/

Greskowiak, J., Prommer, H., Massmann, G. & Nützmann, G. (2006). Modeling Seasonal Redox Dynamics and the Corresponding Fate of the Pharmaceutical Residue Phenazone During Artificial Recharge of Groundwater. *Environmental Science & Technology, 40*(21), 6615-6621, doi:10.1021/es052506t.

Gualtieri, C., Angeloudis, A., Bombardelli, F., Jha, S. & Stoesser, T. (2017). On the Values for the Turbulent Schmidt Number in Environmental Flows. *Fluids, 2*(2), 17.

Gupte, S. K. & Advani, S. G. (1997). Flow near the permeable boundary of a porous medium: An experimental investigation using LDA. *Experiments in Fluids, 22*(5), 408-422, doi:10.1007/s003480050067.

Hancock, P. (2002). Human Impacts on the Stream-Groundwater Exchange Zone. *Environmental management, 29*, 763-781, doi:10.1007/s00267-001-0064-5.

Harper, M. P. & Peckarsky, B. L. (2006). Emergence Cues Of A Mayfly In A High-Altitude Stream Ecosystem: Potential Response To Climate Change. *Ecological Applications, 16*(2), 612-621, doi:10.1890/1051-0761(2006)016[0612:Ecoami]2.0.Co;2.

Harvey, J. W. & Bencala, K. E. (1993). The effect of streambed topography on surface-subsurface water exchange in mountain catchments. *Water Resources Research, 29*(1), 89-98, doi:10.1029/92wr01960.

Harvey, J. W., Böhlke, J. K., Voytek, M. A., Scott, D. & Tobias, C. R. (2013). Hyporheic zone denitrification: Controls on effective reaction depth and contribution to whole-stream mass balance. *Water Resources Research, 49*(10), 6298-6316, doi:10.1002/wrcr.20492.

Harvey, J. W. & Fuller, C. C. (1998). Effect of enhanced manganese oxidation in the hyporheic zone on basin-scale geochemical mass balance. *Water Resour. Res., 34*(4), 623-636.

Harvey, J. W. & Gooseff, M. (2015). River corridor science: Hydrologic exchange and ecological consequences from bedforms to basins. *Water Resources Research, 51*(9), 6893-6922, doi:10.1002/2015wr017617.

Hatch, C. E., Fisher, A. T., Revenaugh, J. S., Constantz, J. & Ruehl, C. (2006). Quantifying surface water–groundwater interactions using time series analysis of streambed thermal records: Method development. *Water Resources Research, 42*(10), doi:10.1029/2005wr004787.

Heberer, T., Massmann, G., Fanck, B., Taute, T. & Dünnbier, U. (2008). Behaviour and redox sensitivity of antimicrobial residues during bank filtration. *Chemosphere, 73*(4), 451-460, doi:10.1016/j.chemosphere.2008.06.056.

Hernandez Murcia, O. E. (2014). *Development of a highly resolved 3-D computational model for applications in water quality and ecosystems.* (Doctor of Philosophy), University of Iowa

Herzog, S. P., Higgins, C. P. & McCray, J. E. (2016). Engineered Streambeds for Induced Hyporheic Flow: Enhanced Removal of Nutrients, Pathogens, and Metals from Urban Streams. *Journal of Environmental Engineering, 142*(1), 04015053, doi:10.1061/(ASCE)EE.1943-7870.0001012.

Hester, E. T. & Gooseff, M. N. (2010). Moving beyond the banks: Hyporheic restoration is fundamental to restoring ecological services and functions of streams. *Environmental Science & Technology, 44*(5), 1521-1525, doi:10.1021/es902988n.

Hester, E. T., Young, K. I. & Widdowson, M. A. (2013). Mixing of surface and groundwater induced by riverbed dunes: Implications for hyporheic zone definitions and pollutant reactions. *Water Resources Research, 49*(9), 5221-5237, doi:10.1002/wrcr.20399.

Hill, A. & Cardaci, M. (2004). Denitrification and Organic Carbon Availability in Riparian Wetland Soils and Subsurface Sediments. *Soil Science Society of America Journal - SSSAJ, 68*, doi:10.2136/sssaj2004.0320.

Hilt, S. (2001). Development of submerged macrophytes in shallow Lake Müggelsee (Berlin, Germany) before and after its switch to the phytoplankton-dominated state. *Archiv fur Hydrobiologie, 152*, 395-409.

Hinkelmann, R. (2005). *Efficient Numerical Methods and Information-Processing Techniques for Modeling Hydro- and Environmental Systems*: Springer-Verlag GmbH.

Hinze, J. O. (1959). *Turbulence: An Introduction to Its Mechanism and Theory*: McGraw-Hill.

Hirt, C. W. & Nichols, B. D. (1981). Volume of fluid (VOF) method for the dynamics of free boundaries. *Journal of Computational Physics, 39*(1), 201-225, doi:10.1016/0021-9991(81)90145-5.

Hoffmann, A. & Gunkel, G. (2011). Bank filtration in the sandy littoral zone of Lake Tegel (Berlin): Structure and dynamics of the biological active filter zone and clogging processes. *Limnologica, 41*(1), 10-19, doi:10.1016/j.limno.2009.12.003.

Huettel, M., Røy, H., Precht, E. & Ehrenhauss, S. (2003). Hydrodynamical impact on biogeochemical processes in aquatic sediments: The Interactions between Sediments and Water (Guest Editor: Brian Kronvang). *Hydrobiologia, 494*, doi:10.1023/A:1025426601773.

Huntscha, S., Singer, H., McArdell, C., Frank, C. & Hollender, J. (2012). Multiresidue analysis of 88 polar organic micropollutants in ground, surface and wastewater using online mixed-bed multilayer solid-phase extraction coupled to high performance liquid chromatography-tandem mass spectrometry. *Journal of chromatography. A, 1268*, doi:10.1016/j.chroma.2012.10.032.

Ibisch, R., I, S. & Borchardt, D. (2009). Influence of periphyton biomass dynamics on biological colmation processes in the hyporheic zone of a gravel bed river (River Lahn, Germany). *Advances in Limnology, 61*, 87-104.

Imholt, C., Gibbins, C. N., Malcolm, I. A., Langan, S. & Soulsby, C. (2010). Influence of riparian cover on stream temperatures and the growth of the mayfly Baetis rhodani in an upland stream. *Aquatic Ecology, 44*(4), 669-678, doi:10.1007/s10452-009-9305-0.

Irvine, D. J., Cranswick, R. H., Simmons, C. T., Shanafield, M. A. & Lautz, L. K. (2015). The effect of streambed heterogeneity on groundwater-surface water exchange fluxes inferred from temperature time series. *Water Resources Research, 51*(1), 198-212, doi:10.1002/2014wr015769.

Issa, R. I. (1986). Solution of the implicitly discretised fluid flow equations by operator-splitting. *Journal of Computational Physics, 62*(1), 40-65, doi:10.1016/0021-9991(86)90099-9.

Ivkovic, K. M. (2009). A top–down approach to characterise aquifer–river interaction processes. *Journal of Hydrology, 365*(3), 145-155, doi:10.1016/j.jhydrol.2008.11.021.

Janse, J. H. (2005). *Model studies on the eutrophication of shallow lakes and ditches.* Wageningen Universiteit Wageninge.

Janssen, F., Cardenas, M. B., Sawyer, A. H., Dammrich, T., Krietsch, J. & de Beer, D. (2012). A comparative experimental and multiphysics computational fluid dynamics study of coupled surface–subsurface flow in bed forms. *Water Resources Research, 48*(8), doi:10.1029/2012wr011982.

Jekel, M. & Czekalla, C. (2016). *Wasseraufbereitung - Grundlagen und Verfahren, DVGW Lehr- und Handbuch Wasserversorgung Bd. 6* Munich: DIV GmbH.

Jin, G., Tang, H., Gibbes, B., Li, L. & Barry, D. A. (2010). Transport of nonsorbing solutes in a streambed with periodic bedforms. *Adv. Water Resour., 33*(11), 1402-1416.

Jin, G., Tang, H., Li, L. & Barry, D. A. (2011). Hyporheic flow under periodic bed forms influenced by low-density gradients. *Geophysical Research Letters, 38*(22), doi:10.1029/2011gl049694.

Jirka, G. H. (2007). *Einführung in die Hydromechanik*: Universitätsverlag Karlsruhe.

Jones, J. B. & Mulholland, P. J. (2000). In *Streams and Ground Waters*. San Diego: Academic Press.

Kalbus, E., Reinstorf, F. & Schirmer, M. (2006). Measuring methods for groundwater – surface water interactions: a review. *Hydrol. Earth Syst. Sci., 10*(6), 873-887, doi:10.5194/hess-10-873-2006.

Kasahara, T. & Wondzell, S. M. (2003). Geomorphic controls on hyporheic exchange flow in mountain streams. *Water Resources Research, 39*(1), SBH 3-1-SBH 3-14, doi:10.1029/2002wr001386.

Keery, J., Binley, A., Crook, N. & Smith, J. W. N. (2007). Temporal and spatial variability of groundwater–surface water fluxes: Development and application of an analytical method using temperature time series. *Journal of Hydrology, 336*(1), 1-16, doi:10.1016/j.jhydrol.2006.12.003.

Kennedy, C. D., Genereux, D. P., Corbett, D. R. & Mitasova, H. (2009). Spatial and temporal dynamics of coupled groundwater and nitrogen fluxes through a streambed in an agricultural watershed. *Water Resources Research, 45*(9), doi:10.1029/2008wr007397.

Khan, H. H. & Khan, A. (2019). Chapter 14 - Groundwater and Surface Water Interaction. In S. Venkatramanan, M. V. Prasanna, & S. Y. Chung (Eds.), *GIS and Geostatistical Techniques for Groundwater Science* (pp. 197-207): Elsevier.

Kinzelbach, W. (1992). *Numerische Methoden zur Modellierung des Transports von Schadstoffen im Grundwasser*: Oldenbourg Wissenschaftsverlag.

Klein, S., Worch, E. & Knepper, T. P. (2015). Occurrence and Spatial Distribution of Microplastics in River Shore Sediments of the Rhine-Main Area in Germany. *Environmental Science & Technology, 49*(10), 6070-6076, doi:10.1021/acs.est.5b00492.

Knapp, C., Dodds, W., Wilson, K., O'Brien, J. & Graham, D. (2009). Spatial Heterogeneity of Denitrification Genes in a Highly Homogenous Urban Stream. *Environmental Science & Technology, 43*, 4273-4279, doi:10.1021/es9001407.

Kobus, H. & Keim, B. (2001). Grundwasser. In *Taschenbuch der Wasserwirtschaft* (pp. 277-313): Blackwell Wissenschaftsverlag.

Krause, S., Hannah, D. M., Fleckenstein, J. H., Heppell, C. M., Kaeser, D., Pickup, R., Pinay, G., Robertson, A. L. & Wood, P. J. (2011). Inter-disciplinary perspectives on processes in the hyporheic zone. *Ecohydrology, 4*(4), 481-499, doi:10.1002/eco.176.

Krause, S., Tecklenburg, C., Munz, M. & Naden, E. (2013). Streambed nitrogen cycling beyond the hyporheic zone: Flow controls on horizontal patterns and depth distribution of nitrate and dissolved oxygen in the upwelling groundwater of a lowland river. *Journal of Geophysical Research: Biogeosciences, 118*(1), 54-67, doi:10.1029/2012jg002122.

Lane, S. N., Hardy, R. J., Elliott, L. & Ingham, D. B. (2002). High-resolution numerical modelling of three-dimensional flows over complex river bed topography. *Hydrol. Processes, 16*, 2261-2272.

Larson, R. E. & Higdon, J. J. L. (1987). Microscopic flow near the surface of two-dimensional porous media. Part 2. Transverse flow. *Journal of Fluid Mechanics, 178*, 119-136, doi:10.1017/S0022112087001149.

Lattermann, E. (2010). *Wasserbau-Praxis: Mit Berechnungsbeispielen Bauwerk-Basis-Bibliothek*: Beuth Verlag GmbH.

Lawrence, J., Skold, M., Hussain, F., Silverman, D., Resh, V., Sedlak, D., Luthy, R. & McCray, J. (2013). Hyporheic Zone in Urban Streams: A Review and Opportunities for Enhancing Water Quality and Improving Aquatic Habitat by Active Management. *Environmental Engineering Science, 30*, 480-501, doi:10.1089/ees.2012.0235.

Lesieur, M. (2007). *Turbulence in Fluids*: Springer, Dordrecht.

Lewandowski, J., Angermann, L., Nützmann, G. & Fleckenstein, J. H. (2011a). A heat pulse technique for the determination of small-scale flow directions and flow velocities in the streambed of sand-bed streams. *Hydrological Processes, 25*(20), 3244-3255, doi:10.1002/hyp.8062.

Lewandowski, J., Arnon, S., Banks, E., Batelaan, O., Betterle, A., Broecker, T., Coll, C., Drummond, J. D., Gaona Garcia, J., Galloway, J., Gomez-Velez, J., Grabowski, R. C., Herzog, S. P., Hinkelmann, R., Höhne, A., Hollender, J., Horn, M. A., Jaeger, A., Krause, S., Löchner Prats, A., Magliozzi, C., Meinikmann, K., Mojarrad, B. B., Mueller, B. M., Peralta-Maraver, I., Popp, A. L., Posselt, M., Putschew, A., Radke, M., Raza, M., Riml, J., Robertson, A., Rutere, C., Schaper, J. L., Schirmer, M., Schulz, H., Shanafield, M., Singh, T., Ward, A. S., Wolke, P., Wörman, A. & Wu, L. (2019). Is the Hyporheic Zone Relevant beyond the Scientific Community? *Water, 11*(11), 2230.

Lewandowski, J., Meinikmann, K. & Krause, S. (2020). Groundwater–Surface Water Interactions: Recent Advances and Interdisciplinary Challenges. *Water, 12*(1), 296.

Lewandowski, J., Putschew, A., Schwesig, D., Neumann, C. & Radke, M. (2011b). Fate of organic micropollutants in the hyporheic zone of a eutrophic lowland stream: results of a preliminary field study. *The Science of the total environment, 409*(10), 1824-1835, doi:10.1016/j.scitotenv.2011.01.028.

Li, B., Liu, X., Kaufman, M. H., Turetcaia, A., Chen, X. & Cardenas, M. B. (2020). Flexible and Modular Simultaneous Modeling of Flow and Reactive Transport in Rivers and Hyporheic Zones. *Water Resources Research, 56*(2), e2019WR026528, doi:10.1029/2019wr026528.

Li, Z., Sobek, A. & Radke, M. (2016). Fate of Pharmaceuticals and Their Transformation Products in Four Small European Rivers Receiving Treated Wastewater. *Environmental Science & Technology, 50*(11), 5614-5621, doi:10.1021/acs.est.5b06327.

Maberly, S. C. (1985a). Photosynthesis by fontinalis antipyretica I. *New Phytologist, 100*(2), 127-140, doi:10.1111/j.1469-8137.1985.tb02765.x.

Maberly, S. C. (1985b). Photosynthesis by fontinalis antipyretica II. *New Phytologist, 100*(2), 141-155, doi:10.1111/j.1469-8137.1985.tb02766.x.

Maberly, S. C., Berthelot, S. A., Stott, A. W. & Gontero, B. (2015). Adaptation by macrophytes to inorganic carbon down a river with naturally variable concentrations of CO2. *Journal of Plant Physiology, 172*, 120-127, doi:10.1016/j.jplph.2014.07.025.

Malcolm, I. A., Soulsby, C., Youngson, A. F. & Hannah, D. M. (2005). Catchment-scale controls on groundwater–surface water interactions in the hyporheic zone: implications for salmon embryo survival. *River Research and Applications, 21*(9), 977-989, doi:10.1002/rra.861.

Maric, T., Höpken, J. & Mooney, K. (2014). *The OpenFOAM technology primer*: [s.l.] : Sourceflux.

Marion, A., Bellinello, M., Guymer, I. & Packman, A. (2002). Effect of bed form geometry on the penetration of nonreactive solutes into a streambed. *Water Resources Research, 38*(10), 27-21-27-12, doi:10.1029/2001wr000264.

Marzadri, A., Tonina, D. & Bellin, A. (2012). Morphodynamic controls on redox conditions and on nitrogen dynamics within the hyporheic zone: Application to gravel bed rivers with alternate-bar morphology. *Journal of Geophysical Research: Biogeosciences, 117*(G3), doi:10.1029/2012jg001966.

McCallum, J. L., Cook, P. G., Berhane, D., Rumpf, C. & McMahon, G. A. (2012). Quantifying groundwater flows to streams using differential flow gaugings and water chemistry. *Journal of Hydrology, 416-417*, 118-132, doi:10.1016/j.jhydrol.2011.11.040.

Mermillod-Blondin, F., Creuze des Chatelliers, M., Marmonier, P. & Dole-Olivier, M.-J. (2000). Distribution of solutes, microbes and invertebrates in river sediments along a riffle-pool-riffle sequence. *Freshwater Biology, 44*(2), 255-269, doi:10.1046/j.1365-2427.2000.00562.x.

Morén, I., Wörman, A. & Riml, J. (2017). Design of Remediation Actions for Nutrient Mitigation in the Hyporheic Zone. *Water Resources Research, 53*(11), 8872-8899, doi:10.1002/2016wr020127.

Mosthaf, K., Baber, K., Flemisch, B., Helmig, R., Leijnse, A., Rybak, I. & Wohlmuth, B. (2011). A coupling concept for two-phase compositional porous-medium and single-phase compositional free flow. *Water Resources Research, 47*(10), doi:10.1029/2011wr010685.

Mutz, M., Kalbus, E. & Meinecke, S. (2007). Effect of instream wood on vertical water flux in low-energy sand bed flume experiments. *Water Resources Research, 43*(10), doi:10.1029/2006wr005676.

Nogaro, G., Datry, T., Mermillod-Blondin, F., Descloux, S. & Montuelle, B. (2010). Influence of streambed sediment clogging on microbial processes in the hyporheic zone. *Freshwater Biology, 55*, 1288-1302, doi:10.1111/j.1365-2427.2009.02352.x.

Nützmann, G. & Mey, S. (2007). Model-based estimation of runoff changes in a small lowland watershed of north-eastern Germany. *Journal of Hydrology, 334*(3), 467-476, doi:10.1016/j.jhydrol.2006.10.026.

O'Connor, B. L. & Harvey, J. W. (2008). Scaling hyporheic exchange and its influence on biogeochemical reactions in aquatic ecosystems. *Water Resources Research, 44*(12), doi:10.1029/2008wr007160.

Ochoa-Tapia, J. A. & Whitaker, S. (1995). Momentum transfer at the boundary between a porous medium and a homogeneous fluid—I. Theoretical development. *International Journal of Heat and Mass Transfer, 38*(14), 2635-2646, doi:10.1016/0017-9310(94)00346-W.

Orghidan, T. (1959). Ein neuer Lebensraum des unterirdischen Wassers: der hyporheische Biotop. *Archiv für Hydrobilogie, 55*, 392–414.

Othman, S., Adlan, M. N. & Selamat, M. (2015). A study on the potential of riverbank filtration for the removal of color, iron, turbidity and E.Coli in Sungai Perak, Kota Lama Kiri, Kuala Kangsar, Perak, Malaysia. *Jurnal Teknologi, 74*, 83-91, doi:10.11113/jt.v74.4877.

Oxtoby, O., Heyns, J. & Suliman, R. (2013, 24.-25.10.). *A finite-volume solver for two-fluid flow in heterogeneous porous media based on OpenFOAM.* Paper presented at the Open Source CFD International Conference, Hamburg, Germany.

Packman, A. I. & Brooks, N. H. (2001). Hyporheic exchange of solutes and colloids with moving bed forms. *Water Resour. Res., 37*(10), 2591-2605.

Packman, A. I., Brooks, N. H. & Morgan, J. J. (2000). A physicochemical model for colloid exchange between a stream and a sand streambed with bed forms. *Water Resources Research, 36*(8), 2351-2361, doi:10.1029/2000wr900059.

Packman, A. I. & Salehin, M. (2003). Relative roles of stream flow and sedimentary conditions in controlling hyporheic exchange. *Hydrobiologia, 494*(1), 291-297, doi:10.1023/A:1025403424063.

Packman, A. I., Salehin, M. & Zaramella, M. (2004). Hyporheic Exchange with Gravel Beds: Basic Hydrodynamic Interactions and Bedform-Induced Advective Flows. *Journal of Hydraulic Engineering, 130*(7), 647-656, doi:10.1061/(ASCE)0733-9429(2004)130:7(647).

Panday, S. & Huyakorn, P. S. (2004). A fully coupled physically-based spatially-distributed model for evaluating surface/subsurface flow. *Advances in Water Resources, 27*(4), 361-382, doi:10.1016/j.advwatres.2004.02.016.

Paton Née Mueller, E., Schaik, N. L. M. B., Blume, T., Bronstert, A., Carus, J., Fleckenstein, J., Fohrer, N., Geissler, K., Gerke, H., Graeff, T., Hesse, C., Hildebrandt, A., Hölker, F., Hunke, P., Körner, K., Lewandowski, J., Lohmann, D., Meinikmann, K., Schibalski, A. & Tietjen, B. (2014). Skalen, Schwerpunkte, Rückkopplungen und Herausforderungen der ökohydrologischen Forschung in Deutschland (Scales, key aspects, feedbacks and challenges of ecohydrological research in Germany). *Hydrologie und Wasserbewirtschaftung, 58*, 221–240, doi:10.5675/HyWa_2014,4_2.

Peter, K. T., Herzog, S., Tian, Z., Wu, C., McCray, J. E., Lynch, K. & Kolodziej, E. P. (2019). Evaluating emerging organic contaminant removal in an engineered hyporheic zone using high resolution mass spectrometry. *Water Research, 150*, 140-152, doi:10.1016/j.watres.2018.11.050.

Peterson, E. W. & Sickbert, T. B. (2006). Stream water bypass through a meander neck, laterally extending the hyporheic zone. *Hydrogeology Journal, 14*(8), 1443-1451, doi:10.1007/s10040-006-0050-3.

Pope, S. B. (2004). Ten questions concerning the large-eddy simulation of turbulent flows. *New Journal of Physics, 6*, 35-35, doi:10.1088/1367-2630/6/1/035.

Prinos, P. (1995). Bed-Suction Effects on Structure of Turbulent Open-Channel Flow. *Journal of Hydraulic Engineering-asce - J HYDRAUL ENG-ASCE, 121*, doi:10.1061/(ASCE)0733-9429(1995)121:5(404).

Putschew, A., Miehe, U., Tellez, A. S. & Jekel, M. (2007). Ozonation and reductive deiodination of iopromide to reduce the environmental burden of iodinated X-ray contrast media. *Water Science and Technology, 56*(11), 159-165, doi:10.2166/wst.2007.827.

Rahimi, M., Essaid, H. I. & Wilson, J. T. (2015). The role of dynamic surface water-groundwater exchange on streambed denitrification in a first-order, low-relief agricultural watershed. *Water Resources Research, 51*(12), 9514-9538, doi:10.1002/2014wr016739.

Regnery, J., Barringer, J., Wing, A., Hoppe-Jones, C., Teerlink, J. & Drewes, J. (2015). Start-up performance of a full-scale riverbank filtration site regarding removal of DOC, nutrients, and trace organic chemicals. *Chemosphere, 127C*, 136-142, doi:10.1016/j.chemosphere.2014.12.076.

Revelli, R., Boano, F., Camporeale, C. & Ridolfi, L. (2008). Intrameander hyporheic flow in alluvial rivers. *Water Resour. Res., 44*(12), W12428-W12428.

Riml, J., Wörman, A., Kunkel, U. & Radke, M. (2013). Evaluating the fate of six common pharmaceuticals using a reactive transport model: Insights from a stream tracer test. *Science of The Total Environment, 458-460*, 344-354, doi:10.1016/j.scitotenv.2013.03.077.

Roche, K. R., Blois, G., Best, J. L., Christensen, K. T., Aubeneau, A. F. & Packman, A. I. (2018). Turbulence Links Momentum and Solute Exchange in Coarse-Grained Streambeds. *Water Resources Research, 54*(5), 3225-3242, doi:10.1029/2017wr021992.

Rodrigues, M. A., Pardela, L., Geraldes, V., Santos, J., Matos, H. A. & Azevedo, E. J. (2011). Theophylline polymorphs by atomization of supercritical antisolvent induced suspensions. *The Journal of Supercritical Fluids, 58*(2), 303-312.

Romero, L. G., Mondardo, R. I., Sens, M. L. & Grischek, T. (2014). Removal of cyanobacteria and cyanotoxins during lake bank filtration at Lagoa do Peri, Brazil. *Clean Technologies and Environmental Policy, 16*(6), 1133-1143, doi:10.1007/s10098-014-0715-x.

Ruehl, C., Fisher, A., Los Huertos, M., Wankel, S., Wheat, C., Kendall, C., Hatch, C. & Shennan, C. (2009). Nitrate dynamics within the Pajaro River, a nutrient-rich, losing stream. *Journal of the North American Benthological Society, 26*, 191-206, doi:10.1899/0887-3593(2007)26[191:NDWTPR]2.0.CO;2.

Sachse, R., Petzoldt, T., Blumstock, M., Moreira, S., Pätzig, M., Rücker, J., Janse, J. H., Mooij, W. M. & Hilt, S. (2014). Extending one-dimensional models for deep lakes to simulate the impact of submerged macrophytes on water quality. *Environmental Modelling & Software, 61*, 410-423, doi:10.1016/j.envsoft.2014.05.023.

Saenger, N. (2002). Estimation of flow velocities within the hyporheic zone. *SIL Proceedings, 1922-2010, 28*(4), 1790-1795, doi:10.1080/03680770.2001.11901935.

Saenger, N., K. Kitanidis, P. & Street, R. (2005). *A numerical study of surface-subsurface exchange processes at a riffle-pool pair in the Lahn River, Germany* (Vol. 41).

Schaper, J. L., Posselt, M., Bouchez, C., Jaeger, A., Nuetzmann, G., Putschew, A., Singer, G. & Lewandowski, J. (2019). Fate of Trace Organic Compounds in the Hyporheic Zone: Influence of Retardation, the Benthic Biolayer, and Organic Carbon. *Environmental Science & Technology, 53*(8), 4224-4234, doi:10.1021/acs.est.8b06231.

Schaper, J. L., Posselt, M., McCallum, J. L., Banks, E. W., Hoehne, A., Meinikmann, K., Shanafield, M. A., Batelaan, O. & Lewandowski, J. (2018). Hyporheic Exchange Controls Fate of Trace Organic Compounds in an Urban Stream. *Environmental Science & Technology, 52*(21), 12285-12294, doi:10.1021/acs.est.8b03117.

Schuetz, T. & Weiler, M. (2011). Quantification of localized groundwater inflow into streams using ground-based infrared thermography. *Geophysical Research Letters, 38*(3), doi:10.1029/2010gl046198.

Schulze, L. & Thorenz, C. (2014, 2014). *The Multiphase Capabilities of the CFD Toolbox OpenFOAM for Hydraulic Engineering Applications.* Paper presented at the ICHE 2014, Hamburg.

Shen, H. W., Fehlman, H. M. & Mendoza, C. (1990). Bed Form Resistances in Open Channel Flows. *Journal of Hydraulic Engineering, 116*(6), 799-815, doi:10.1061/(ASCE)0733-9429(1990)116:6(799).

Shen, Y. & Diplas, P. (2008). Application of two- and three-dimensional computational fluid dynamics models to complex ecological stream flows. *J. Hydrol., 348*(1-2), 195-214.

Silliman, S. E. & Booth, D. F. (1993). Analysis of time-series measurements of sediment temperature for identification of gaining vs. losing portions of Juday Creek, Indiana. *Journal of Hydrology, 146*, 131-148, doi:10.1016/0022-1694(93)90273-C.

Smagorinsky, J. (1963). General circulation experiments with the primitive equations. *Monthly Weather Review, 91*(3), 99-164, doi:10.1175/1520-0493(1963)091<0099:Gcewtp>2.3.Co;2.

Smith, J. W. N. (2005). *Groundwater-Surface Water Interactions in the Hyporheic Zone*: Environment Agency Science Report.

Solder, J. E., Gilmore, T. E., Genereux, D. P. & Solomon, D. K. (2016). A Tube Seepage Meter for In Situ Measurement of Seepage Rate and Groundwater Sampling. *Groundwater, 54*(4), 588-595, doi:10.1111/gwat.12388.

Sophocleous, M. (2002). Interactions between groundwater and surface water: the state of the science. *Hydrogeology Journal, 10*(1), 52-67, doi:10.1007/s10040-001-0170-8.

Starov, V. & Zhdanov, V. (2001). Effective viscosity and permeability of porous media. *Colloids and Surfaces A-physicochemical and Engineering Aspects - COLLOID SURFACE A, 192*, 363-375, doi:10.1016/S0927-7757(01)00737-3.

Stieber, M., Putschew, A. & Jekel, M. (2008). Reductive dehalogenation of iopromide by zero-valent iron. *Water Science and Technology, 57*(12), 1969-1975, doi:10.2166/wst.2008.602.

Stoesser, T., Braun, C., García-Villalba, M. & Rodi, W. (2008). Turbulence Structures in Flow over Two-Dimensional Dunes. *J. Hydraul. Eng., 134*(1), 42-55.

Stofleth, J. M., Shields Jr, F. D. & Fox, G. A. (2008). Hyporheic and total transient storage in small, sand-bed streams. *Hydrological Processes, 22*(12), 1885-1894, doi:10.1002/hyp.6773.

Stonedahl, S. H., Harvey, J. W. & Packman, A. I. (2013). Interactions between hyporheic flow produced by stream meanders, bars, and dunes. *Water Resources Research, 49*(9), 5450-5461, doi:10.1002/wrcr.20400.

Stonedahl, S. H., Harvey, J. W., Wörman, A., Salehin, M. & Packman, A. I. (2010). A multiscale model for integrating hyporheic exchange from ripples to meanders. *Water Resources Research, 46*(12), doi:10.1029/2009wr008865.

Thibodeaux, L. J. & Boyle, J. D. (1987). Bedform-generated convective transport in bottom sediment. *Nature, 325*(6102), 341-343, doi:10.1038/325341a0.

Thorenz, C. & Strybny, J. (2012). *On the numerical modelling of filling-emptying system for locks*. Paper presented at the Proceedings of 10th International Conference onHydroinformatics, Hamburg, Germany.

Tonina, D. (2012). Surface water and streambed sediment interaction: The hyporheic exchange. In *Fluid Mechanics of Environmental Interfaces*. London: CRC Press.

Tonina, D. & Buffington, J. M. (2007). Hyporheic exchange in gravel bed rivers with pool-riffle morphology: Laboratory experiments and three-dimensional modeling. *Water Resources Research, 43*(1), doi:10.1029/2005wr004328.

Tonina, D. & Buffington, J. M. (2009a). Hyporheic Exchange in Mountain Rivers I: Mechanics and Environmental Effects. *Geography Compass, 3*, 1063-1086.

Tonina, D. & Buffington, J. M. (2009b). A three-dimensional model for analyzing the effects of salmon redds on hyporheic exchange and egg pocket habitat. *Canadian Journal of Fisheries and Aquatic Sciences, 66*(12), 2157-2173, doi:10.1139/F09-146.

Toran, L. (2017). *Groundwater-Surface water interactions: A review for Encyclopedia of Water*.

Trauth, N., Schmidt, C., Maier, U., Vieweg, M. & Fleckenstein, J. (2013). Coupled 3-D stream flow and hyporheic flow model under varying stream and ambient groundwater

flow conditions in a pool-riffle system. *Water Resources Research, 49*(9), 5834-5850, doi:10.1002/wrcr.20442.

Trauth, N., Schmidt, C., Vieweg, M., Maier, U. & Fleckenstein, J. H. (2014). Hyporheic transport and biogeochemical reactions in pool-riffle systems under varying ambient groundwater flow conditions. *Journal of Geophysical Research: Biogeosciences, 119*(5), 910-928, doi:10.1002/2013jg002586.

Trauth, N., Schmidt, C., Vieweg, M., Oswald, S. E. & Fleckenstein, J. H. (2015). Hydraulic controls of in-stream gravel bar hyporheic exchange and reactions. *Water Resour. Res., 51*, 2243-2263.

Triska, F. J., Kennedy, V. C., Avanzino, R. J., Zellweger, G. W. & Bencala, K. E. (1989). Retention and Transport of Nutrients in a Third-Order Stream in Northwestern California: Hyporheic Processes. *Ecology, 70*(6), 1893-1905, doi:10.2307/1938120.

van der Molen, D. T., Breeuwsma, A. & Boers, P. C. M. (1998). Agricultural Nutrient Losses to Surface Water in the Netherlands: Impact, Strategies, and Perspectives. *Journal of Environmental Quality, 27*(1), 4-11, doi:10.2134/jeq1998.00472425002700010002x.

van Gent, M. (1995). *Wave Interaction with Permeable Coastal Structures* (Vol. 95). Amsterdam, Netherlands: Elsevier Science.

VanderKwaak, J. E. (1999). *Numerical Simulation of Flow and Chemical Transport in Integrated Surface-Subsurface Hydrologic Systems.* (Ph.D. thesis), University of Waterloo Waterloo, Canada.

Vaux, W. (1968). Intragravel flow and interchange of water in a streambed. *Fishery Bulletin of the Fish and Wildlife Service, 66*(3), 479-489.

Voermans, J., Ghisalberti, M. & Ivey, G. (2017). *The variation of flow and turbulence across the sediment–water interface* (Vol. 824).

Ward, A. S. (2016). The evolution and state of interdisciplinary hyporheic research. *WIREs Water, 3*(1), 83-103, doi:10.1002/wat2.1120.

Ward, A. S., Morgan, J. A., White, J. R. & Royer, T. V. (2018). Streambed restoration to remove fine sediment alters reach-scale transient storage in a low-gradient fifth-order river, Indiana, USA. *Hydrological Processes, 32*(12), 1786-1800, doi:10.1002/hyp.11518.

Wasserbetriebe, B. (2015). *Data on pumping rates provided by Berlin water works (Berliner Wasserbetriebe)*.

Wehrly, K. E., Wang, L. & Mitro, M. (2007). Field-Based Estimates of Thermal Tolerance Limits for Trout: Incorporating Exposure Time and Temperature Fluctuation. *Transactions of the American Fisheries Society, 136*(2), 365-374, doi:10.1577/T06-163.1.

Westbrook, D. R. (1985). Analysis of inequality and residual flow procedures and an iterative scheme for free surface seepage. *International Journal for Numerical Methods in Engineering, 21*(10), 1791-1802, doi:10.1002/nme.1620211006.

Westhoff, M. C., Savenije, H. H. G., Luxemburg, W. M. J., Stelling, G. S., van de Giesen, N. C., Selker, J. S., Pfister, L. & Uhlenbrook, S. (2007). A distributed stream temperature model using high resolution temperature observations. *Hydrol. Earth Syst. Sci., 11*(4), 1469-1480, doi:10.5194/hess-11-1469-2007.

White, D. & Hendricks, S. (2000). Lotic Macrophytes and Surface–Subsurface Exchange Processes. In (Vol. 40, pp. 363-379).

Wiese, B., Massmann, G., Jekel, M., Heberer, T., Dünnbier, U., Orlikowski, D. & Grützmacher, G. (2011). Removal kinetics of organic compounds and sum parameters under field conditions for managed aquifer recharge. *Water Research, 45*(16), 4939-4950, doi:10.1016/j.watres.2011.06.040.

Winter, T. C., Harvey, J. W., Franke, O. L. & Alley, W. M. (1998). *Ground water and surface water; a single resource* (1139). Retrieved from

Woessner, W. W. (2000). Stream and Fluvial Plain Ground Water Interactions: Rescaling Hydrogeologic Thought. *Groundwater, 38*(3), 423-429, doi:10.1111/j.1745-6584.2000.tb00228.x.

Wondzell, S. M. & Gooseff, M. (2013). *Geomorphic Controls on Hyporheic Exchange Across Scales: Watersheds to Particles* (Vol. 9).

Wu, L., Singh, T., Gomez-Velez, J., Nützmann, G., Wörman, A., Krause, S. & Lewandowski, J. (2018). Impact of Dynamically Changing Discharge on Hyporheic Exchange Processes Under Gaining and Losing Groundwater Conditions. *Water Resources Research, 54*(12), 10,076-010,093, doi:10.1029/2018wr023185.

Yang, G., Coltman, E., Weishaupt, K., Terzis, A., Helmig, R. & Weigand, B. (2019). On the Beavers–Joseph Interface Condition for Non-parallel Coupled Channel Flow over a Porous Structure at High Reynolds Numbers. *Transport in Porous Media, 128*(2), 431-457, doi:10.1007/s11242-019-01255-5.

Young, D. F., Munson, B. R., Okiishi, T. H. & Huebsch, W. W. (2010). *A Brief Introduction to Fluid Mechanics*: John Wiley.

Yue, W., Lin, C. L. & Patel, V. C. (2005). Large eddy simulation of turbulent open-channel flow with free surface simulated by level set method. *Phys. Fluids, 17*(2), 025108-025108.

Zaramella, M., Packman, A. & Marion, A. (2003). Application of the transient storage model to analyze advective hyporheic exchange with deep and shallow sediment beds. *Water Resources Research, 39*, doi:10.1029/2002WR001344.

Zarnetske, J. P., Haggerty, R., Wondzell, S. M. & Baker, M. A. (2011). Dynamics of nitrate production and removal as a function of residence time in the hyporheic zone. *Journal of Geophysical Research: Biogeosciences, 116*(G1), doi:10.1029/2010jg001356.